Heat Transfer Enhancement in Plate-Fin Heat Exchangers Using Longitudinal Vortex Generators

by
R. VASUDEVAN

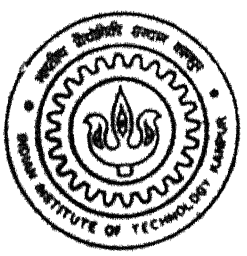

DEPARTMENT OF MECHANICAL ENGINEERING
INDIAN INSTITUTE OF TECHNOLOGY KANPUR

March, 2000

Heat Transfer Enhancement in Plate-Fin Heat Exchangers Using Longitudinal Vortex Generators

A Thesis Submitted
in Partial Fulfilment of the Requirements
for the degree of

DOCTOR OF PHILOSOPHY

by
R. VASUDEVAN

to the
DEPARTMENT OF MECHANICAL ENGINEERING
INDIAN INSTITUTE OF TECHNOLOGY
MARCH, 2000

Certificate

It is certified that the work contained in the thesis entitled *"Heat Transfer Enhancement In Plate Fin Heat Exchangers Using Longitudinal Vortex Generators"* by **R.Vasudevan** has been carried out under our supervision and that this work has not been submitted elsewhere for a degree.

Dr. V.Eswaran
Dept. of Mech. Engineeering
I.I.T. Kanpur

Gautam Biswas
Dr. Gautam Biswas
Dept. of Mech. Engineering
I.I.T. Kanpur

March 2000`

To my daughter
Nivedita

Synopsis

An innovative design of secondary fins for enhancing the heat transfer rate in plate-fin heat exchangers is proposed. Triangular fins that are used as inserts between the plates of a plate-fin heat exchanger are to be provided with longitudinal vortex generators in the form of delta wings or delta winglets on their slant surfaces. When the fluid flows past such an enhanced surface longitudinal vortices develop along the edge of the vortex generator due to the pressure difference between the front surface facing the flow and the rear surface. These streamwise vortices interact with an otherwise two-dimensional boundary layer and produce a three dimensional swirling flow that mixes near-wall fluid with the free stream. This mechanism strongly enhances the exchange of fluid between the wall and the core region of the flow field, which brings about significant enhancement in heat transfer.

The performance of the proposed design is evaluated for different angles of attack and different thermal boundary conditions. The flow regime is assumed to be laminar because, usually the fin spacing is so small and the mean velocity is such that the Reynolds numbers of interest are below the critical Reynolds number. The computational domain for a punched delta winglet is the rhomboid shown in Figure S-1. The governing equations of the problem are the three dimensional Navier-Stokes and energy equations which can be written in their conservative form in tensor notation as

$$\frac{\partial U_i}{\partial X_i} = 0$$

$$\frac{\partial U_i}{\partial \tau} + \frac{\partial U_i U_j}{\partial X_j} = -\frac{\partial P}{\partial X_i} + \frac{1}{\mathrm{Re}}\left[\frac{\partial}{\partial X_j}\left(\frac{\partial U_i}{\partial X_j} + \frac{\partial U_i}{\partial X_i}\right)\right]$$

$$\frac{\partial \theta}{\partial \tau} + \frac{\partial (\theta U_j)}{\partial X_j} = \frac{1}{\mathrm{Re.Pr}} \frac{\partial}{\partial X_j} \left(\frac{\partial \theta}{\partial X_j} \right)$$

The three dimensional velocity and temperature fields are obtained in the form of numerical solution to these equations using a modified version of the Marker and Cell (MAC) method. The computational domain has a triangular stamping lying in the middle as shown in Figure S-1. Presence of fluid on either side of the stamping rules out the use of fictitious cells. Hence in the present formulation, the numerical implementation of boundary conditions is accomplished without resorting to the use of fictitious cells.

Figure S-2 shows the distribution of combined spanwise average Nusselt number in the channel having a winglet with an angle of attack of 30° for two different Reynolds numbers. The heat transfer enhancement effect of the winglet is clearly evident from the steady increase in the Nusselt number along the length of the winglet. The purpose of using heat transfer enhancement techniques is to reduce the size of the heat exchanger for a given heat transfer load. To this end the results of the computation are expressed in terms of the compactness achievable using the proposed design. The only price to be paid for enhancing heat transfer using longitudinal vortex generators is the additional pumping power required to force the fluid through the heat exchanger. This quantity is also computed to confirm that the increase is sufficiently small.

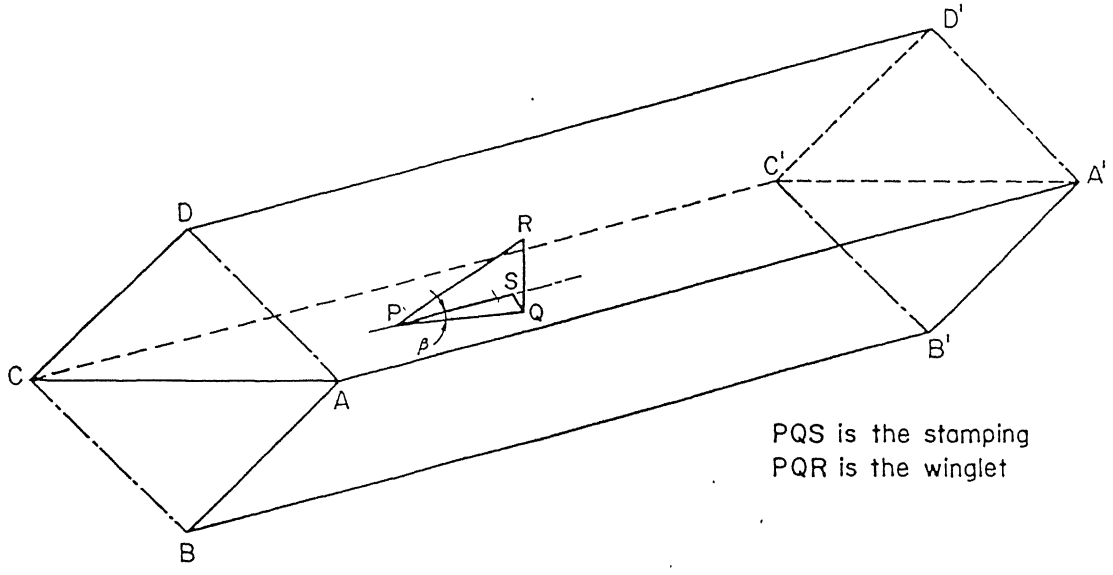

Figure S-1 Computational domain for the punched delta winglet

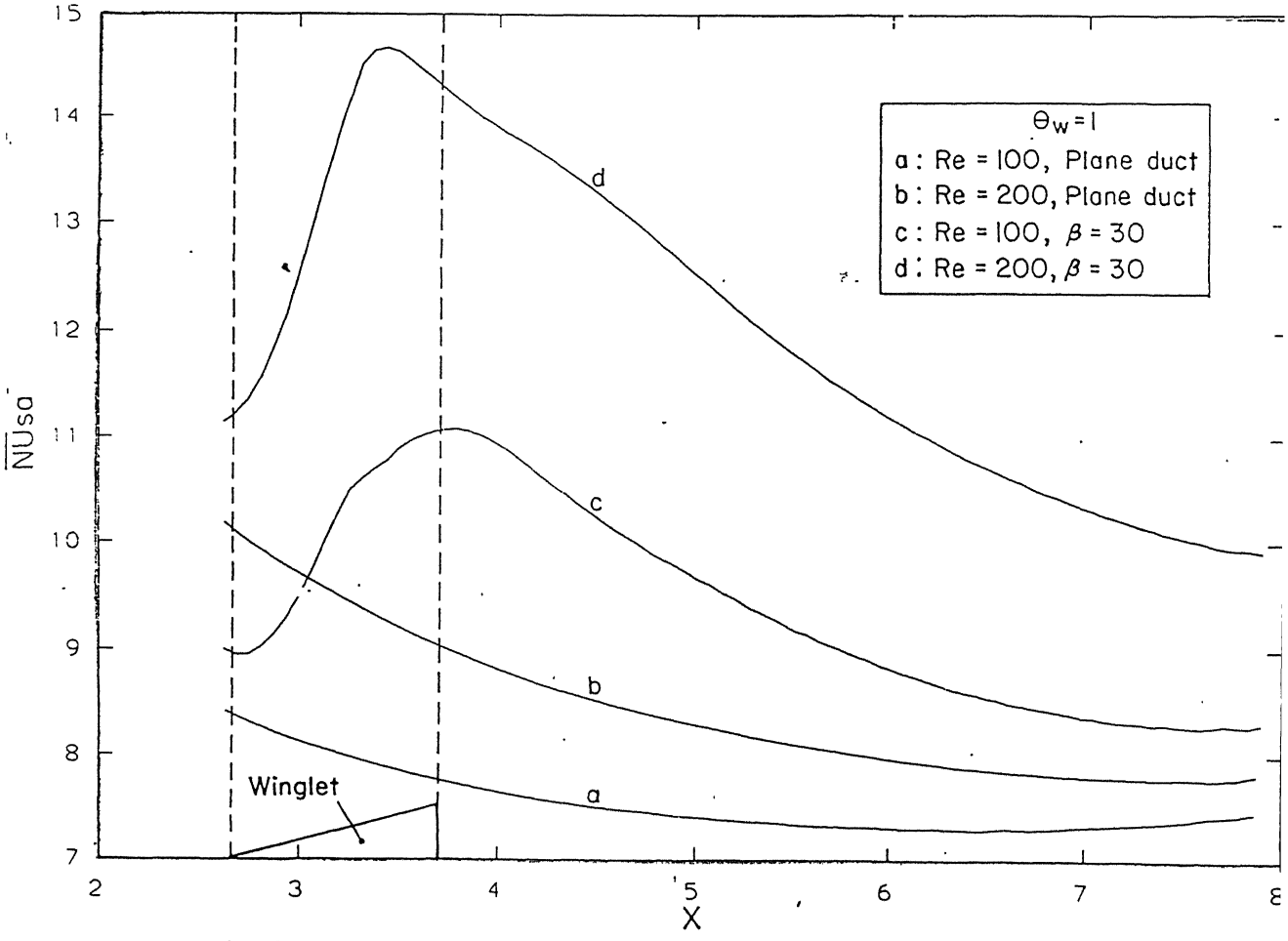

Figure S-2 Distribution of combined spanwise average Nusselt number in the channe

Acknowledgements

At the outset, I would like to express my solemn gratitude to Late Prof. N.K. Mitra of Thermo and Fluid Dynamics Institute , Ruhr University Bochum, Germany. His untimely demise on October 14, 1999 created a vacuum in the scientific community of Heat and Mass Transfer. In fact, following his advice, the Britannia Heat Transfer Limited Birmingham has manufactured the secondary fins for the Plate-Fin Heat Exchangers. The photographs of these fins have been used in this thesis. I am deeply indebted to him for many innovative ideas.

I would like to record my heartfelt gratitude to my thesis supervisors Dr. Gautam Biswas and Dr. Vinayak Eswaran for their invaluable help, constant encouragement and sagacious advice throughout my Ph.D program. It was Prof. Biswas who initiated me into the field of *Computational Fluid Dynamics.* It was from him that I learnt the technique of working systematically and meticulously. The numerous discussions I had with Prof. Eswaran instilled in me the confidence needed to crack formidable problems in CFD. I will always cherish my association with Dr. Keshav Kant whose friendly advice and support helped me sail through difficult times.

I owe the progress of my Ph.D work to the facilities available in the CFD lab. But for the ideal working environment of this lab, assiduously built up by Prof. Gautam Biswas, my research work could not have been completed in time. I would also like to thank all my colleagues at the CFD lab for their help and cooperation. Mr. Kushwaha, Draftsman of Mechanical Engineering Department deserves a special mention for all the help he rendered in preparing the drawings. My family members silently bore the pain of separation for three long years. I can never adequately thank them for the moral support provided by them during this period.

R.Vasudevan

Contents

List of Figures

Nomenclature

A_c	area of cross section of the duct
h	heat transfer coefficient
H	characteristic length dimension (distance between the plates)
k	.thermal conductivity of the fluid
Nu	local Nusselt number based on bulk temperature of the fluid
$\overline{Nu}$	combined average Nusselt number
p	static pressure
P	nondimensional static pressure
P′	prime pressure correction
Pr	Prandtl number
q	heat flux
Re	Reynolds number
t	time
T	temperature
u, v, w	axial, normal and spanwise components of velocity
U, V, W	axial, normal and spanwise components of velocity (nondimensional)
U_{av}	average velocity of the fluid at the channel inlet
U_c	mean channel outflow velocity
x, y, z	axial, normal and spanwise dimension of coordinates
X, Y, Z	axial, normal, and spanwise coordinates (normalised by H)

Greek symbols

β	angle of attack of the vortex generator
ν	kinematic viscosity of the fluid
θ	temperature (nondimensional)
τ	nondimensional time
ϕ	dependent variable, U, V, W or θ

Subscripts

w	wall
b	bulk condition
av	average
sa	spanwise combination of channel walls
∞	inlet condition for the temperature

Chapter 1

Introduction

1.1 Perspective

A heat exchanger is a device whose primary purpose is to exchange thermal energy between two fluids. Many applications require the space occupied by the exchanger to be kept as low as possible. The compact heat exchangers serve this purpose together with the required amount of energy exchange and low fluid inventory. The compactness of a heat exchanger is measured in terms of the heat transfer surface area per unit volume of the exchanger. Heat exchangers having a high value of this ratio are known as compact heat exchangers.

Heat exchangers are widely used in power and process industries, so improvements in their performance are of great technical, economical, and not the least, ecological importance. Performance improvement becomes particularly necessary in heat exchangers with gases because the thermal resistance of gases can be 10 to 50 times as large as that of liquids. Typical values of the gas side heat transfer surface area per unit volume of a compact heat exchanger lie between 700 and 1000 m^2 / m^3 (Tiggelbeck et al., 1992) . This results in very low hydraulic diameters (of a few millimetres) on the gas side. Larger heat transfer area on the gas side is necessary because, the higher heat transfer resistance for such

equipment lies on the gas side. The heat transfer rate at the gas side is often increased by adding fins to compensate for the poor heat transfer properties of the gases. In designing a compact heat exchanger the requisite heat transfer rate has to be achieved while ensuring that the size of the exchanger is small enough and the pumping power required is not very high. In accomplishing this goal, the use of enhanced heat transfer surfaces is a very effective technique for the designer. The present work is undertaken to compute the enhancement levels achievable in a plate-fin heat exchanger by using triangular inserts with built-in vortex generators in the form of delta wings and delta winglets.

1.2 Classification of Heat Exchangers

Heat exchangers can be classified into three categories, namely (1) Regenerators; (2) Open-type exchangers ; and (3) Closed type exchangers, or recuperators. Regenerators are exchangers in which the hot and cold fluids flow alternately through the same space with as little physical mixing between the two streams as possible. Open-type heat exchangers are devices wherein the two fluid streams physically mix with each other. Hot and cold fluids enter the open-type heat exchanger and leave as a single stream. In the closed type of heat exchanger, most widely used for industrial applications, the hot and cold fluids are separated by a wall, across which heat is transferred from the hot fluid to the cold fluid.

1.2.1 Classification of Closed-Type Heat Exchangers

Based on the number of passes made by each fluid, closed type heat exchangers are classified into single pass and multi-pass types; and based on the relative directions of the two streams, into parallel flow,

counterflow and crossflow types. Figures 1.1 to 1.4 show different closed-type heat exchangers that are commonly in use.

1.3 Design considerations for closed-type heat exchangers

The design of a heat exchanger involves a consideration of both the heat transfer rate between the fluids and the mechanical pumping power expended to overcome fluid friction while moving the fluids through the heat exchanger. For a heat exchanger operating with high-density fluids, the friction-power expenditure is generally small relative to the heat transfer rate, with the result that the friction power expenditure is seldom of controlling influence. However, for low density fluids, such as gases it is very easy to expend as much mechanical energy in overcoming friction power as is transferred as heat (Kays and London., 1984). And in most thermal power systems mechanical energy is worth 4 to 10 times as much as its equivalent in heat. For flow passages typically used for the heat transfer surfaces of a closed type heat exchanger, the heat transfer rate per unit of surface area can be increased by increasing fluid-flow velocity, and this heat transfer rate varies as something less than the first power of the velocity. The friction power expenditure is also increased with flow velocity, but in this case the power varies by as much as the cube of the velocity and never less than the square. This behaviour enables the designer to match both heat transfer rate and friction (pressure drop) specifications. If the friction-power expenditure in a particular application tends to be high, the flow velocities can be reduced by increasing the number of flow passages in the heat exchanger. This will also decrease the heat transfer rate per unit of surface area, but according to the above relations the reduction in heat

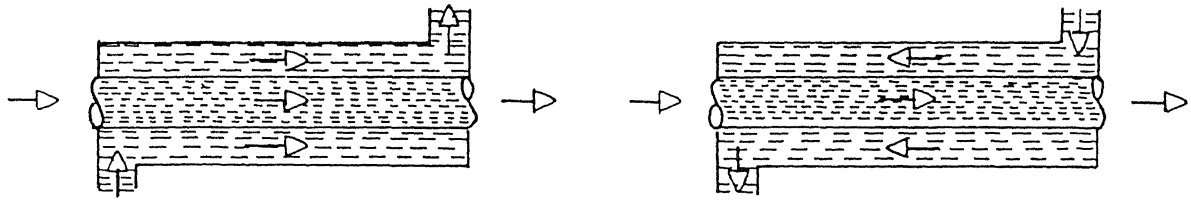

Figure 1.1 Concentric tube heat exchangers (a) Parallel flow. (b) Counterflow.

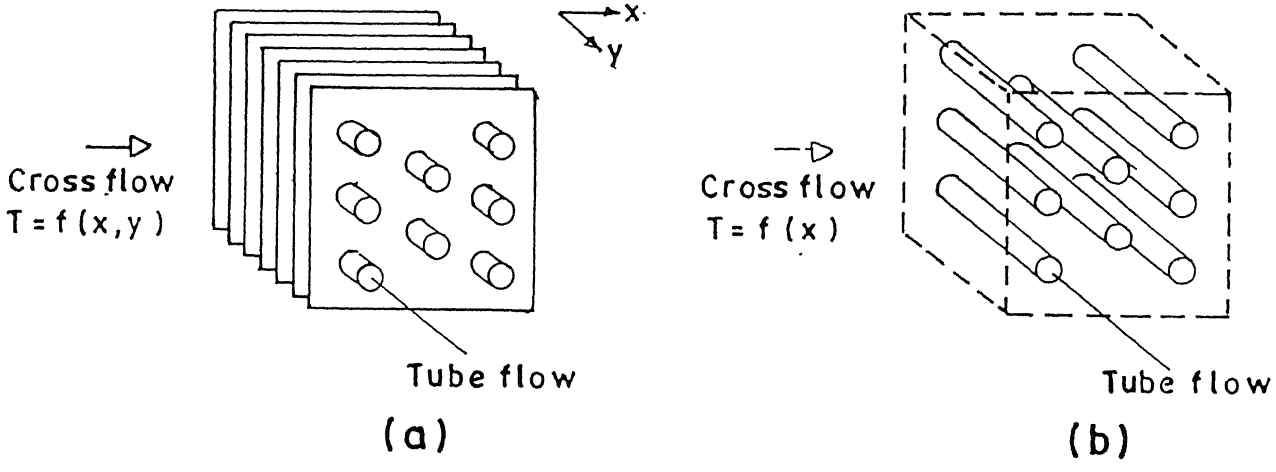

Figure 1.2 Cross-flow heat exchangers (a) Finned with both fluids unmixed (b) Unfinned with one fluid mixed and the other unmixed.

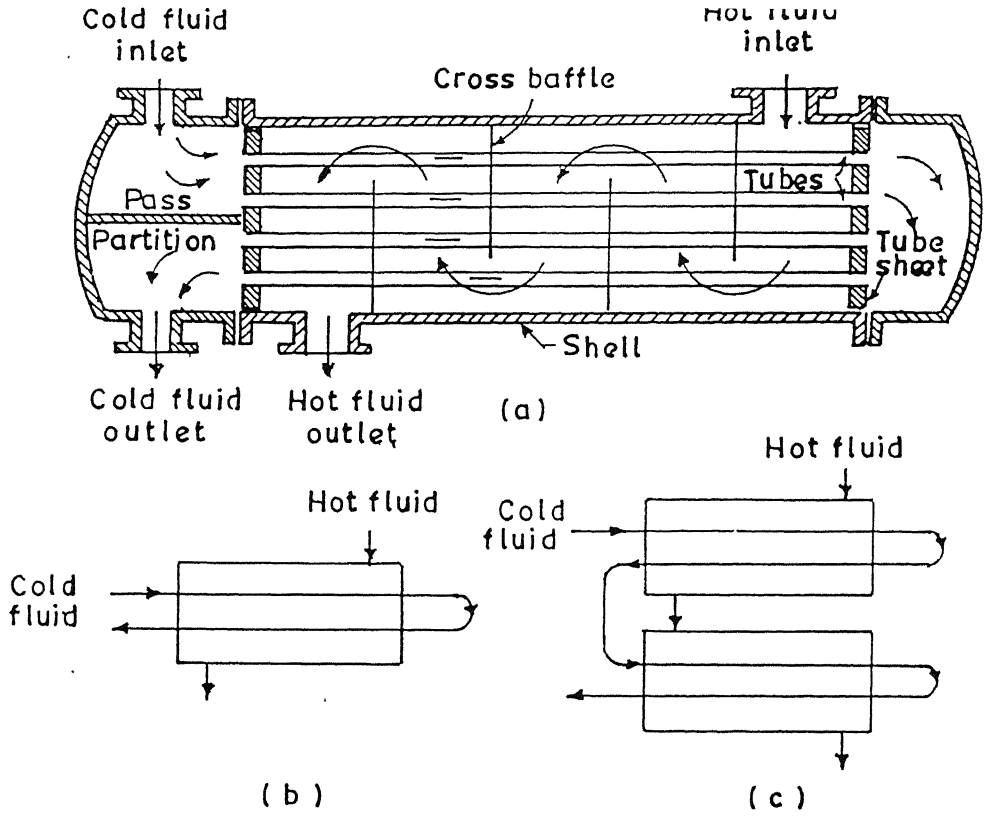

Figure. 1.3 Multiple pass heat exchangers: (a),(b) one shell pass and two tube passes; (c) two shell passes four tube passes.

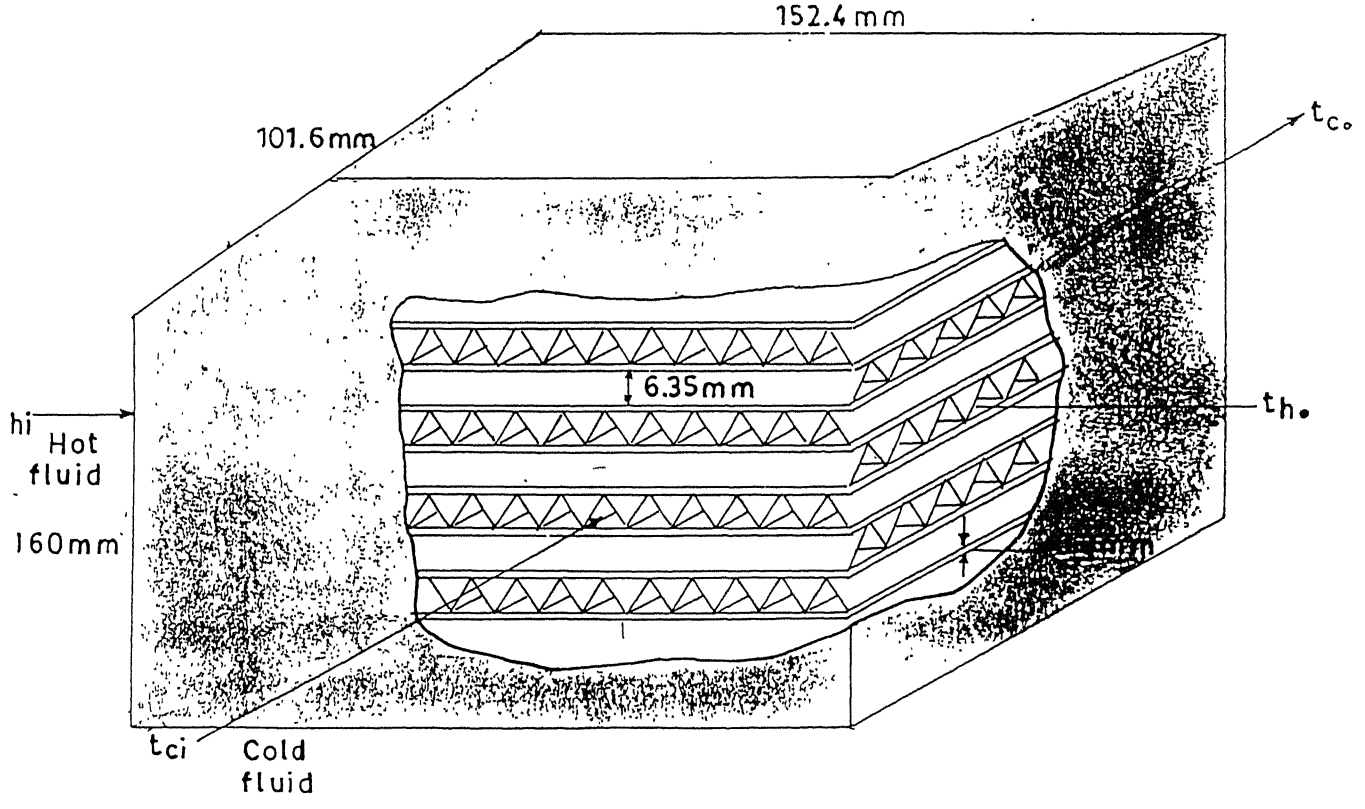

Figure. 1.4 Compact cross flow heat exchanger.

transfer rate will be considerably less than the friction-power reduction. The loss of heat transfer rate is then made up by increasing the surface area (lengthening the tubes), which in turn also increases the friction power expenditure, but only in the same proportion as the heat transfer surface area is increased.

In gas-flow heat exchangers the friction-power limitations generally force the designer to arrange for moderately low velocities. Low velocities, together with the low thermal conductivities of gases (low relative to most liquids), result in low heat transfer rates per unit of surface area. Thus large surface areas are typical of gas-flow heat exchangers. Gas-to gas heat exchangers may require up to 10 times the surface area of condensers or evaporators or liquid-to-liquid heat exchangers of comparable total heat transfer rates and pumping powers. For example, a regenerator for a gas turbine plant requires several times as much heat transfer surface as the combined boiler and condenser in a steam power plant of comparable power capacity. These considerations have led to the development of new heat transfer surfaces having high surface area density for gas flow applications. Such surfaces are termed as compact heat transfer surfaces.

Figure 1.5 shows some typical examples of compact heat exchanger surfaces. The circular tube bundle arrangement shown in Figure 1.5(a) has long been used for both high and low-density fluids, but the only way in which surface area density can be substantially increased is to decrease the diameter of the tubes. Fabrication difficulties and cost restrict the minimum diameter to 0.006 m. An effective way to increase the surface area density is to make use of secondary surfaces, or fins, on one or both fluid sides of the surface. Figure 1.5(b) illustrates a finned circular tube surface in which circular fins have been attached to the outside of circular tubes. Such an arrangement is frequently used in gas-to-liquid heat exchangers where optimum design demands a

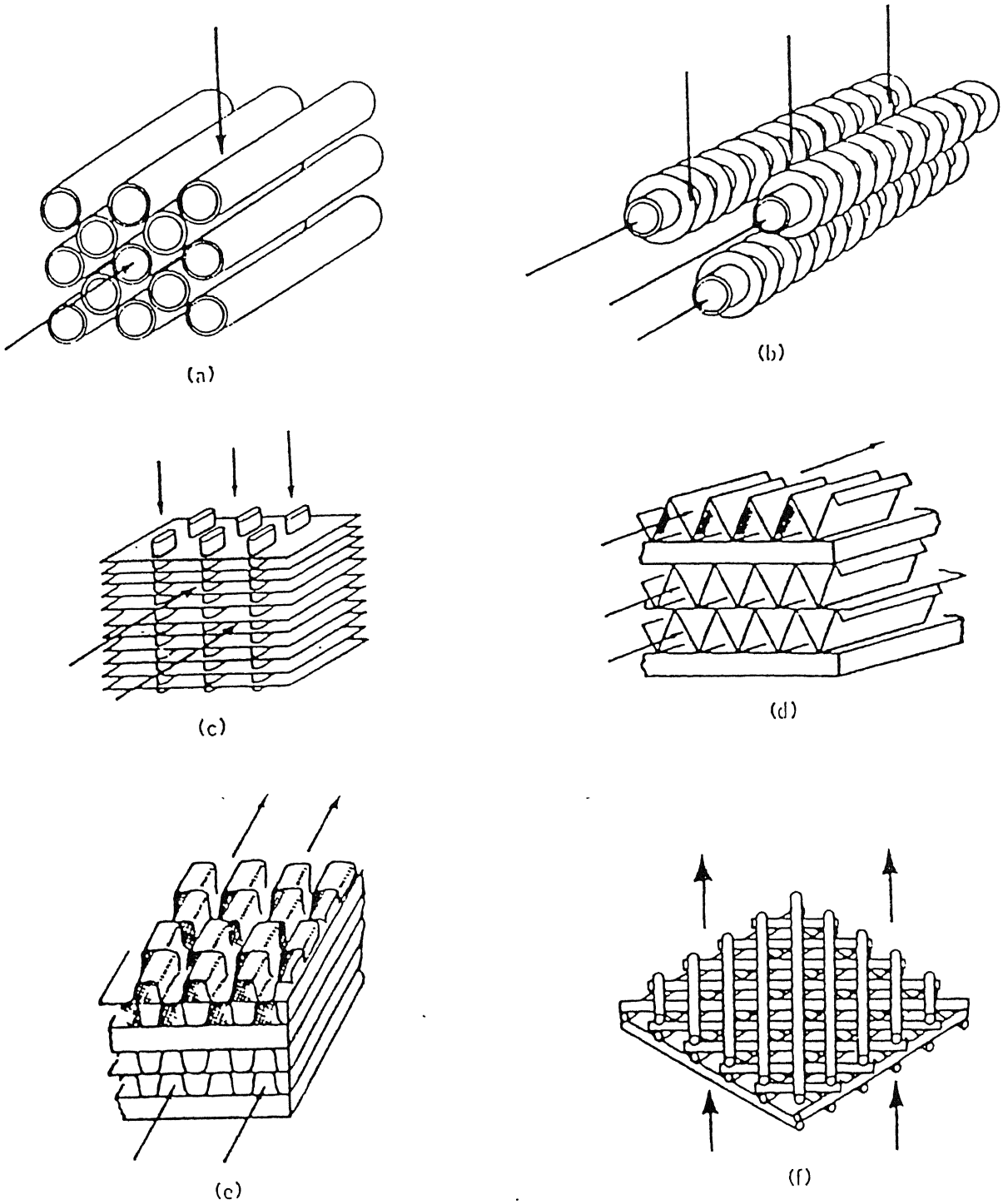

Figure 1.5 Compact heat exchanger surtaces

maximum of surface area on the gas side. Figure 1.5(c) shows another popular variation of the finned-tube arrangement. In this illustration flattened tubes are used though circular tubes are also in vogue. In compact gas-to gas heat exchangers, a large area density is desirable on both fluid sides and Figure 1.5(d) shows one way of accomplishing this by using the plate-fin arrangement. The heat exchanger is built up as a sandwich of flat plates bonded to interconnecting fins. The two fluids are carried between alternate pairs of plates and can be arranged in either counterflow or crossflow. Figure 1.5(e) illustrates another variation in which the fins are interrupted rather than continuous. In the periodic flow type heat exchanger, energy is transferred by convection and stored in a matrix, from which it is later given up to the other fluid. Figure 1.5(f) illustrates one such compact matrix, which could be built up of stacks of solid rods or stacks of wire screens.

1.4 Principle of Enhancement in Heat Exchangers

In plate-fin and fin-tube heat exchangers shown in Figure 1.6, the heat transfer rate can be enhanced by manipulating the surface geometry of the plates by employing a suitable enhancement technique. The principle behind this technique is as follows. The basic equation for the heat transfer rate in a two fluid heat exchanger (Figure 1.7) is given by

$$q = U . A . \Delta T_m \qquad (1.1)$$

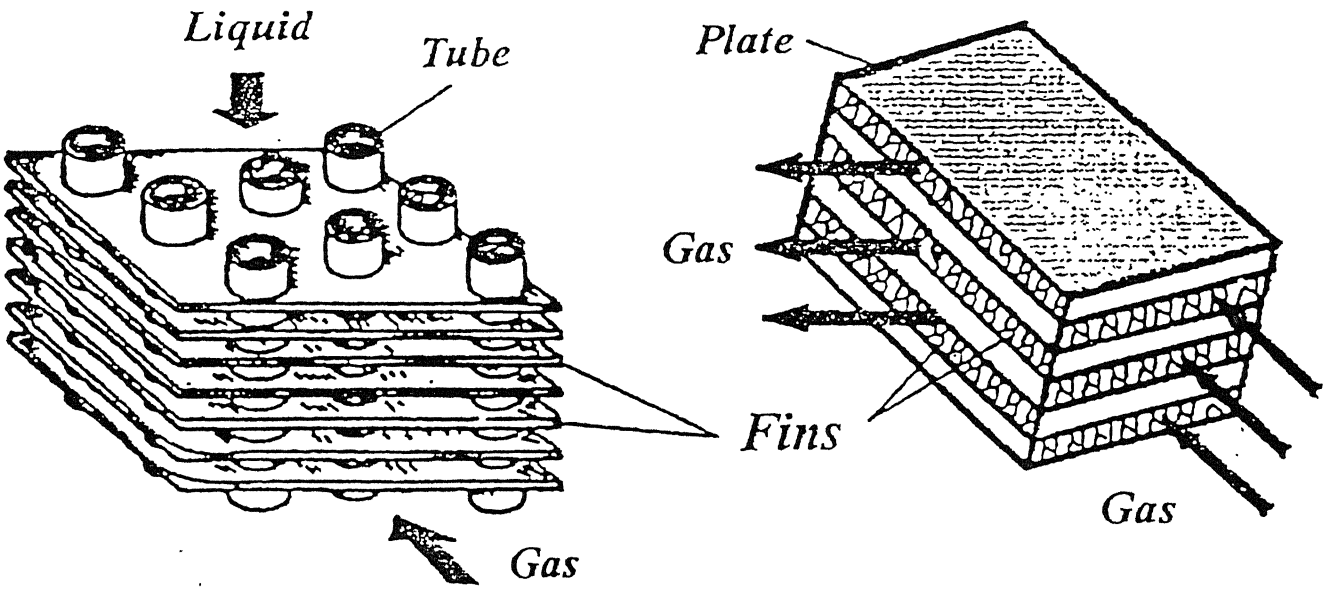

Figure 1.6 Schematic of compact heat exchangers

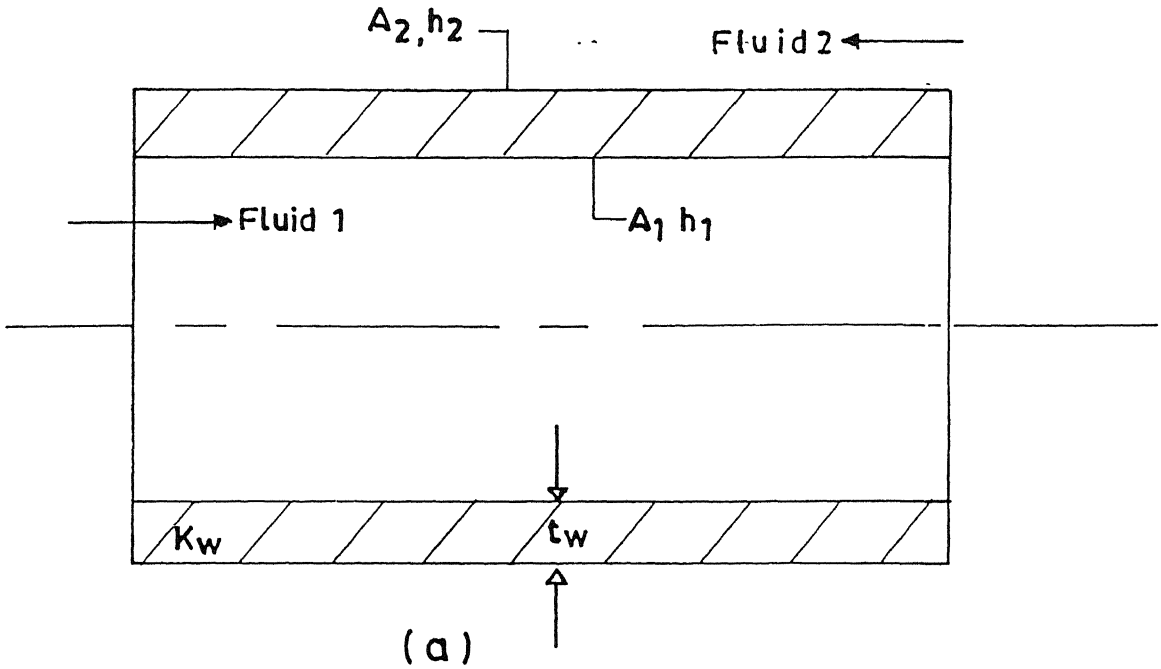

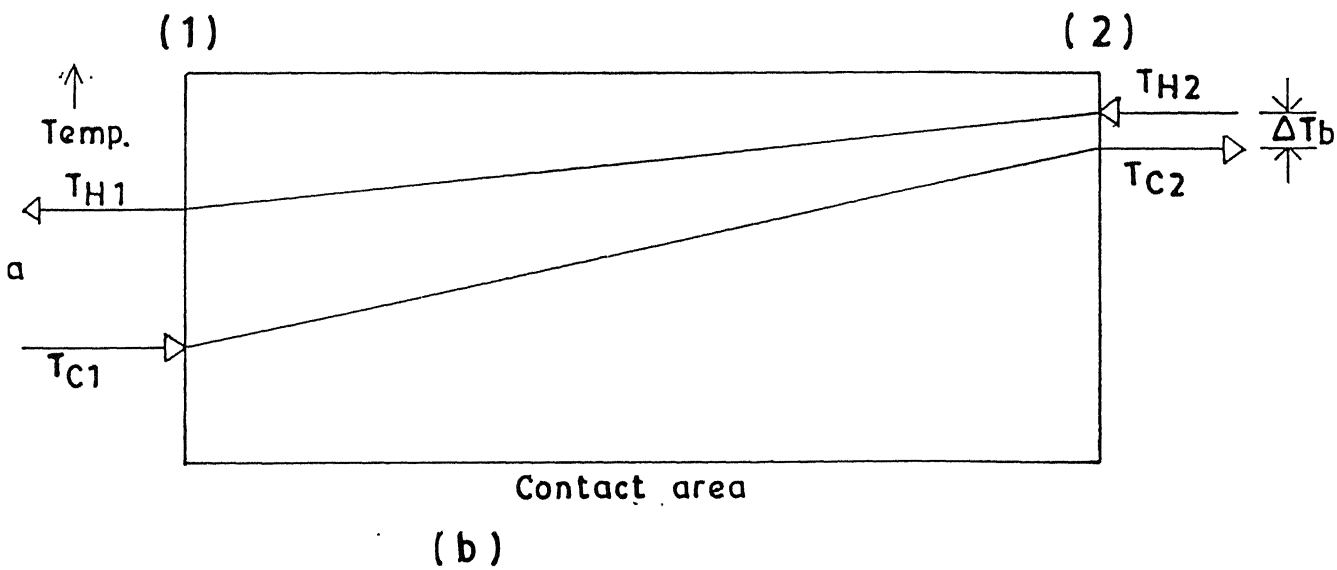

igure 1.7(a)Cross-section of a counter-flow heat exchanger
(b)Temperature vs contact area for a single-pass counter flow heat exchanger

Where q is the rate of heat transfer; U is the overall heat transfer coefficient based on area A, which is either of the areas A_1 or A_2 , the tube side and shell side areas respectively as shown in Figure 1.7(b) ; and ΔT_m is the logarithmic mean temperature difference defined as

$$\Delta T_m = \frac{(\Delta T_b - \Delta T_a)}{\ln\left(\frac{\Delta T_b}{\Delta T_a}\right)} \qquad (1.2)$$

where $\Delta T_a = (T_{H1} - T_{C1})$; and $\Delta T_b = (T_{H2} - T_{C2})$ being the temperature differences between the hot and cold fluids at sections (1) and (2) respectively as shown in Figure 1.7 (b). The overall thermal resistance is given by

$$\frac{1}{UA} = \frac{1}{h_1 A_1} + \frac{1}{h_2 A_2} + \frac{t_w}{k_w A_w} \qquad (1.3)$$

where A_1 and A_2 are the tube side and shell side heat transfer areas respectively; h_1 and h_2 are the corresponding convective heat transfer coefficients; t_w is the wall thickness; k_w is the thermal conductivity of the wall material and A_w is the average of the inner and outer areas of the tube.

When the surfaces are enhanced the thermal resistance of the enhanced system is given by

$$\frac{1}{UA} = \frac{1}{(\varepsilon_1 h_2 A_2)} + \frac{1}{(\varepsilon_2 h_2 A_2)} + \frac{1}{(k_w A_w)} \qquad (1.4)$$

The values of both ε_1 and ε_2 are higher than 1 leading to a reduction in the overall thermal resistance. The size of the heat exchanger remains the same as before, because the values of A_1 and A_2 are not altered.

Thus the heat transfer rate increases while the space occupied by the heat exchanger remains the same. Alternatively, for a desired heat transfer rate, the volume of the heat exchanger can be reduced. Therefore this technique is ideally suited for the design of compact heat exchangers where an optimal use of space is very important. A large number of methods for increasing the gas side heat transfer have been described by Kays and London (1984) These methods deal with structuring the flow and temperature fields by means of geometrical modifications of the gas side heat transfer surface, using roughness elements, turbulators or secondary fins. The offset strip-fin and the louvered fin (Figure 1.8(a)) have been widely used for this purpose (Fiebig et al (1995)). The basic mechanism involved in these devices is the periodic interruption of the boundary layer by separation, wake recovery and the generation of thin developing boundary layers with high Nusselt numbers (Figure 1.8(b)).

A somewhat different method of reducing the thermal resistance is by inducing longitudinal streamwise vortices in the flow field. The longitudinal vortices can be generated by mounting delta wing or delta winglet type vortex generators on the flat surfaces of the plates as shown in Figure 1.9. These vortices develop along the edge of the vortex generator due to the pressure difference between the front surface facing the flow and the back surface. These vortices are mainly longitudinal (Figure 1.10), so-called because their axes of rotation are aligned to the direction of the main flow. These streamwise vortices interact with an otherwise two-dimensional boundary layer and produce a three dimensional swirling flow that mixes near-wall fluid with the free stream. This mechanism strongly enhances the exchange of fluid between the wall and the core region of the flow field , which causes high heat transfer augmentation. The use of longitudinal vortices for boundary layer control is well known (Pearcy, 1961] and vortex generators are

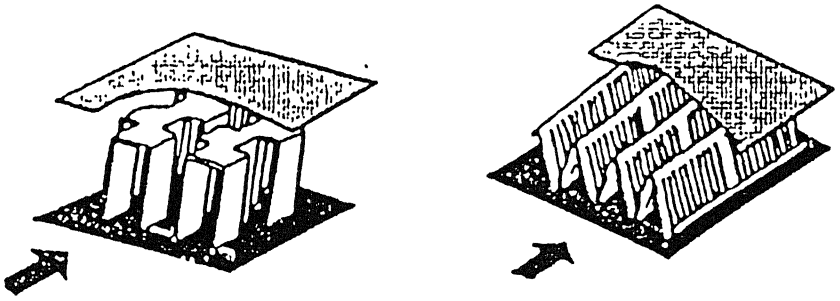

(a)

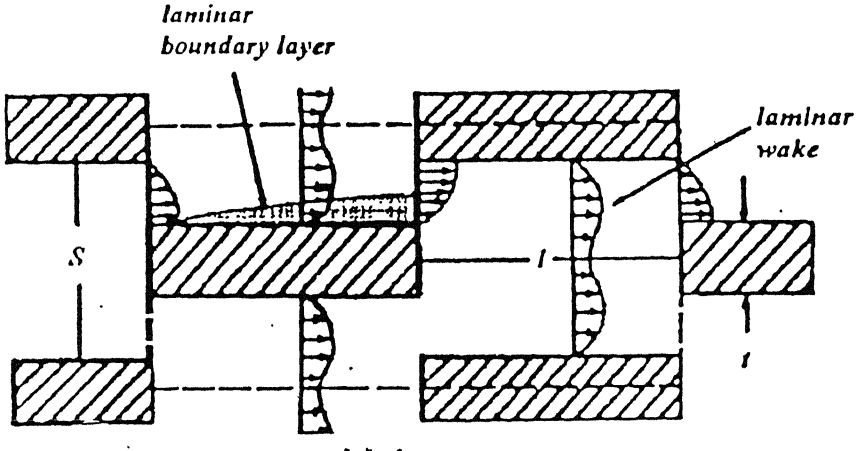

(b)

Figure 1.8(a) High performance fins (b) Schematic of flow structure for offset strip fin and louvered fin arrays. The enhancement mechanism is periodic flow seperation, wake recovery and developing boundary layer.

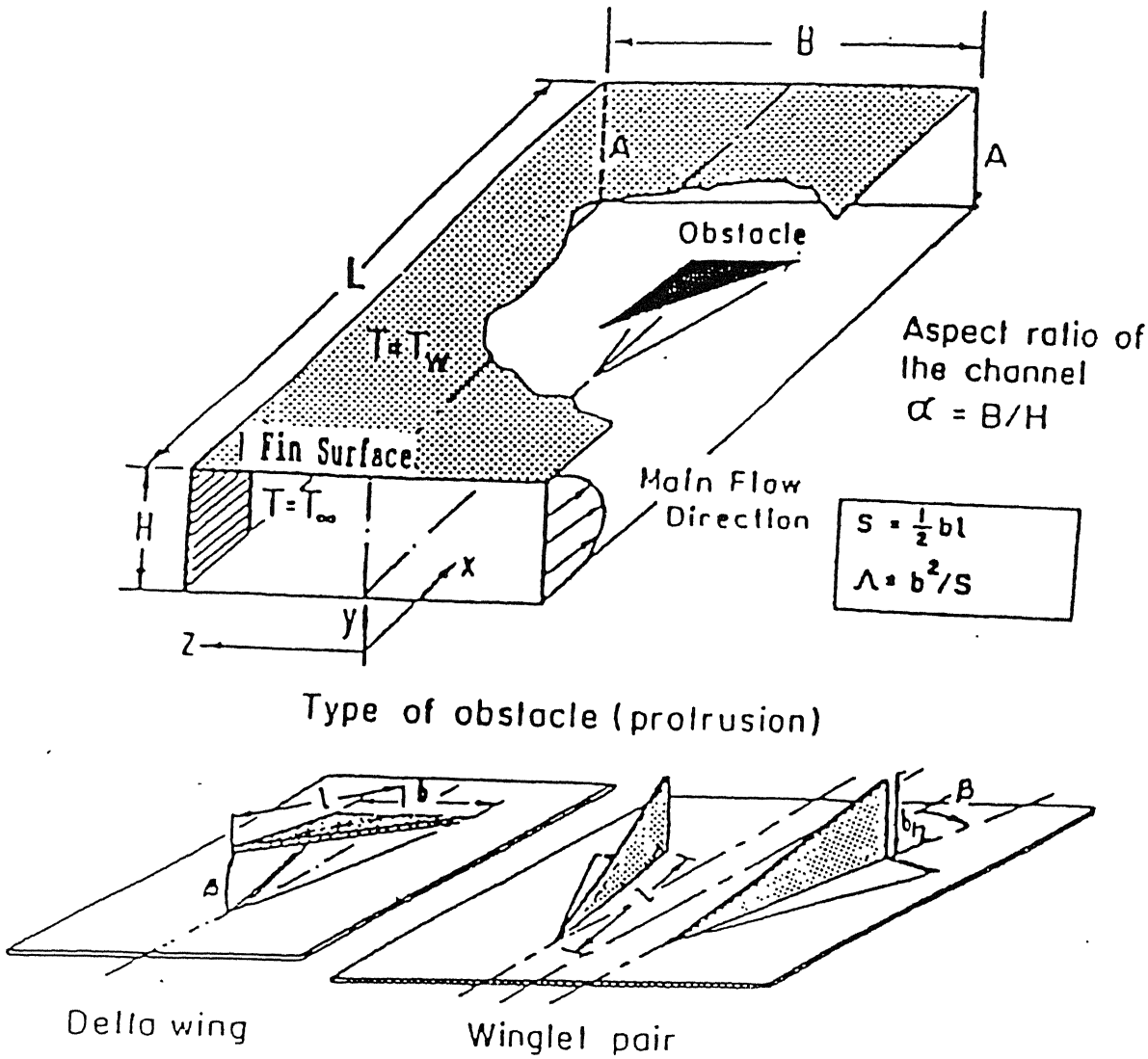

Figure 1.9 Longitudinal vortex generators

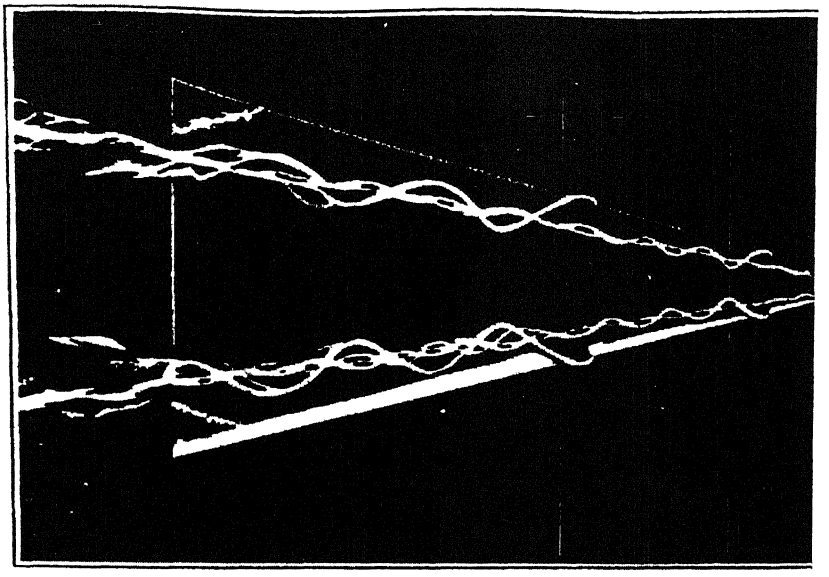

(a)

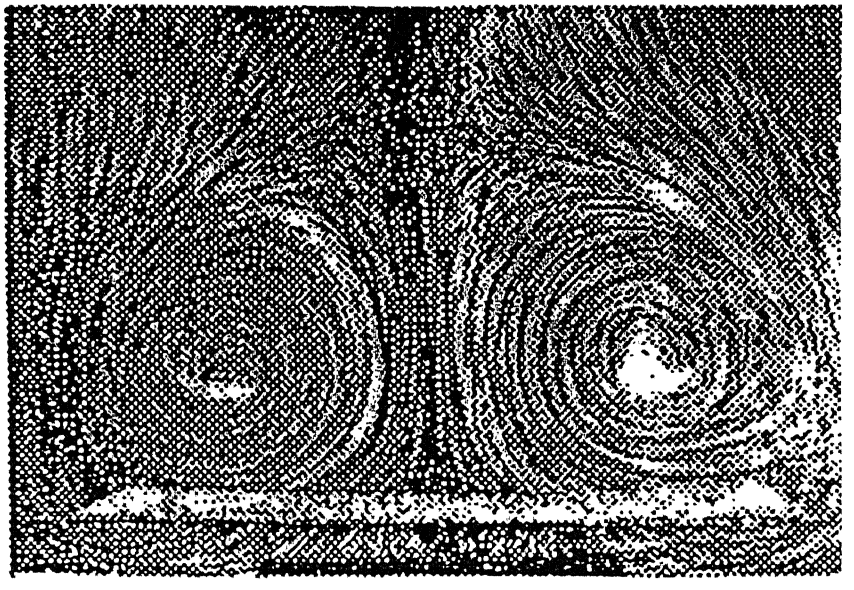

(b)

Fig. I.10 Longitudinal vortices above a delta wing with 30° vertex angle at 20° angle of attack and Reynolds number 20000. (a) Lines of coloured fluid in water show the longitudinal vortices. (b) Tiny air bubbles in water show the cross flow of the vortex pair; from van Dyke (1988)

commonly used in commercial aeroplanes for this purpose. The vortex generator obstructs the flow and hence adds to the pumping cost. However the additional pressure loss due to the use of delta wings or winglets is very modest, because the form drag for these slender bodies is low. Further, this increase in pumping power will be insignificant when the complete ducting of the equipment is considered. A large number of investigations, both experimental as well as computational, have been carried out to understand the basic mechanism of heat transfer enhancement by longitudinal vortices, and also to predict quantitatively the extent of heat transfer augmentation which can be achieved by using different types of vortex generators viz., delta wings, delta winglet pairs, and rectangular wings (Fiebig et al. 1995, Biswas et al 1995). The present work is a study of an innovative secondary fin configuration proposed for use in plate-fin heat exchangers.

1.5 Motivation for the present work

In a fin-tube heat exchanger (Figure 1.6), one of the fluids flows through the tube while the other fluid (shell side fluid) flows through the space between the adjacent plates. For such an arrangement, an enhancement of the transport coefficients on the plate surface is easily accomplished by punching vortex generators in the form of delta wings, or delta winglets. The manufacturing process involves making a triangular cut on the plate surface, and then pushing out the slender body along the edges of the cut. As a result, a triangular stamping is formed on the plate surface just beneath the vortex generator, and fluid can flow from one side of the plate to the opposite side across this stamping. Since the same fluid flows on both sides of the plates in a fin-

tube heat exchanger, the presence of the stamping poses no problem. On the other hand, in the case of a plate-fin heat exchanger, (Figure 1.6) the hot and cold fluids flow on the opposite sides of the plates. Physical mixing of the two is not permissible. Therefore, punching out of delta wings or winglets on the plates of a plate-fin heat exchanger is ruled out. Hence, the only option available is to attach these vortex generators to the plate surface using a welding process. Though the stamping is eliminated, the additional cost and complexity involved in this method of welding the vortex generators to the plate surface are significant.

The present work proposes a way out of this difficulty. The solution suggested is to punch out the vortex generators on the plane surfaces of a triangular insert which is placed in the gap between the adjacent plates. The stamped winglets may be termed as secondary fins. Thus the final configuration of the fin geometry is the triangular fin with punched out secondary fins on the slant surfaces. Figure 1.11 shows the various fin geometries currently used to enhance the heat transfer rate in plate-fin heat exchanger. The proposed device is an innovative combination of the plain triangular fin (Figure 1.11(c)) and the perforated fin (Figure 1.11(f)) to form a triangular fin which is provided with the delta winglet or delta wing type vortex generators on its slant surface. With such an arrangement there is no scope for the mixing of hot and cold fluids Figure 1.12 shows a fin-design currently being used by Britannia Heat Transfer Limited, Birmingham, U.K. In the present study, the enhancement potential of such a combination is evaluated by computing the numerical solution to the governing equations for mass, momentum, and energy.

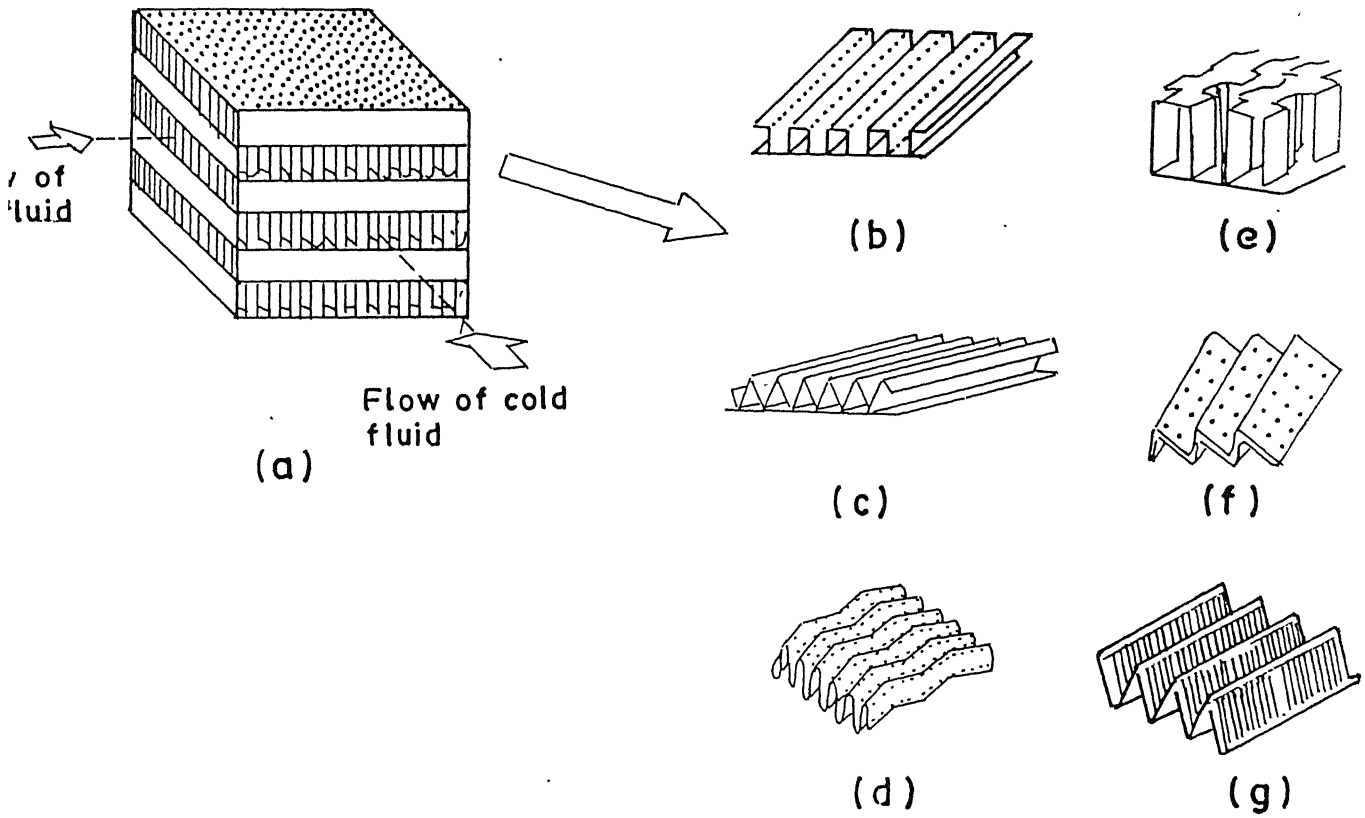

ure 1.11 Plate-fin heat exchanger and its surface geometries:
(b) Plain rectangular fins (c) Plain triangular fins
(d) Wavy fins (e) Offset strip fins (f) Perforated fins
(g) Louvered fins; after Webb (1987)

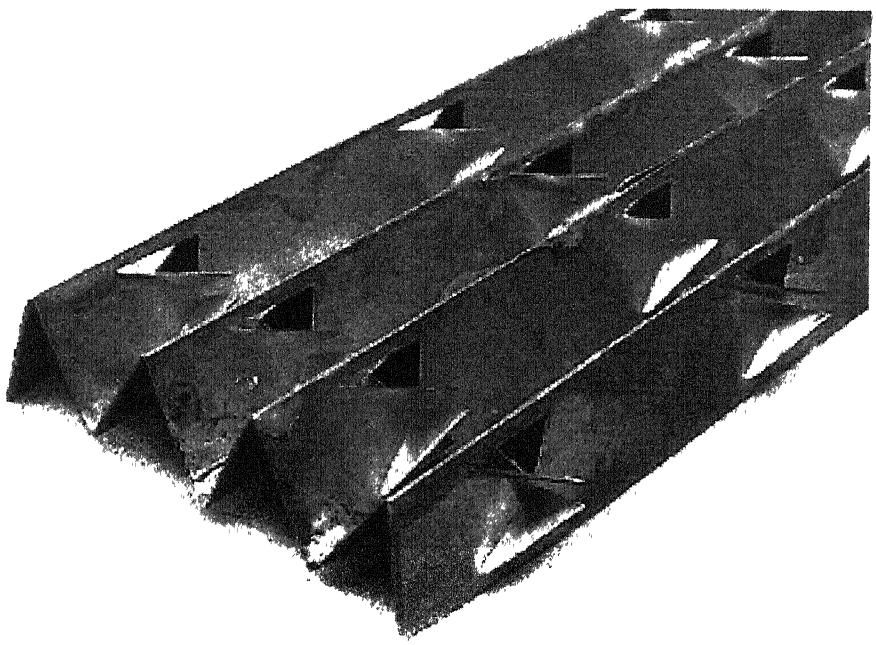

Fig 1.12 Secondary fin with delta winglet vortex generators for plate-fin heat exchanger

1.6 Layout of the Thesis

Chapter-2 of the thesis provides a review of literature of the field of *Heat Transfer Enhancement* with an emphasis on the application of vortex generators. A brief survey of the various numerical techniques developed for solving Navier-Stokes equations is also presented. The mathematical formulation of the problem is explained in Chapter-3. All the details regarding the geometry, the governing equations, the boundary conditions, the method adopted for the numerical implementation of the boundary conditions and the algorithm used to obtain the numerical solution are given here. Chapter-4 presents the results of the computations for the delta winglet. The performance of delta winglet in enhancing the heat transfer as well as the associated increase in pumping power for , different Reynolds numbers, angles of attack and different thermal boundary conditions are presented. Chapter-5 provides the results for the case of delta wing.. Chapter-6 contains the conclusions of the present work besides scope for future work in the same area.

Chapter 2

Review of Literature

2.1 Introduction

A substantial amount of research in the area of heat transfer augmentation is available both in the form of experimental results and as predictions of numerical investigations. In this chapter, a summary of these findings is presented in order to put the present problem in perspective. The literature is reviewed from three different viewpoints. In the first section, an overview of the field of heat transfer enhancement is presented. The next section focuses on those investigations which have evaluated the utility of vortex generators (in the form of delta wings, delta winglet pairs and rectangular wings) in enhancing the heat transfer in heat exchangers. In the third section, the numerical techniques developed for the purpose of computing flow fields by solving the full Navier-Stokes equations are reviewed.

2.2 Augmentation of Heat Transfer

The subject of heat transfer enhancement is of great importance in the design of compact heat exchangers where the emphasis is on

minimising the space occupied by the equipment for a desired rate of heat transfer. A large number of enhancement techniques have been developed in the last few decades and these are applicable to diverse areas such as, (1) single phase flows, (2) two phase flows and convective mass transfer. A number of recent review articles and handbooks (Bergles, 1978, 1983, 1985) deal with the augmentation of heat transfer for different applications. A detailed account of the theory of heat transfer enhancement is provided by R. L. Webb (1987) The growing importance of this field is underlined by the spurt in the number of research publications and patents pertaining to heat transfer enhancement. It has emerged as an inter-disciplinary area which involves the principles of heat transfer as well as those of manufacturing technology.

2.2.1 Classification of Heat Transfer Augmentation Techniques

A detailed account of the various techniques of heat transfer augmentation is available in the Handbook of Heat Transfer Applications by Bergles (1985). The following section has been largely influenced by the above mentioned documentation.

Augmentation techniques can be classified either as *passive* methods, which require no direct application of external power, or as *active* schemes, which require external power. The effectiveness of both types depends strongly on the mode of heat transfer, which might range from single-phase free convection to dispersed-flow film boiling. Some of the passive techniques are:

(a) *Treated surfaces* which involve fine-scale alternation of the surface finish or coating (continuous or discontinuous) They are used for

boiling and condensing modes of heat transfer; the roughness height is below that which affects single-phase heat transfer.

(b) *Rough Surfaces* are produced in many configurations ranging from random sandgrain-type roughness to discrete protruberances (Figure 2.1). The configuration is generally chosen to promote turbulence rather than to increase the heat transfer surface area. The application of rough surfaces is directed primarily toward single-phase flow.

(c) *Extended surfaces* are routinely employed in many heat exchangers (Figure 2.2). The development of new types of extended surfaces, such as integral inner-fin tubing, and the improvement of heat transfer coefficients on extended surfaces by shaping or interrupting the surfaces are of particular interest.

(d) *Displaced enhancement devices* (Figure 2.3) are inserted into the flow channel so as to alter flow characteristics and indirectly improve energy transport at the heated surface. They are used with forced flow.

(e) *Swirl flow devices* (Figure 2.4) include a number of geometrical arrangements or tube inserts for forced flow which create rotating and/or secondary flow: coiled tubes, inlet vortex generators, twisted tape inserts, and axial-core inserts with a screw type winding fall under this category.

(f) *Surface tension devices* (Figure 2.5) consist of wicking or grooved surfaces to direct the flow of liquid in boiling or condensing.

(g) *Additives for liquids* include solid particles and gas bubbles in single-phase flows and liquid trace additives for boiling systems.

(h) *Additives for gases* are liquid droplets or solid particles, either dilute phase (gas-solid suspensions) or dense phase (fluidised beds)

The active techniques of enhancement are:

(a) *Mechanical aids* which stir the fluid by mechanical means or by rotating the surface. 'Surface scraping' widely used for viscous liquids in the chemical process industry, can also be applied to duct flow of

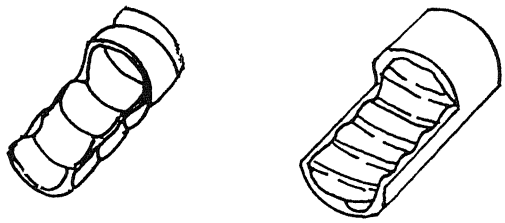

(a)

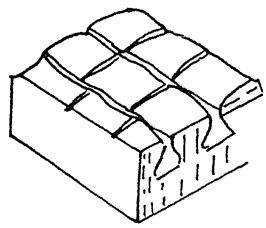

(b)

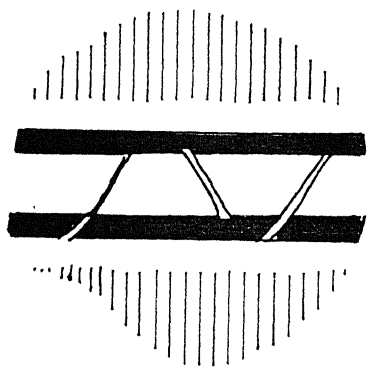

(c)

Figure 2.1 Roughness elements

(a) Tubeside roughness for singlephase or two phase flow

(b) Rough surface for nucleate boiling

(c) Wire coil insert

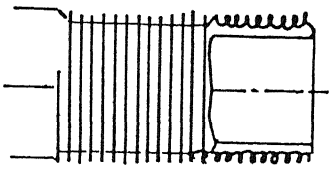

(a)

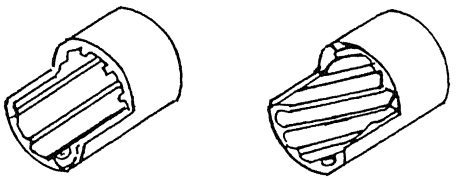

(b)

(c)

(d)

Fig. 2.2 (a) Integral fins on outer tube surface. (b) Intcmally finned tubes (axial and helical fins) (c) Cross sections of multiply internally finned tubes. (d) Tube with aluminum star insert.

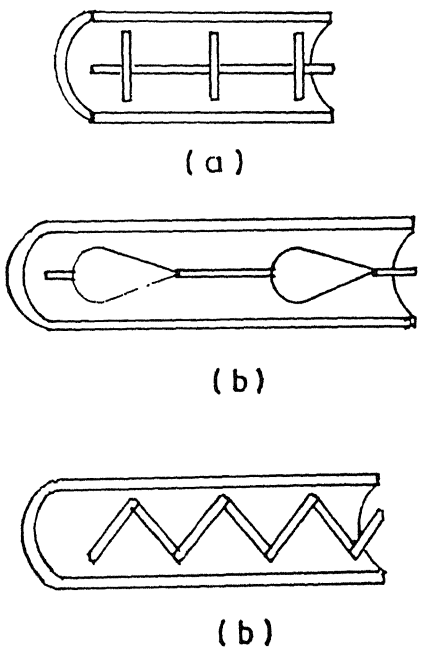

Figure.2.3 Displaced enhancement devices (a) Spaced disk devices (b) Spaced streamline shaped insert devices (c) Displaced wire coil insert (From Webb[1987])

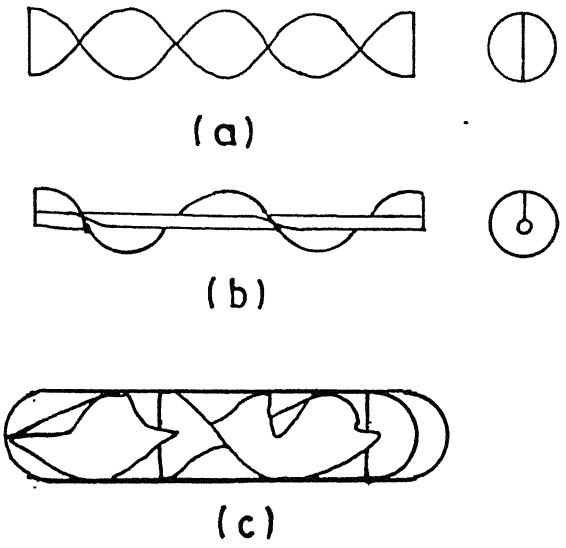

Figure 2.4 Swirl flow inserts (a) Twisted tape insert. (b) Helical vane insert; (c) Static mixer.

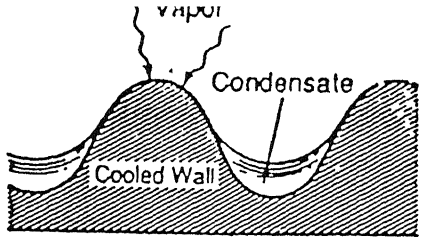

(a)

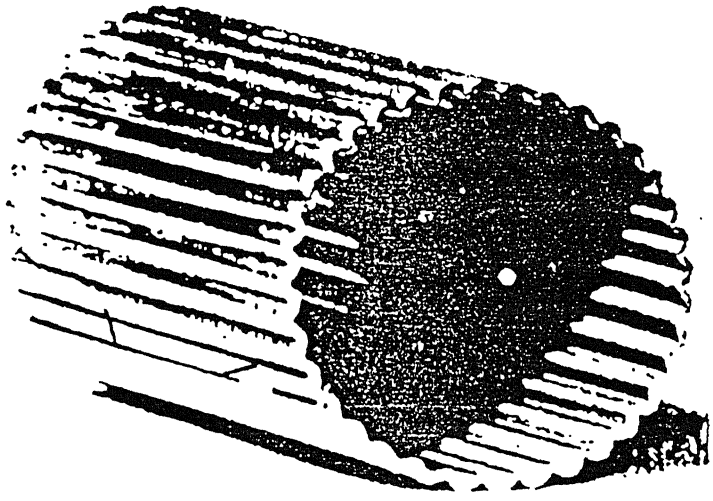

(b)

Figure 2.5 Surface tension devices

(a) Illustration of surface tension drainage from the flutes into the drainage channels

(b) Fluted tube used for condensation

gases. Equipment with rotating heat exchanger ducts is found in commercial practice.

(b) *Surface vibration* at either low or high frequency has been used primarily to improve single-phase heat transfer.

(c) *Fluid vibration* is the most practical type of vibration enhancement, given the mass of most heat exchangers. The vibrations range from pulsations of about 1 Hz to ultrasound. Single-phase fluids are of primary concern.

(d) *Electrostatic fields (dc or ac)* are applied in many different ways to dielectric fluids. Generally speaking, electrostatic fields can be directed to cause greater bulk mixing of fluid in the vicinity of the heat transfer surface. An electrical field and a magnetic field may be combined to provide a forced convection or electromagnetic pumping.

(e) *Suction* involves either vapour removal through a porous heated surface in nucleate or film boiling, or fluid withdrawal through a porous heated surface in single-phase flow.

Two or more of the above techniques may be utilised simultaneously to produce an enhancement larger than that produced by either technique. This simultaneous use is termed compound augmentation. Some examples for single-phase flows are

(1) Rough tube with twisted-tape insert;

(2) Finned tubes in fluidised beds; and

(3) Rough cylinder with acoustic vibrations

One important consideration while studying enhanced heat transfer is to assess the effect of an inherent condition on heat transfer. Examples of such inherent conditions are roughness produced by standard manufacturing, surface vibration resulting from rotating machinery or flow oscillations, and electric fields present in electrical equipment.

2.2.2 Prospects for the future

As energy and material shortages become more important factors in the overall cost of thermal systems, it is expected that heat transfer augmentation techniques will find increasing utility. Therefore, it is appropriate to view augmentation techniques as 'second-generation' heat transfer technology. Such new technology normally requires several phases of development for successful commercialisation. The steps involved are as follows.

1. Basic performance data for heat transfer and pressure drop, if applicable, must be obtained. General correlations should be developed to predict heat transfer and pressure drop as a function of the geometrical characteristics.
2. Criteria for performance evaluation must be developed to facilitate selection of the optimum surface geometry for the various techniques and particular applications.
3. A suitable manufacturing technology at a viable cost must be available for the desired surface geometry and material.
4. Pilot plant tests of the proposed design are required to permit a complete economic evaluation and to establish the long-term fouling and corrosion characteristics.

Several augmentation techniques have gone through all these steps required for commercialisation. It is reasonable to assume that, there will be a broader acceptance of enhancement techniques by the industry in the years to come.

2.3 Vortex generators

In the following sections, specific results reported by different investigators on various aspects of heat transfer enhancement using vortex generators are summarised. From aeronautics, it is well known that vortices can generate large forces. Small aeroplanes are forbidden to fly in the wake of huge ones, because the latter's strong trailing vortices might spin the small aeroplane out of control. The wings of an aircraft can be regarded as specially designed vortex generators to generate strong forces. The axial and tangential velocities generated by longitudinal vortices are often of the same magnitude as the primary velocity, Delery *et al.* (1984). Vortices can also have a strong influence on heat transfer and can be used in heat exchangers for augmentation of heat transfer rates. This enhancement is caused by the mixing, due to the vortices, of the mid-stream and boundary layer fluids, which causes steeper temperature gradients to develop near the wall.

Detailed investigations of the enhancement potential of vortex generators have been carried out in the last two decades (Fiebig *et al.* (1986), Turk and Junkhan (1986), Eibeck and Eaton (1986) , Fiebig *et al* (1989), Amon (1989), Dong (1989), Zhang (1989), Tiggelbeck (1992), Yanagihara and Torri (1990), Fiebig *et al.* (1990), Fiebig *et al* (1991), Sanchez (1989), Valencia (1992), Fiebig *et al.* (1993b), Biswas *et al.* (1994) and Valencia (1996). The idea of using vortex generators in compact heat exchangers has already been implemented by the industry. Figure 2.6 shows an enhanced heat transfer surface having delta winglets produced by Britannia Heat Transfer Limited, Birmingham, U K.

Transverse vortex generators, such as ribs and corrugations in channels generate vortices whose axes are mainly transverse to the

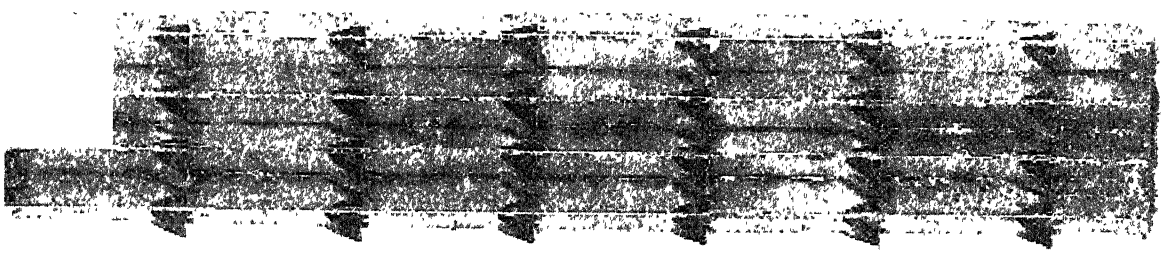

g 2.6 Enhanced heat transfer surface having delta winglet vortex generators

primary flow direction (Figure 2.7), whereas, longitudinal vortex generators, such as delta wings, rectangular wings, and delta winglets generate vortices having axes mainly along the primary flow direction (Figure 2.8). So far, all experimental and theoretical investigations point out that longitudinal vortex generators are preferable to transverse vortex generators for compact heat exchangers when both heat transfer enhancement and flow loss are taken into account. The enhancement mechanism for transverse vortices requires unsteady flow and implies reversed flow regions which increase flow resistance. On the other hand the enhancement mechanism for longitudinal vortices consists of strong swirling flow around an axis essentially aligned with the main flow direction which causes a strong exchange of core and wall fluid. Intuitively it seems clear, that for the same exchange rate of wall and core fluid, less energy is needed to turn the flow around an axis aligned with the main flow direction than for the generation of swirl around an axis perpendicular to the main flow direction which requires reversed flow. It has been shown by Grosse-Gorgemann *et al.* (1993b) for periodically ribbed channels that for steady flow conditions transverse vortices do not cause any global enhancement of heat transfer, but increased friction factors. Only when unsteadiness sets in does global heat transfer enhancement occur. The periodic exchange of core and wall fluid caused by the (time and space) periodic Karmann vortex streets is the heat transfer enhancement mechanism. It also gives rise to enhanced pressure losses, but to a lesser extent than turbulent flow (Grosse-Gorgemann (1993a)).

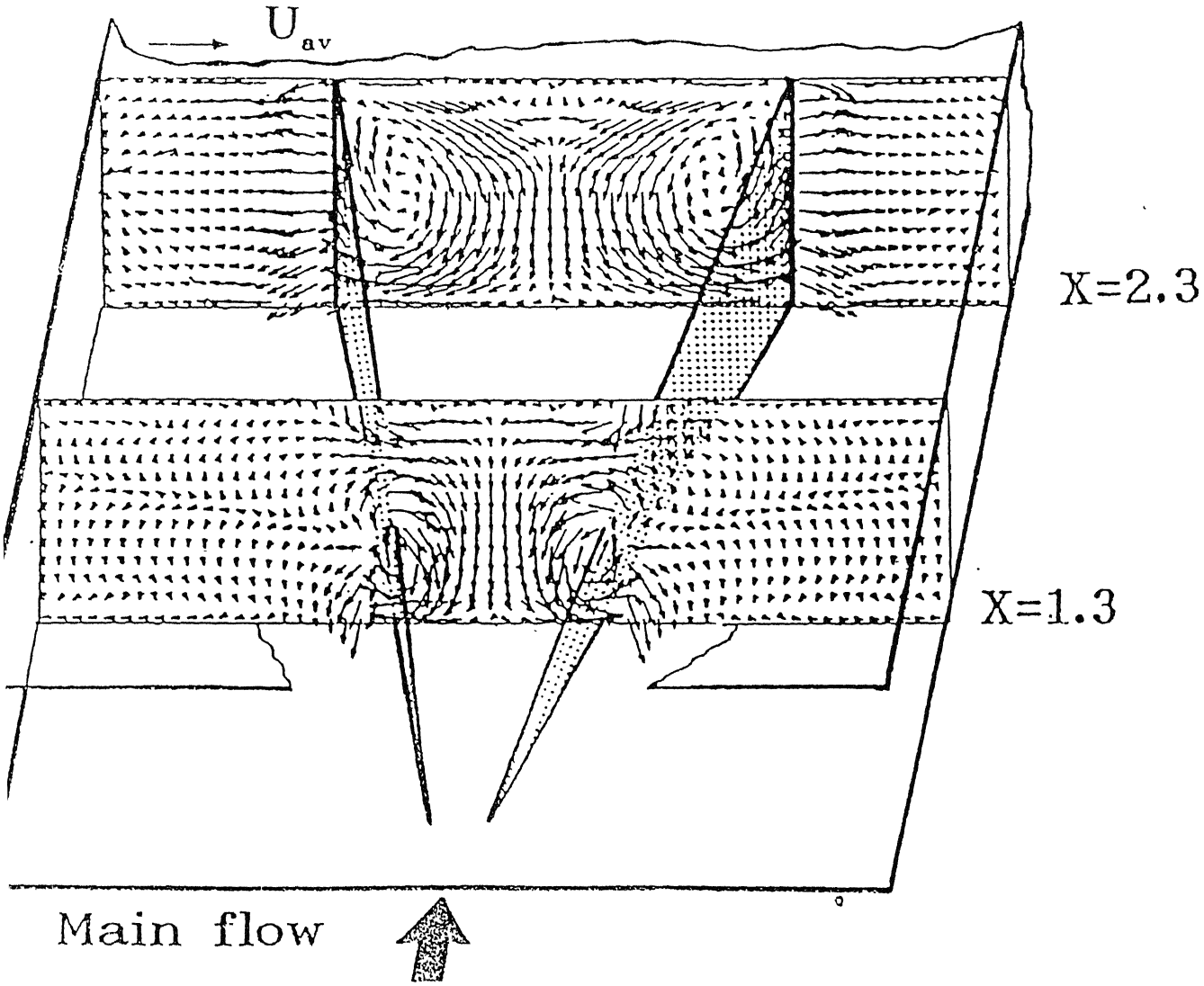

Figure 2.8 Longitudinal vortices generated by a delta winglet pair.

2.3.1 Longitudinal vortex generators

Longitudinal vortices have been observed by researchers in many different complex flow configurations. The interaction of these vortices with the boundary layer and the resultant effect on the heat transfer rate has been investigated in detail by several researchers. Taylor-Gortler vortices in boundary layers on concave curved surfaces, horseshoe vortices (Figure 2.9) formed by an obstruction protruding from a surface and wingtip vortices impinging on a downstream surface are all examples of such vortices. The embedded vortex is capable of strongly perturbing the boundary layer and influencing the heat transfer rates. Moreover, these longitudinal vortices usually maintain their coherence over a long streamwise distance. Consequently the heat transfer rates behind a vortex generator are very persistent. Pioneering work in this area was done by Eibeck and Eaton (1987), Westphal and Mehta (1987). In their experiments on longitudinal vortices embedded in a turbulent boundary layer Eibeck and Eaton have observed as much as 24 percent increase in local Stanton number.

The formation of streamwise longitudinal vortices behind a slender aerodynamic object has generated considerable research interest for many years. Both theoretical and experimental investigations on flow past a delta wing have been reported in the literature by a number of researchers. Among them Winter (1956), Fink, (1956), Marsden *et al.* (1958) and Lawford (1964) are noteworthy early works.. The physics of vortex formation has been explained by Brown *et al.* (1954). More recently experimental investigations due to Edwards and Alker (1974), Russels *et al.* (1982), Fiebig *et al* (1986), (Fiebig *et al* (1991) and Tiggelbeck *et al.* (1992) can be referred to in connection with augmentation of heat transfer by means of longitudinal vortices. Fiebig

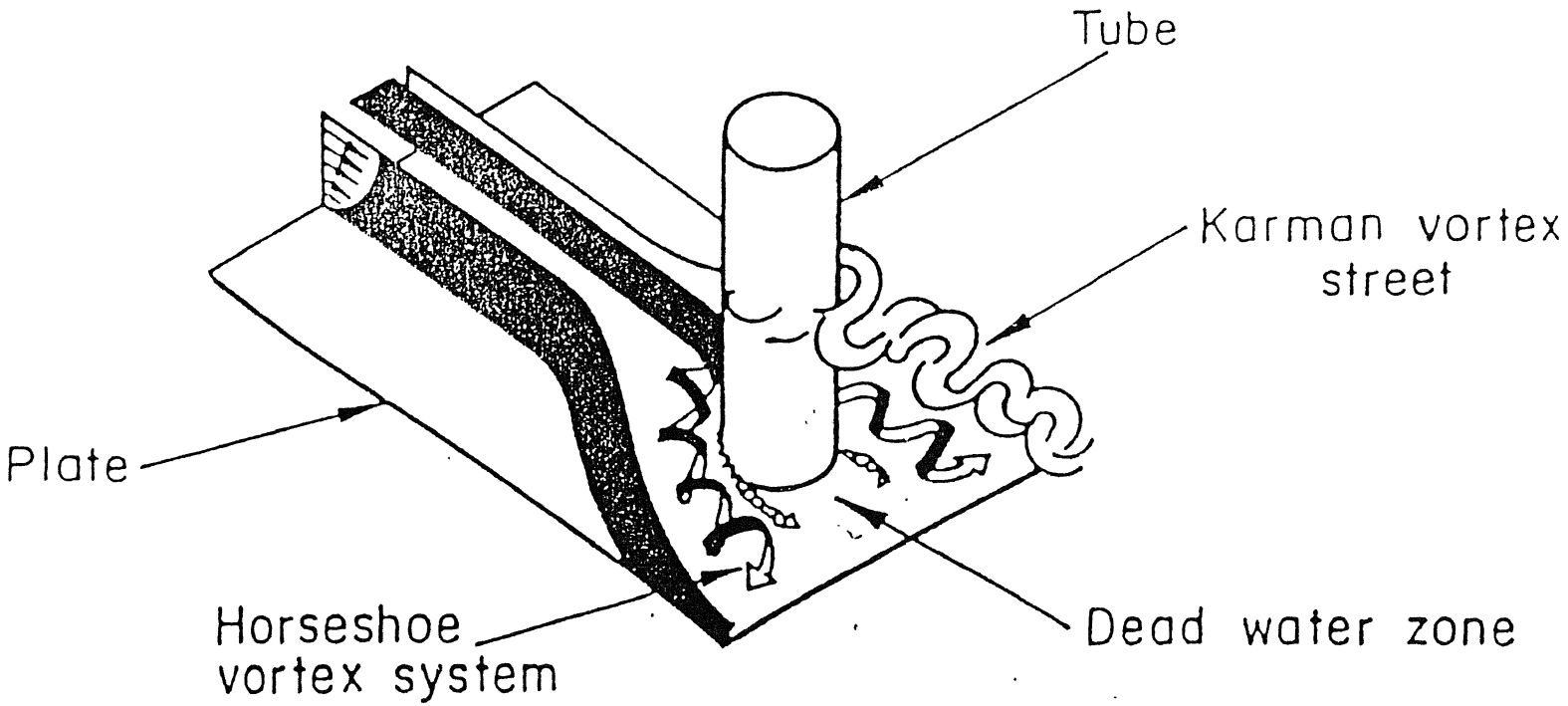

Figure 2.9 Flow around a tube on a plate

and his co-workers (Fiebig *et al.*, 1986) experimentally observed enhancement in heat transfer on punching vortex generators on the primary heat transfer surface. Subsequently a host of other investigations were taken up by different groups and the use of vortex generators evolved as a device for enhancement of convective heat transfer. The investigations due to Eibeck and Eaton (1987), Fiebig *et al* (1989), Biswas *et al* (1989), Fiebig *et al* (1990), Yanagihara and Torri (1990), Fiebig *et al* (1991), Biswas and Chattopadhyay (1992), Biswas *et al* (1994a), Biswas *et al* (1994b), Tiggelbeck *et al* (1992), Deb *et al* (1995) and Valencia (1996) revealed the effectiveness of using vortex generators in compact heat exchangers. Biswas and Chattopadhyay (1992) considered the influence of Reynolds number and angle of attack on skin friction and Nusselt number. In this computational study, the effect of a stamped hole underneath the wing was considered ; such a hole results when fin material is used to form the wing or winglet type vortex generators.

The experiments of Fiebig *et al.* (1991) is the first systematic study to compare the performance of different kinds of vortex generators, viz., delta wing, rectangular wing, delta winglet pair and rectangular winglet pair in the Reynolds number range of 1360 to 2270. Their findings reveal that the delta wing is the best vortex generator from the heat transfer point of view. Further, it was reported that the heat transfer coefficient increases with increase in the angle of attack till the vortex breakdown occurs. Tiggelbeck *et al.* (1992) observed the influence of multiple rows of vortex generators in an aligned arrangement within a channel on the flow structure. It was found that the flow structure in the wake of the second row is qualitatively similar to that of the first row. Using flow visualisation by a laser light sheet they pointed out that the concentrated vortex pair generated by a small aspect ratio delta wing at a large angle of attack has an elliptic shape due to the influence of the channel walls.

The experimental results of Fiebig *et al* (1986) have been simulated numerically by Biswas *et al* (1989) and the agreement was quite satisfactory. The numerical simulations of Fiebig *et al.* (1995) also showed excellent comparison with the experimental results of Tiggelbeck *et al.* (1994). Although, with regard to augmentation of heat transfer in a channel, the delta wings showed better performance (Fiebig *et al.*,1986 , 1990) it was argued that the delta winglet pair is a more appropriate choice with respect to the effective use of energy (Biswas *et al.*, 1994a). In a recent study by Biswas and Mitra (1998), the performance of the delta winglet has been compared to that of a rectangular winglet pair.

Biswas *et al.* (1994b) have compared the enhancement levels of two different arrangements of a row of winglets (Figure 2.10). The co-rotating vortex was found to be the superior one because of the more thorough mixing of the upwash and downwash vortices in this case (Figure 2.11). In contrast to this, there are alternate zones of 'common flow down' and 'common flow up' in the case of the counter rotating arrangement. It was further observed that the flow regime is usually laminar. The disturbance in the form of a vortex generator can lead to one of the three possibilities, viz. (a) the flow remains laminar; (b) the flow becomes fully turbulent, which is not desirable because of the high flow losses associated with turbulent flow; and (c) the flow becomes unsteady periodic with one or two dominating frequencies. In the last case besides the swirling effect of the longitudinal vortices there is also the effect of unsteadiness. This results in a self-sustaining oscillatory type of situation and the flow does not tend to become fully turbulent. As a result, the laminar boundary layer is found to undulate. This situation is most desirable as it leads to the maximum enhancement in heat transfer.

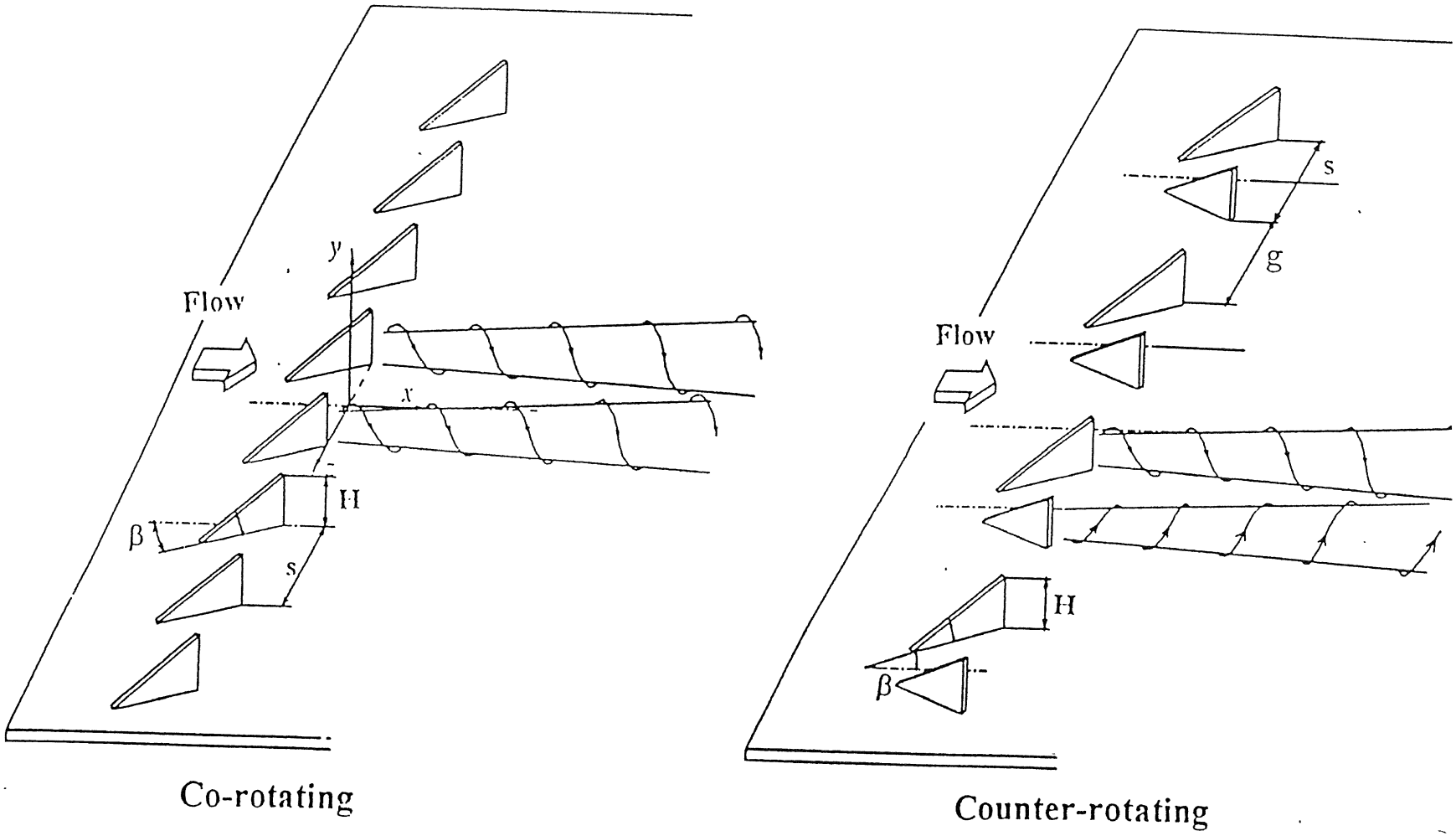

Figure 2.10 Winglets with corotating and counterrotating arrangement.

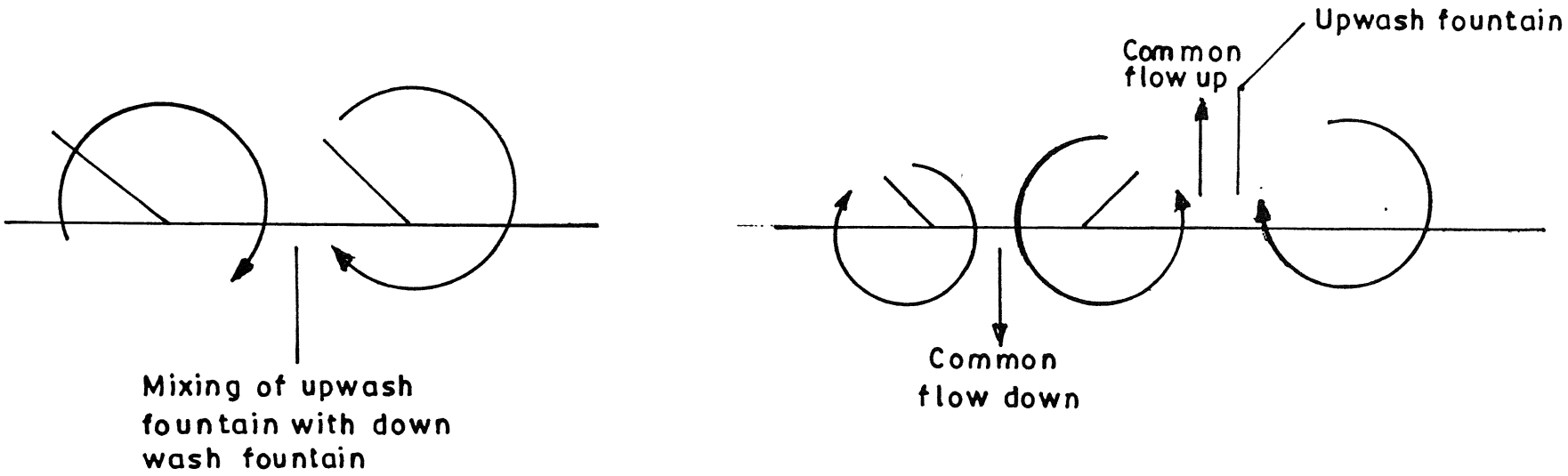

Figure 2.11 Flow structure due to delta winglets.

When the flow velocity is not very high, and the temperature difference between the body surface and the fluid is large, flow and heat transfer characteristics are strongly influenced by thermal buoyancy forces. Even without a vortex generator, buoyancy can induce longitudinal vortices and multiple plumes which can enhance heat transfer and alter the length of the entrance region in mixed convection flows in ducts (Patankar *et al.* 1978; Incropera and Schutt (1985); Incropera *et al.* (1987). Biswas *et al.* (1989) studied the mixed convection, caused by buoyancy driven secondary flows that form counter rotating longitudinal vortices and enhance heat transfer. In another study, Biswas *et al.*(1990) observed that the critical Reynolds number in a channel flow with built-in obstacle may be lower in the case of mixed convection than in the case of forced convection alone.

2.4 Internal Flows in Tubes and Ducts

For tubular heat exchangers, enhancement is desirable for the inner side, outer side or both sides of the tube. Figure 2.12 shows some doubly enhanced tubes where the enhancement is applied to both inner and outer surfaces. Enhancement of the inner side is generally achieved by imparting a swirl to the flowing fluid. Date (1974) has performed numerical computations for the twisted tape in fully developed laminar flow for constant heat flux with constant properties. His analysis shows that the Nusselt number increases with increasing Prandtl and Reynolds numbers, contrary to laminar flow in smooth tubes which is independent of Reynolds and Prandtl numbers. Date (1973) has also proposed a correlation for the friction factor for the range $5000 < Re < 70{,}000$. Bergles *et al.* (1980) have reported a detailed bibliography of different

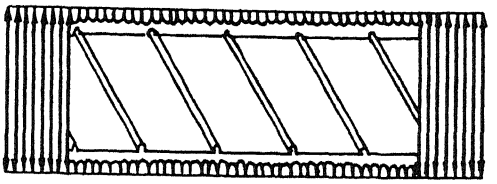

(a)

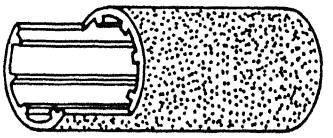

(b)

P_t = Axial distance through which the tape is twisted by 180°

Twist ratio
$r_t = p_t / 2d_i$

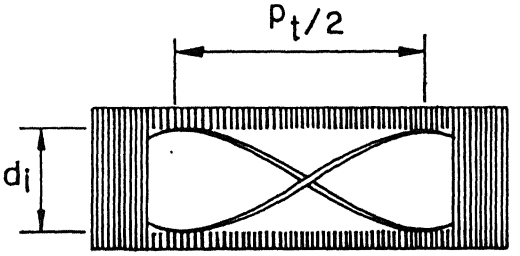

(c)

Fig.2.12 Various methods of making enhanced tubes: (a) Helical ribson inner surface and integral fin on outer surface (b) Internal fins on inner surface and porous coating on outer surface. (c) Twisted tape insert on inner surface and integral fins on outer surface.

augmentation techniques. Bergles and Joshi (1983) provide an excellent summary of performance data on the twisted tape inserts.

Non-decaying swirl flow has been the subject of many investigations (Kreith and Margdis, 1959; Gambill and Bundy, 1963; Smithberg and Landis, 1964; Hong and Bergles, 1976). Blum and Oliver (1966) and Migay and Golubev (1970) have shown that there is significant increase in heat transfer due to free swirling flow. Sparrow and Chaboki (1984) have performed an experimental study on swirl affected turbulent air flow and heat transfer in a tube. The swirling motion has been found to enhance heat transfer substantially in the initial portion of the tube.

Junkan *et al.* (1985) have conducted experimental studies of three different types of tape inserts for fire tube boilers. These tapes are termed as turbulators. Two commercial turbulators consisting of narrow, thin metal strips bent and twisted in a zig-zag fashion to allow periodic contact with tube wall have caused 135 and 175 percent increase in heat transfer coefficient at a high Reynolds number. A third turbulator, in the form of a twisted strip, with a width slightly less than the tube diameter, provided a 65 percent increase in the heat transfer coefficient while the increase in the friction factor is small as compared to the other two turbulators.

2.5 Flows in Parallel Plate Channels

In the present work, the focus is on the enhancement of heat transfer in plate fin heat exchangers and on the gas side of fin-tube heat exchangers (with flat fins). A study of various investigations in this particular area is presented now.

Augmentation of heat transfer is of special interest in channel flows where the rate of heat transfer between the fluid and the channel walls deteriorates as the boundary layer grows along the channel walls and the flow tends to become fully developed. The evolution towards a fully developed flow can be disturbed by suitable manipulation of the surface of the channel. Using multi-louvered surface geometry is an option. Achaichia and Cowell (1988) have provided detailed performance data for louvered fin surfaces. However, in using louvered fins, enhancement is obtained at the price of a high pressure drop. This difficulty can be circumvented by using protrusions in the form of slender delta wings or winglets.

As has already been mentioned, the gas side heat transfer coefficient in gas-liquid fin-tube cross flow heat exchangers is small as compared to that of the liquid side. The mechanism of heat transfer between the gas and the solid surfaces in such cases is to be studied in detail. Figure 2.9. shows a single tube on a plate-fin . The flow field consists of a horseshoe vortex system, and a dead water zone at the juncture of the tube and the plate and a von-Karman vortex street in the middle. In order to enhance heat transfer in such a flow configuration, vortex generators can be mounted on the plates.

Dong (1989) and Valencia (1992) have conducted experimental investigations to observe the influence of winglet type vortex generators in a channel with a built-in circular tube. Sanchez *et al.*(1989) have computed the laminar flow around a circular cylinder in a rectangular channel with a pair of delta winglets on the bottom plate of the channel. Their results show that the longitudinal vortices generated by the winglets placed in the wake, control the spread of the wake zone behind the cylinder and damp the periodic vortex street. Biswas *et al.* (1994) have observed that in the absence of winglet type vortex generators, relatively little heat transfer takes place in the downstream of the circular tube which is a recirculation region with low velocity fluid. However, very

high heat transfer enhancement , of upto 240 percent was observed in the wake region behind the cylinder in the presence of winglet type vortex generators.

Computational studies have also been done with periodic configurations of the form of plate-fin heat exchangers with perforated fins or slotted channels. Heat transfer surfaces periodically interrupted along the streamwise direction have been widely used for enhancing the heat transfer rates.. In slotted channels, for example, Each slot enables the interruption of the thermal boundary layer where the highest resistance to heat transfer occurs and a new boundary layer with lower thermal resistance begins. Such channels have been classified as communicating channels. They allow a very good mixing of the flow with self-sustained oscillations when the system is operating above the critical Reynolds number. That is, above a certain critical value of the Reynolds number, much within the laminar regime, the initially steady flow becomes unsteady and attains a time periodic self-sustaining oscillatory regime. Appreciable transport augmentation takes place in this range of Reynolds numbers (Majumdar and Amon, 1992).

Webb and Ramadhyani (1985) have analysed fluid flow and heat transfer characteristics through a parallel plate channel with transverse ribs which act as vortex generators. They have reported significant levels of heat transfer augmentation for fluids such as water and flourocarbons.

2.6 Development of Numerical Methods for Solving Navier- Stokes Equations

In the past three decades many researchers have tried to develop numerical schemes to solve the incompressible Navier-Stokes equations

in three dimensions. The main difficulty in incompressible flow simulation arises from the absence of any explicit equation for pressure and due to the nature of spatial coupling of the pressure and the velocity. For incompressible flow problems, pressure does not have the usual thermodynamical meaning. Here it is a relative variable which adjusts itself instantaneously for the condition of zero divergence to be satisfied at all computational cells. This behaviour is related to the well known fact that in an incompressible fluid the speed of sound becomes infinite. As a consequence, the pressure field can not be calculated by an explicit time advancement procedure, instead it requires at least a partially implicit determination which takes into account the coupling existing between the pressure and the velocity fields as well as the effects of the velocity boundary conditions. This aspect is the most distinctive feature of the primitive variable formulation of the incompressible Navier-Stokes equations.

The difficulties associated with the determination of the pressure field have led to the development of methods which eliminate pressure from the governing equations. In two dimensions, the elimination of pressure from the two momentum equations by cross differentiation leads to the vorticity transport equation. This equation, along with the definition of stream function for steady two-dimensional flows forms the basis of the well known stream function-vorticity method. However this approach does not work for three-dimensional flows because of the absence of a single scalar stream function. A primitive variable formulation involving the velocity components and pressure can be used for solving the Navier-Stokes equations for two-dimensional as well as three-dimensional flows. Such a formulation also allows boundary conditions to be applied in a straightforward manner.

A three-dimensional problem requires a primitive-variable approach. Efforts have been made so that two-dimensional as well as three-dimensional problems could be computed following a primitive

variable approach without encountering non-physical wiggles in pressure distribution. As a remedy, it has been suggested to employ a different grid for each dependent variable. Harlow and Welch (1965) have used such a staggered grid for the dependent variables in their well known MAC (Marker and Cell) method. The MAC method of Harlow and Welch is one of the earliest and widely used explicit methods for solving the full Navier-Stokes equations. In this method, solutions of velocities are obtained using a two step procedure. In the first step called the predictor step provisional values of velocity components are computed explicitly using advection, diffusion and pressure gradients of the earlier time step. The velocity field obtained in this manner need not be divergence free. Hence, in the second step called the corrector step, the pressure and velocity components are corrected so that the velocity field satisfies the continuity equation. This is done through the solution of a Poisson equation for pressure. A related technique developed by Chorin (1967) involves a simultaneous iteration of pressure and velocity components. Vicelli (1971) has shown that the two methods as applied to MAC are equivalent.

The original version of the MAC method has been modified by Harlow and Amsden (1970), Nichols and Hirt (1971) and Hirt and Cook (1972) for application to free surface flows. The MAC method uses a layer of imaginary cells around the boundary of the physical domain necessitating the updating of boundary conditions after every change in internal velocity and pressure values. The MAC method has been extensively used by many researchers to solve for the flow field in complex geometries. For example, Braza, Chassaing and Ha-Minh (1986) have obtained the unsteady wake behind a circular cylinder using the MAC method. Mukhopadhyay, Biswas and Sundararajan(1993) have obtained the periodic wake behind a rectangular obstacle. In fact, the MAC method has been successfully used even to simulate highly unsteady turbulent flows (Robichaux, Tafti and vanka, 1992). It has been

experienced that the MAC method is indeed very efficient in the studies of temporal flow development but it has stability restrictions on the time step values which slow down the calculations for steady flow considerably.

Since implicit methods have no such restrictions, they are more attractive. Patankar and Spalding (1972) have introduced an efficient method known as SIMPLE (Semi-Implicit Method for Pressure Linked Equations). This method is based on a finite-volume discretisation of the governing equations on a staggered grid. In order to improve the convergence involved in the pressure-velocity coupling, several variants of SIMPLE algorithm have been developed. The SIMPLER algorithm of Patankar (1981) and the SIMPLEC algorithm of van Doormaal and Raithby (1984) are improvements on SIMPLE. Although the changes that are required to incorporate SIMPLEC into SIMPLE algorithm are minor, the consequences can be great as it eliminates the approximations made in SIMPLE while deriving the pressure-velocity corrections. A comparative illustration of the operator splitting algorithm, viz., the PISO of Issa (1986) and the SIMPLE family of algorithms has been reported by Jang, Jetli and Acharya (1986).

Garg and Maji (1987) have applied SIMPLEC (Van Doormall and Raithby, 1984) method for solution of viscous flows through periodically converging - diverging tubes. In another numerical investigation, Velusamy and Garg (1993) have solved the complete set of Navier-Stokes equations for three-dimensional developing flow in elliptic cross-section ducts. Application of finite volume methods using non-orthogonal coordinates and collocated grids is reported by Rhie and Chow (1983) and Peric (1985). Peric *et al* (1988) have shown that the collocated arrangement converges faster than the staggered variable arrangement and has advantages when extensions such as multigrid techniques and non-orthogonal grids are considered. A finite volume based procedure has been successfully developed by Majumdar *et al*

(1992) using such collocated velocities and pressure. The concept of momentum interpolation of cell face pressure from nodal values has established an effective equivalence in the methods of staggered and collocated arrangements. Mukhopadhyay *et al.* (1993) have developed a numerical method for predicting viscous flows in complex geometries. The physical domain is divided into a number of non-orthogonal control volumes which are isoparametrically mapped onto standard regular cells. Numerical integration for unsteady momentum equations is performed over such non-orthogonal cells.

Verma and Eswaran (1996) and Verma (1997) have developed a finite volume based flow solver for complex geometries using overlapping control volumes. The algorithm has been tested successfully on some model problems. Kobayashi and Pereira (1991) modified the momentum interpolation method suggested by Peric (1995) and named it as Pressure- Weighted Interpolation Method - Corrected (PWIMC). In this method, the non-orthogonal terms in the momentum equations were solved explicitly, whereas in the pressure-correction equations they were dropped. Roychowdhury *et al* have further modified the PWIMC method. In this work the governing equations have been discretised in the physical plane itself without coordinate transformation. The non-orthogonal terms and QUICK type corrections for the convective terms in the momentum equations are treated explicitly, while the other terms are taken in implicit form. In the pressure correction equation, the non-orthogonal terms were dropped altogether. The scheme has been able to demonstrate excellent convergence properties even for highly skewed grids.

Chapter 3

Problem Formulation

3.1 Introduction

The present work is undertaken to evaluate the performance of an innovative design of secondary fins, described briefly in chapter 1, to be used to enhance the heat transfer rate in plate-fin heat exchangers. The velocity and temperature fields inside the domain of interest need to be computed first. From these results the level of enhancement in heat transfer and the increase in pumping power associated with the proposed design can be calculated. In order to arrive at the optimum design, the effect of varying the Reynolds number and the angle of attack of the vortex generator are to be studied.

3.2 Statement of the Problem

A portion of a compact cross-flow heat exchanger having plain triangular fins is shown in Figure 3.1. The passage formed by the surfaces of the triangular fin and that of the plate of the plate-fin heat exchanger can be considered as a triangular channel as shown in Figure

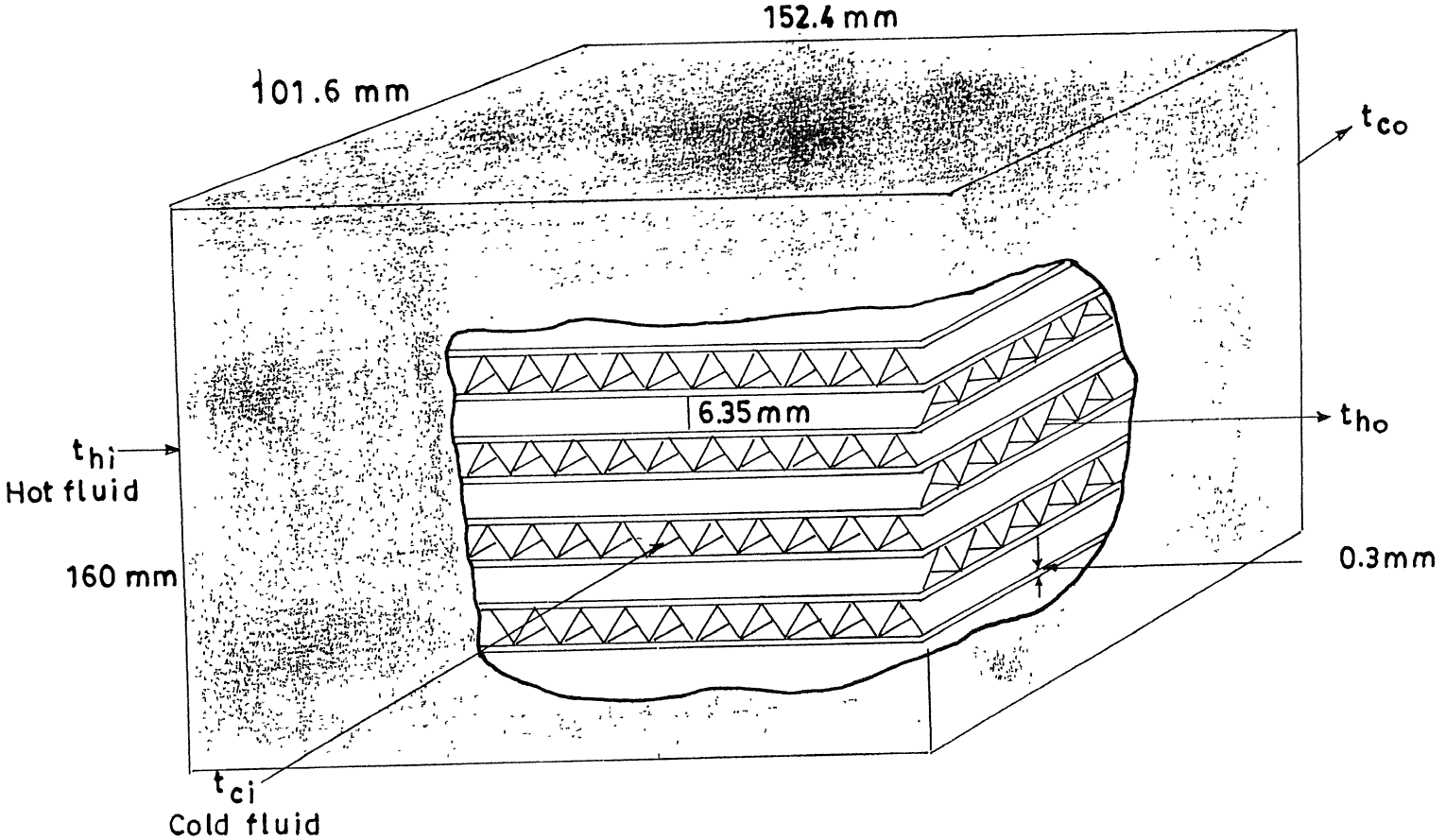

Figure 3.1 Compact cross flow heat exchanger having triangular fins.

The primary objective is to compute the flow structure and temperature distribution of the fluid flowing in this channel in the presence of a vortex generator. These vortex generators , in the form of delta wings or delta winglets are either mounted on or punched out of the slant faces *AB* and *AD* of the triangular fin as shown in Figures 3.3 and 3.4. It is much easier to compute the flow field if the surface on which the vortex generator is mounted is horizontal. This is ensured by rotating the whole set up such that the slant face *AB* of the triangular fin becomes horizontal, as shown in Figures 3.3 and 3.4. The plane of the vortex generator makes an angle β with the direction of flow. This angle is called the angle of attack of the vortex generator. The dimensions and location of the vortex generator are shown in Figures 3.3 and 3.4.

The following two cases are to be considered in this study.

Case 1: When the winglets (or wings) are mounted on (i.e., not stamped out of) the sides of *AB* and *AD*, the flow field is partitioned by *AB* and is symmetric with respect to the midplane *AC* (Fig. 3.3a). Hence only one half of the triangular channel, viz., *ABC*A′B′C′ needs to be considered for computation (Figure 3.3 b).

Case 2: When the winglets (or wings) are punched out of the fin surface the punching operation leaves a triangular stamping on the fin surface and fluid can flow across this stamping. The computational domain in this case is the rhomboid shown *ABCD*A′B′C′D′ shown in Figures 3.5 and 3.6.

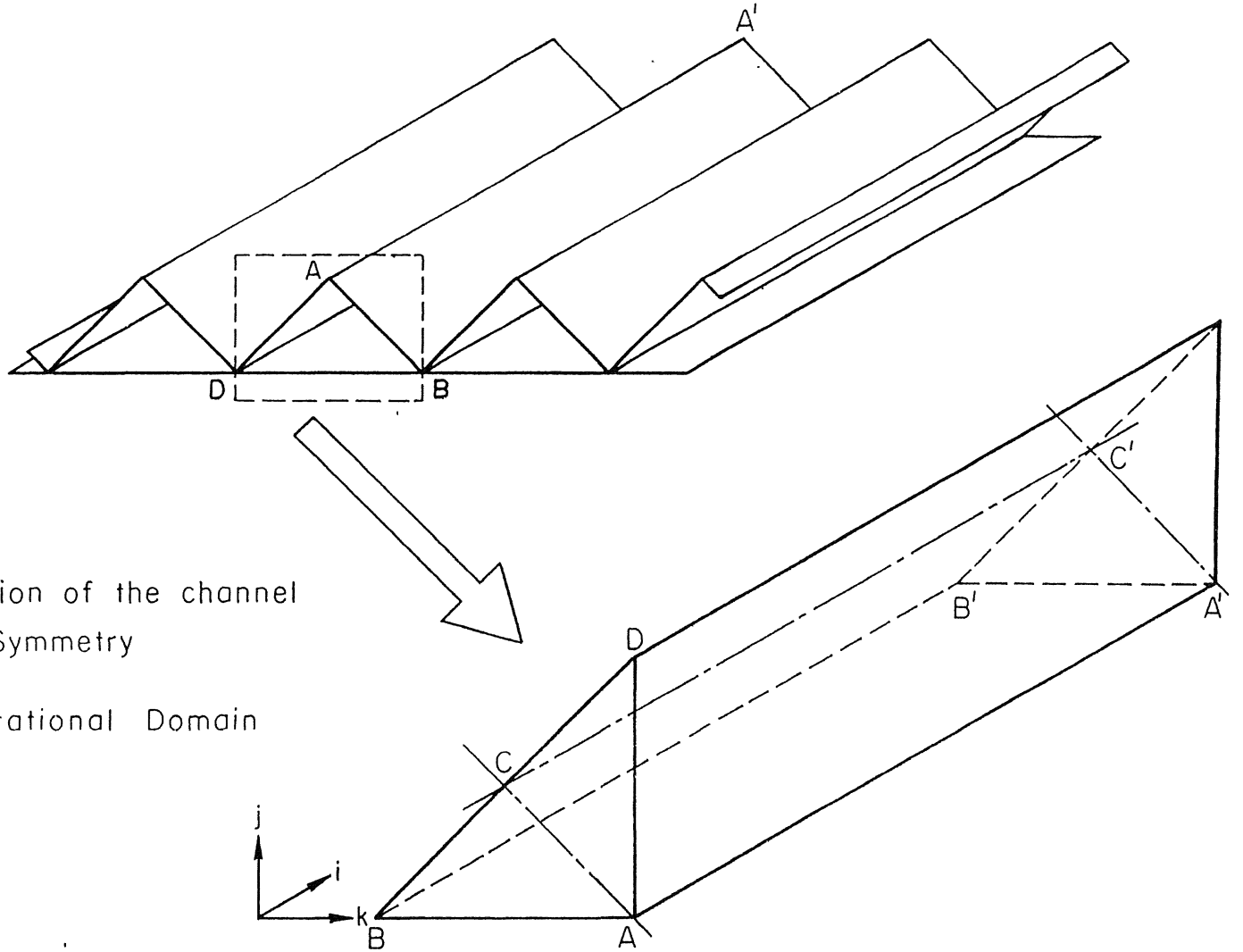

ABD : Cross-section of the channel

ACC'A' :Plane of Symmetry

ABCC'A'B' Computational Domain

Figure 3.2 Triangular channel (after rotation)

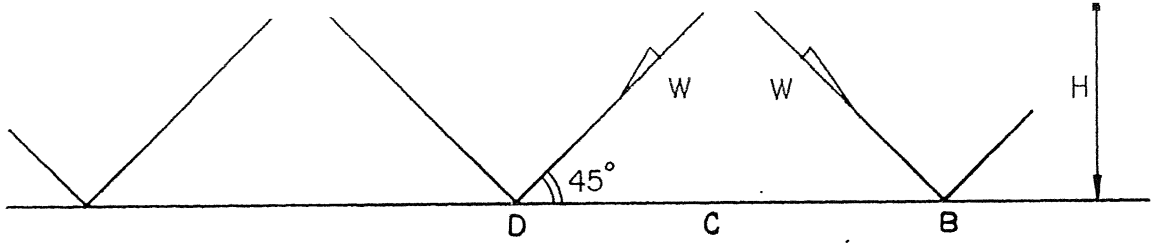

W,W : Winglets

Winglet Geometry
PQ = 1.05
QR = 0.318
Xi = 2.64

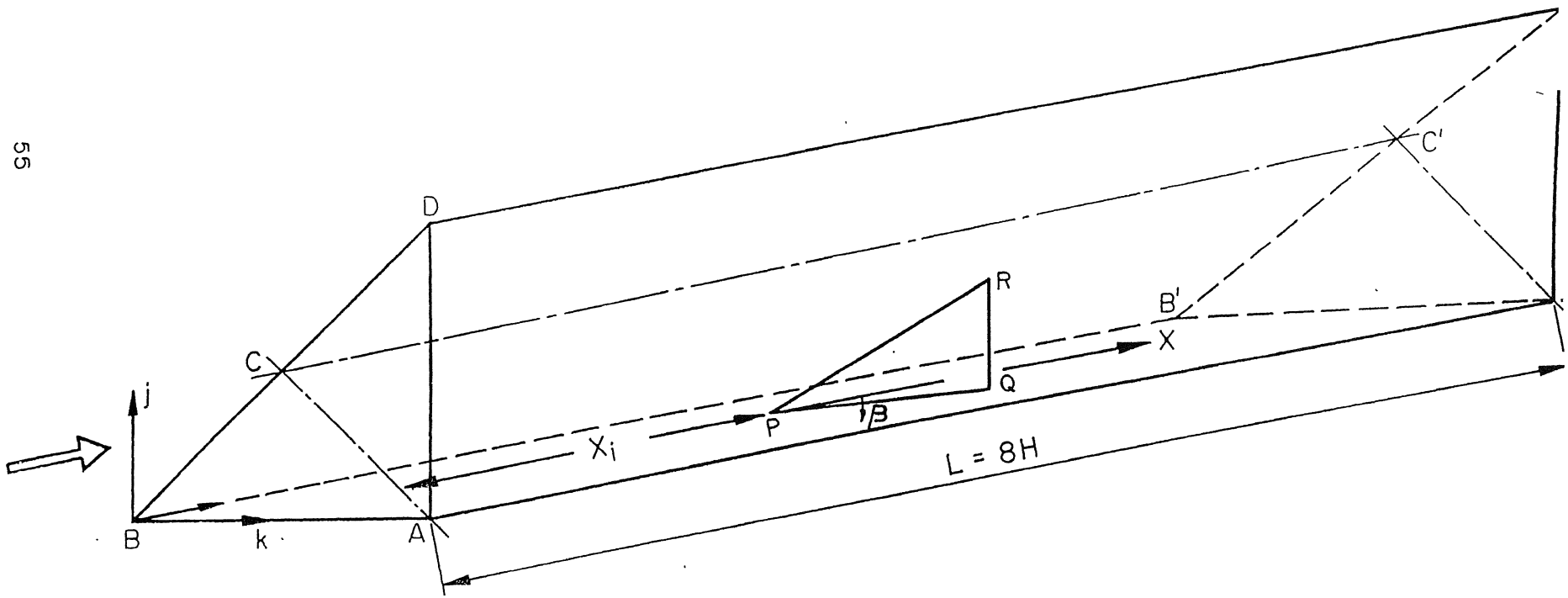

Figure 3.3 Triangular channel with a mounted delta winglet

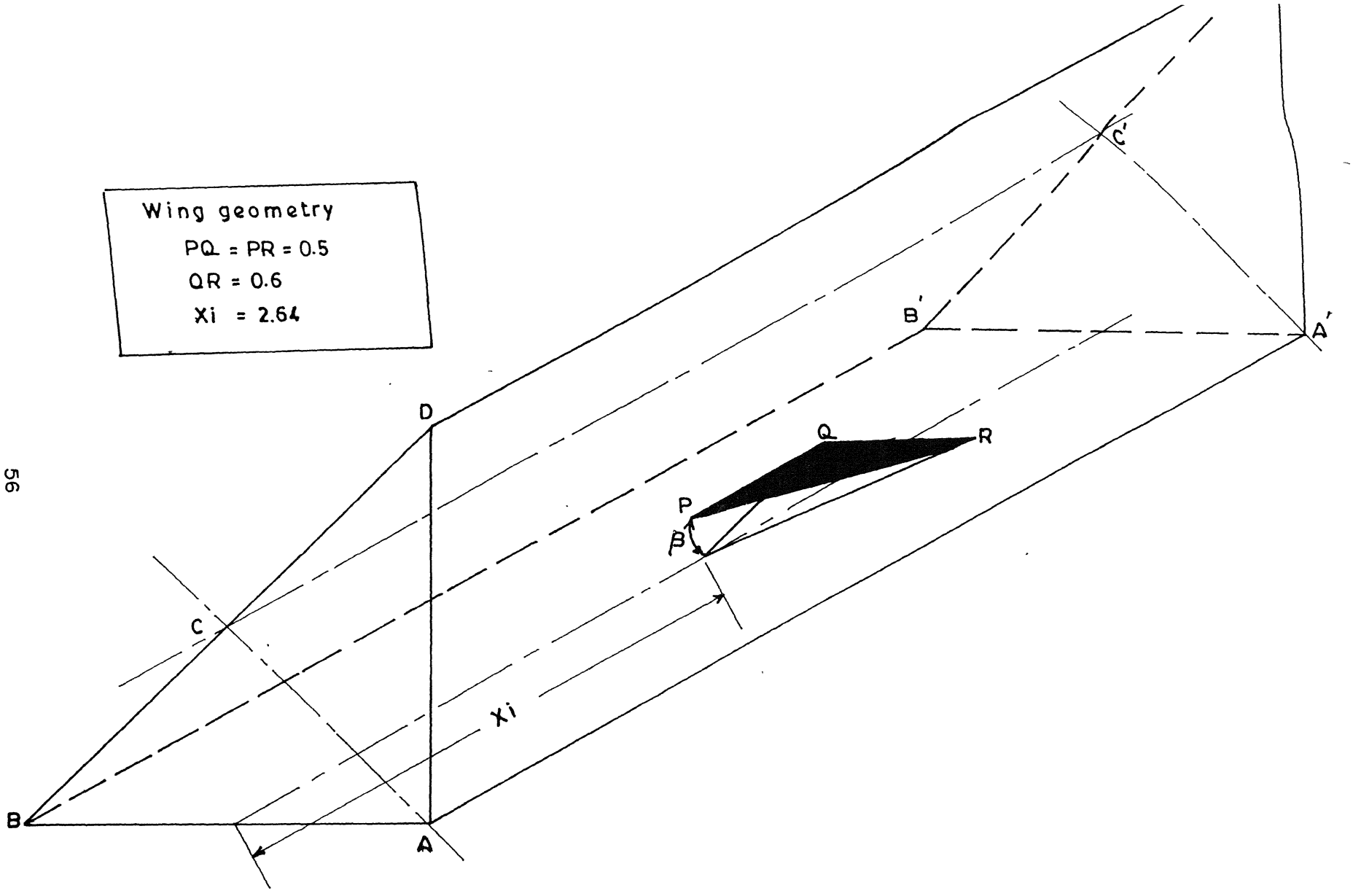

Figure 3.4 Triangular channel with a mounted delta wing

for the case of a constant wall temperature boundary condition; and as

$$\theta = \frac{(T - T_\infty)}{(q_w H / k)} \tag{3.6}$$

for the case of a constant wall heat flux boundary condition, where T_w is the temperature of the wall, T_∞ is the temperature of the incoming fluid and q_w is the value of the uniform heat flux along the walls.

3.2.2 Boundary Conditions

The boundary conditions to be specified for the confining walls of the channel and the surface of the vortex generator are discussed in this section. The procedure used to implement these conditions numerically is described in section 3.5.

3.2.2.1 Confining Walls

(a) Velocity Boundary Conditions:

There are two types of boundary surfaces, namely no-slip boundaries and the plane of symmetry. The velocity boundary conditions for a no-slip boundary are

$$U = V = W = 0 \tag{3.7}$$

And for a plane of symmetry (the plane $ACC'A'$ in Figure 3.2)

$$V = W = 0 \tag{3.8}$$

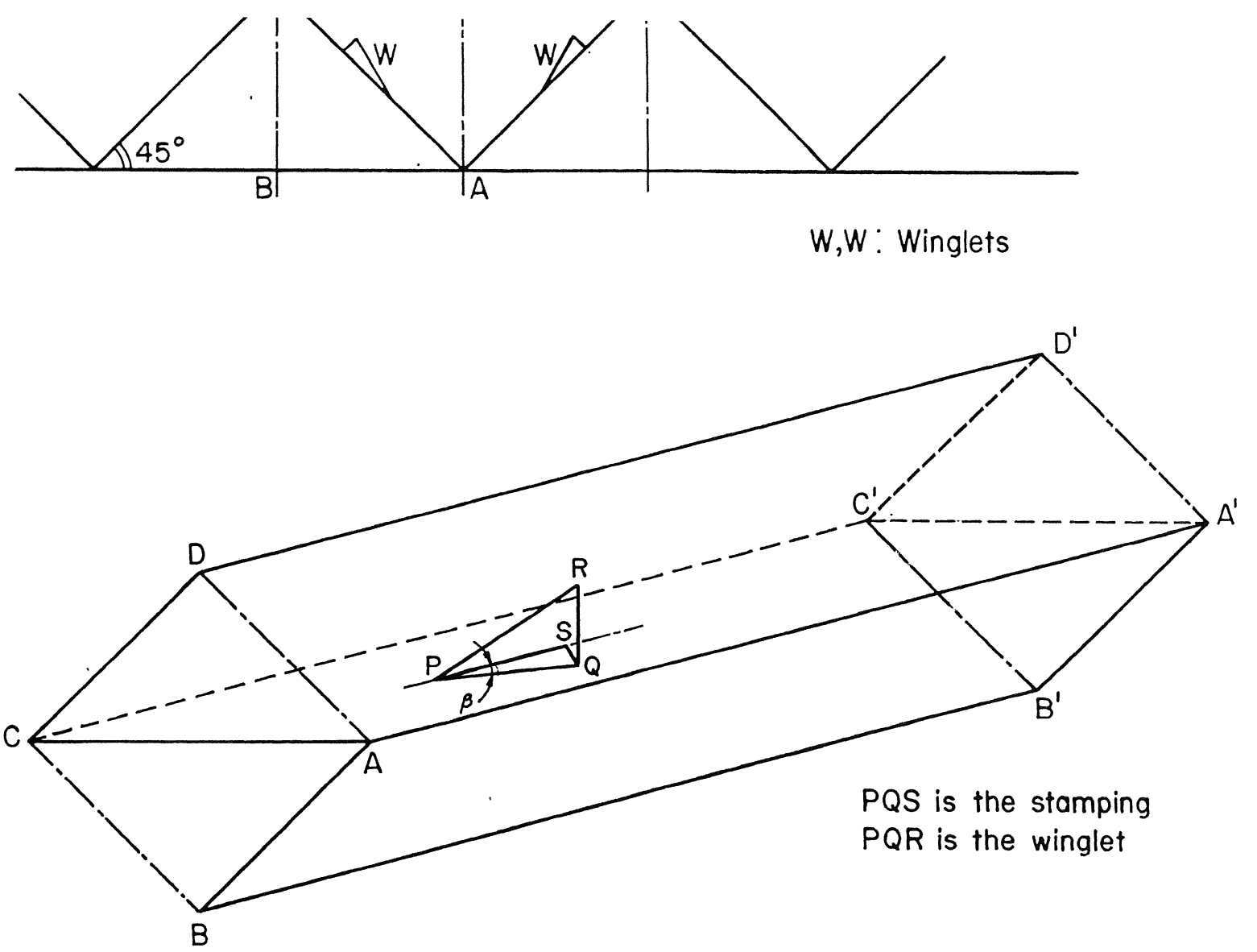

Figure 3.5 Computational domain for the punched delta winglet

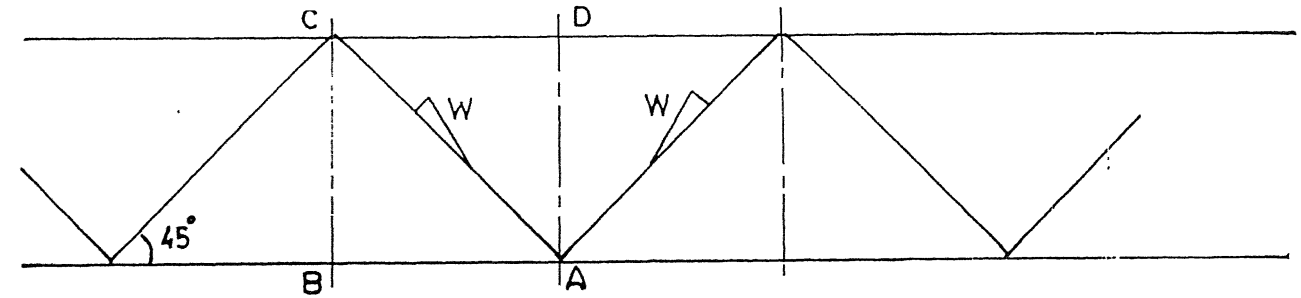

W.W : Delta wings

(a)

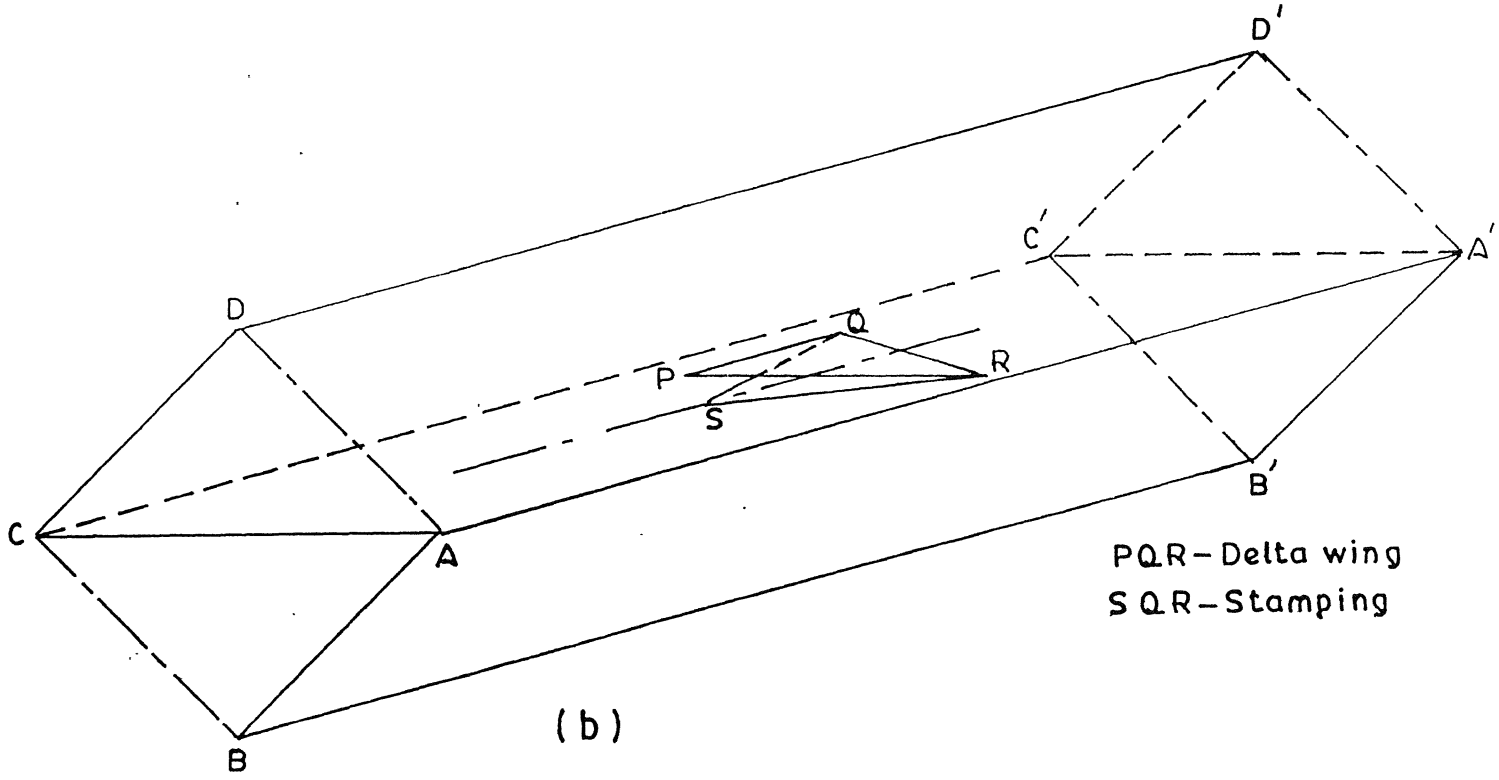

PQR – Delta wing

SQR – Stamping

(b)

Figure 3.6 Computational domain for the punched delta wing.

(This follows from the fact that any non-zero value for the V or W component will make the velocity field asymmetric.) and U is symmetric across this plane. In other words, the U- component of velocity has the same value at points which lie on opposite sides of the plane of symmetry at equal distance. In the case of a mounted vortex generator the computational domain $ABCA'B'C'$ (Figures 3.3 and 3.4) has two no-slip walls viz., $ABB'A'$ and $BCC'B'$ and a plane of symmetry $ACC'A'$. In the case of a punched vortex generator the computational domain $ABCDA'B'C'D'$ (Figures 3.5 and 3.6) is twice as large and has three no-slip boundaries namely, $ABB'A'$, $CDD'C'$ and $ACC'A'$; and two planes of symmetry viz., $BCC'B'$ and $ADD'A'$. The boundary conditions specified in equations 3.7 and 3.8 are applicable in both these cases. However, in the case of the punched vortex generator the fin surface $ACC'A'$ is a no-slip surface everywhere except along the stamping (PQS in Figure 3.5 and SQR in Figure 3.6). This aspect is taken care of while numerically implementing the boundary conditions as explained in section 3.5.
At the channel inlet uniform flow conditions are assumed:

$$U = 1 \quad \text{and} \quad V = W = 0 \tag{3.9}$$

At the exit a smooth transition through the outflow boundary is ensured by setting the condition due to Orlanski (1976)

$$\frac{\partial \Phi}{\partial \tau} + U_c \frac{\partial \Phi}{\partial X} = 0 \tag{3.10}$$

where ϕ is the dependent variable U, V, W or θ The quantity U_c is the mean channel outflow velocity which is equal to 1 in the present case.

(b) Thermal Boundary Conditions

Two idealised situations are considered viz., (1) uniform wall temperature and (2) uniform wall heat flux. In the case of uniform wall temperature, the thermal boundary condition for the channel walls is

$$\theta_w = 1 \qquad (3.11)$$

In other words, the slant surfaces of the triangular fin as well as the plate surface of the plate-fin heat exchanger are assumed to be at the same common temperature T_w . Strictly speaking, the slant surfaces of the triangular fin are not in direct contact with the hot fluid, but $\theta_w = 1$ has been used for these as well, because otherwise the analysis would involve solving the conjugate heat transfer problem. In the case of uniform wall heat flux the thermal boundary condition for the channel walls is

$$q_w = \text{constant.} \qquad (3.12)$$

The thermal boundary condition applicable to the plane of symmetry is that the values of temperature at points which are equidistant from the plane of symmetry, but on opposite sides of this plane are equal. While computing the case of stamped vortex generator no boundary conditions are implemented along the triangular stamping. This is because fluid flows across the stamping and hence the latter is not a boundary surface.

3.2.3 Boundary conditions for the vortex generator

The vortex generator can be considered as a surface of zero thickness. Since it is a no-slip surface the velocity boundary condition is

$$U = V = W = 0 \tag{3.13}$$

and the thermal boundary condition is

$$\theta_w = 1 \tag{3.14}$$

for the case of uniform wall temperature. In the case of uniform wall heat flux, the surface of the vortex generator is not treated as a source of heat or even that it is thermally interacting with the flow. Its role is confined to the generation of vortices and no thermal boundary condition is specified. The exact procedure used to implement these boundary conditions numerically is explained in section 3.5.

3.2.3. Parametric Study

In order to arrive at the optimum design, the performance of the proposed fin design is to be computed for various angles of attack. Three different values of $\beta = 15°, 30°, 45°$ are considered. The computations are done for two different values of the Reynolds number viz., Re = 100 and Re = 200.

3.3 Grid System Used

The computational domain is divided into a set of rectangular cells (Figure 3.7) and a staggered grid arrangement is used such that the velocity components are defined at the centre of the cell faces to which they are normal. The pressure and temperature are defined at the centre of the cell. With such an arrangement, it is well-known (Patankar 1977) that the pressure velocity computations converge properly and quickly. Another important advantage of such a grid system is that the transport rates across the faces of the control volumes can be computed without interpolation of velocity components.

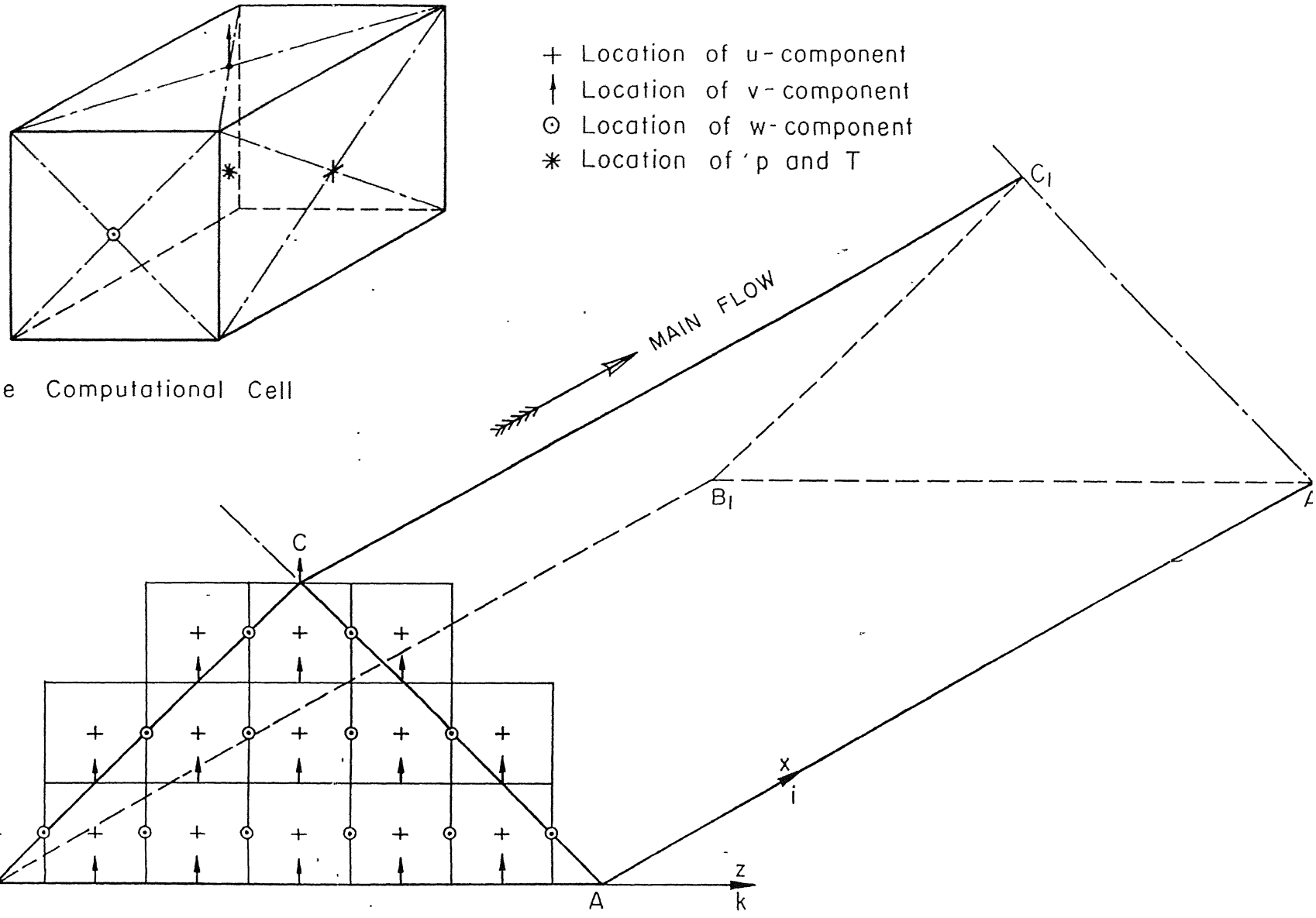

Figure 3.7 Staggered grid arrangement.

3.4 Method of Solution

A modified version of Marker and Cell (MAC) method due to Harlow and Welch (1965) and Hirt and Cook (1972) is used to obtain the numerical solution of the governing equations

3.4.1 MAC Algorithm

In the staggered grid arrangement used, (Figure 3.8)the velocities are not defined at the nodal points. Whenever required, the velocities at the nodal points are to be found by interpolation. For example, with uniform grids, we can write

$$U_{i+1/2,j,k} = 0.5\left(U_{i+1,j,k} + U_{i,j,k}\right) \qquad (3.15)$$

Where a product or a square of such a quantity appears, it is to be averaged first and then the product is to be formed. Because of the staggered grid being used, the location of the velocity grid points depend upon the component being described. For example if the centre of the cell (i, j, k) is at (X_i, Y_j, Z_k) then the pressure $P_{i,j,k}$ and temperature $T_{i,j,k}$ will be evaluated at (X_i, Y_j, Z_k) ,but $U_{i,j,k}$ will be evaluated at ($X_i + \Delta X/2, Y_j, Z_k$), $V_{i,j,k}$ at ($X_i, Y_j + \Delta Y/2, Z_k$),and $W_{i,j,k}$ at ($X_i, Y_j, Z_k + \Delta Z/2$) respectively as shown in Figure 3.8. This should be kept in mind while interpreting the discretized equations given below.

Convective terms of the momentum equations are discretised using a weighted average of second upwind and space centered scheme (Hirt et *al.*, 1975). Diffusive terms are discretised by a central difference scheme. The discretised terms of the x-momentum equation are presented below. The quantities in | | denote absolute values.

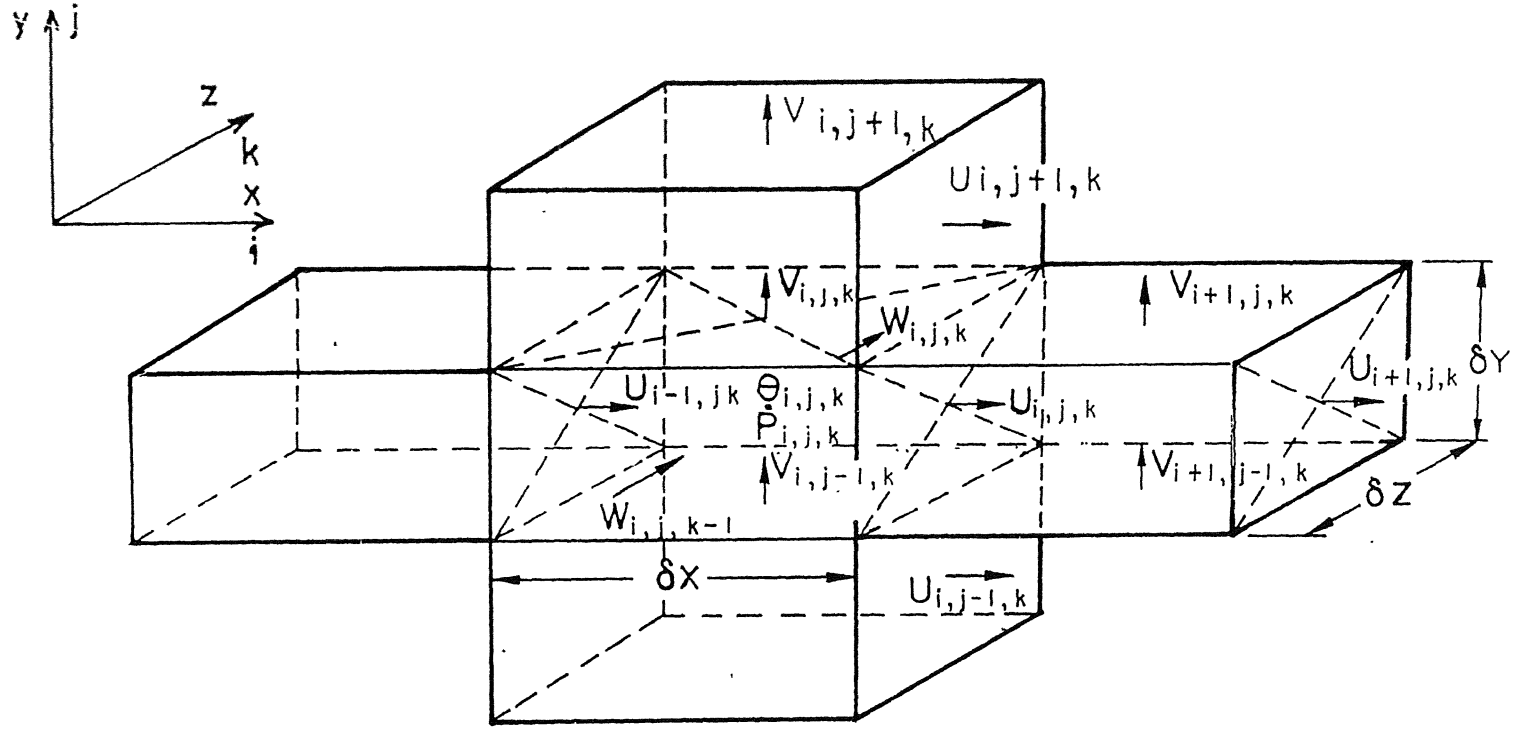

Figure 3.8 Velocity locations in the staggered grid

$$\left[\frac{\partial U^2}{\partial X}\right] = \frac{1}{4\delta X}\Big[\left(U_{I,J,k} + U_{I+1,J,k}\right)\left(U_{I,J,k} + U_{I+1,J,k}\right)$$

$$+\alpha_P \left|\left(U_{i,j,k} + U_{i+1,j,k}\right)\right| \left(U_{I,J,k} - U_{i+1,J,k}\right)$$

$$-\left(U_{I-1,J,k} + U_{I,J,k}\right)\left(U_{I-1,J,k} + U_{I,J,k}\right)$$

$$-\alpha_P \left|\left(U_{i-1,j,k} + U_{I,j,k}\right)\right| \left(U_{i-1,J,k} - U_{I,J,k}\right) \Big]$$

$$\equiv \text{DUUDX} \qquad (3.16)$$

$$\left[\frac{\partial UV}{\partial Y}\right] = \frac{1}{4\delta Y}\Big[\left(V_{I,j,k} + V_{i+1,j,k}\right)\left(U_{I,J,k} + U_{I,J+1,k}\right)$$

$$+ \quad \alpha_P \left|\left(V_{i,J,k} + V_{I+1,J,k}\right)\right| \left(U_{i,j,k} - U_{I,J+1,k}\right)$$

$$-\left(V_{i,j-1,k} + V_{i+1,J-1,k}\right)\left(U_{i,J-1,k} + U_{I,J,k}\right)$$

$$-\alpha_P \left|\left(V_{i,j-1,k} + V_{i+1,j-1,k}\right)\right| \left(U_{I,J-1,k} - U_{i,j,k}\right)$$

$$\equiv \text{DUVDY} \qquad (3.17)$$

$$\left[\frac{\partial UW}{\partial Z}\right] = \frac{1}{4\delta Z}\Big[\left(W_{i,j,k} + W_{i+1,j,k}\right)\left(U_{I,j,k} + U_{I,J,k-1}\right)$$

$$+ \quad \alpha_P \left|\left(W_{i,j,k} + W_{i+1,J,k}\right)\right| \left(U_{I,J,k} - U_{I,J,k-1}\right)$$

$$-\left(W_{i,j,k-1} + W_{i+1,J,k-1}\right)\left(U_{i,J,k-1} + U_{i,J,k}\right)$$

$$-\alpha_P \left|\left(W_{i,j,k} + W_{i+1,j,k-1}\right)\right| \left(U_{i,J,k-1} - U_{I,J,k}\right) \Big]$$

$$\equiv \text{DUWDZ} \qquad (3.18)$$

$$\frac{\partial P}{\partial X} = \frac{P_{i+1,j,k} - P_{i,j,k}}{\delta X} \equiv DPDX \qquad (3.19)$$

$$\frac{\partial^2 U}{\partial X^2} = \frac{U_{i+1,j,k} - 2U_{i,j,k} + U_{i-1,j,k}}{(\delta X)^2} \equiv D2UDX2 \qquad (3.20)$$

$$\frac{\partial^2 U}{\partial Y^2} = \frac{U_{i,j+1,k} - 2U_{i,j,k} + U_{i,j-1,k}}{(\delta Y)^2} \equiv D2UDY2 \qquad (3.21)$$

$$\frac{\partial^2 U}{\partial Z^2} = \frac{U_{i,j,k+1} - 2U_{i,j,k} + U_{i,j,k-1}}{(\delta Z)^2} \equiv D2UDZ2 \qquad (3.22)$$

The quantity α_p is the upwinding factor. With, α_p = 1, the scheme is second order upwind and if α_p = 0 the scheme is space centered. The factor α_p is chosen so as to incorporate some upwinding for the sake of stability. A typical value of α_p is between 0.2 and 0.3.

To satisfy both the Navier Stokes equation as well as the continuity equation it is necessary that the pressure term be evaluated implicitly, i.e., pressure has to be treated as an unknown along with the velocity. However, without knowing the pressure we cannot know the velocities at the new time step. To circumvent this problem solutions for the velocities are obtained in a two step *predictor -corrector* procedure. First the velocity components are advanced explicitly using the previous state of flow, having calculated accelerations caused by convection, diffusion and pressure gradients through a time step of $\delta\tau$. The resultant predicted velocity field need not necessarily satisfy the continuity equation i.e. the value of divergence may not be zero in all the cells.. Therefore in the second *corrector* step the adjustment of pressure and velocity is done by an iterative process in order to ensure mass conservation in each cell. If

the explicitly advanced predicted velocity is termed as $\tilde{U}^{n+1}_{i,j,k}$ then from equation 3.2 we can write

$$\tilde{U}^{n+1}_{i,j,k} = U^{n}_{i,j,k} + \delta\tau[\mathrm{CONDIFU}]^{n}_{i,j,k} - \delta\tau[DPDX]^{n}_{i,j,k} \qquad (3.23)$$

where

$$[CONDIFU]^{n}_{i,j,k} = \Big[\big(-DUUDX - DUVDY - DUWDZ\big) + (1/\mathrm{Re})(\mathrm{D2UDX2} + \mathrm{D2UDY2} + \mathrm{D2UDZ2})\Big] \qquad (3.24)$$

In a similar manner we evaluate

$$\tilde{V}^{n+1}_{i,j,k} = V^{n}_{i,j,k} + \delta\tau[CONDIFV]^{n}_{i,j,k} - \delta\tau[DPDY]^{n}_{i,j,k} \qquad (3.25)$$

$$\tilde{W}^{n+1}_{i,j,k} = W^{n}_{i,j,k} + \delta\tau[CONDIFW]^{n}_{i,j,k} - \delta\tau[DPDZ]^{n}_{i,j,k} \qquad (3.26)$$

As discussed earlier, the explicitly advanced predicted velocities may not necessarily lead to a flow field with zero mass divergence in each cell. This implies that at this stage the pressure distribution is not correct. Pressure in each cell will need to be corrected in such a way that there is no net mass flow into or out of any cell. In the original MAC method, the corrected pressures are obtained from the solution of a Poisson equation for pressure. A related technique developed by Chorin (1967) involved a simultaneous iteration of pressures and velocity components. Vicelli (1971) has shown that the two methods as applied to the MAC algorithm are equivalent. In the present computation, the iterative correction procedure of Chorin (1967) has been used for obtaining a divergence-free velocity field. The mathematical methodology

of this iterative pressure-velocity correction procedure is presented below.

The relationship between the explicitly advanced predicted velocity component and the velocity at the previous time step may be written as

$$\tilde{U}^{n+1}_{i,j,k} = U^{n}_{i,j,k} - \frac{\delta\tau\left[P^{n}_{i+1,j,k} - P^{n}_{i,j,k}\right]}{\delta X} + \delta\tau[CONDIFU]^{n}_{i,j,k} \qquad (3.27)$$

where, on the other hand, the corrected velocity-component (unknown) will be related to the correct pressure (also unknown) in the following way:

$$U^{n+1}_{i,j,k} = U^{n}_{i,j,k} - \frac{\delta\tau\left[P^{n+1}_{i+1,j,k} - P^{n+1}_{i,j,k}\right]}{\delta X} + \delta\tau[CONDIFU]^{n}_{i,j,k} \qquad (3.28)$$

From equations (3.27) and (3.28) we can write

$$U^{n+1}_{i,j,k} - \tilde{U}^{n+1}_{i,j,k} = \frac{\delta\tau\left[P'_{i+1,j,k} - P'_{i,j,k}\right]}{\delta X} \qquad (3.29)$$

Where the pressure correction may be defined as

$$P'_{i,j,k} = P^{n+1}_{i,j,k} - P^{n}_{i,j,k} \qquad (3.30)$$

Neither the pressure corrections nor $U^{n+1}_{i,j,k}$ are known explicitly at this stage so one cannot be calculated with the help of the other. Calculations are done in an iterative cycle and we write

$$U^{n+1}_{i,j,k} = \tilde{U}^{n+1}_{i,j,k} + \frac{\delta\tau\left[P'_{i+1,j,k} - P'_{i,j,k}\right]}{\delta X} \qquad (3.31)$$

In a similar way we have

Corrected Estimated Correction

$$V_{i,j,k}^{n+1} \rightarrow \tilde{V}_{i,j,k}^{n+1} + \frac{\delta\tau\left[P'_{i,j+1,k} - P'_{i,j,k}\right]}{\delta Y} \tag{3.32}$$

$$W_{i,j,k}^{n+1} \rightarrow \tilde{W}_{i,j,k}^{n+1} + \frac{\delta\tau\left[P'_{i,j,k+1} - P'_{i,j,k}\right]}{\delta Z} \tag{3.33}$$

Substituting the above relationships into the continuity equation (3.1) we obtain

$$\delta\tau\left[\frac{P'_{i+1,j,k} - 2P'_{i,j,k} + P'_{i-1,j,k}}{(\delta X)^2} + \frac{P'_{i,j+1,k} - 2P'_{i,j,k} + P'_{i,j-1,k}}{(\delta Y)^2} + \frac{P'_{i,j,k-1} - 2P'_{i,j,k} + P'_{i,j,k-1}}{(\delta Z)^2}\right]$$

$$= \left[\frac{\tilde{U}_{i,j,k}^{n-1} - \tilde{U}_{i-1,j,k}^{n+1}}{\delta X} + \frac{\tilde{V}_{i,j,k}^{n+1} - \tilde{V}_{i,j-1,k}^{n+1}}{\delta Y} + \frac{\tilde{W}_{i,j,k}^{n+1} - \tilde{W}_{i,j,k-1}^{n+1}}{\delta Z}\right]$$

$$- \left[\frac{U_{i,j,k}^{n-1} - U_{i-1,j,k}^{n+1}}{\delta X} + \frac{V_{i,j,k}^{n+1} - V_{i,j-1,k}^{n+1}}{\delta Y} + \frac{W_{i,j,k}^{n+1} - W_{i,j,k-1}^{n+1}}{\delta Z}\right] \tag{3.34}$$

The last term in square brackets is put to zero to satisfy continuity. Therefore we have

$$\delta\tau\left[\frac{P'_{i+1,j,k} - 2P'_{i,j,k} + P'_{i-1,j,k}}{(\delta X)^2} + \frac{P'_{i,j+1,k} - 2P'_{i,j,k} + P'_{i,j-1,k}}{(\delta Y)^2} + \frac{P'_{i,j,k-1} - 2P'_{i,j,k} + P'_{i,j,k-1}}{(\delta Z)^2}\right]$$

$$= \left[\frac{\tilde{U}_{i,j,k}^{n-1} - \tilde{U}_{i-1,j,k}^{n+1}}{\delta X} + \frac{\tilde{V}_{i,j,k}^{n+1} - \tilde{V}_{i,j-1,k}^{n+1}}{\delta Y} + \frac{\tilde{W}_{i,j,k}^{n+1} - \tilde{W}_{i,j,k-1}^{n+1}}{\delta Z}\right] \tag{3.35}$$

The right side of this equation is known and is denoted by $D^n_{i,j,k}$. Substitution of this yields a Poisson equation for pressure

$$\delta\tau \left[\nabla^2 P'\right] = D_{i,j,k} \tag{3.36a}$$

From the above equation the $P'_{i,j,k}$ can be obtained by Guass-Seidel iterations by repeatedly iterating

$$P'_{i,j,k} = \frac{-(D)_{i,j,k}}{\left[2\delta\tau\left(\frac{1}{\delta X^2}+\frac{1}{\delta Y^2}+\frac{1}{\delta Z^2}\right)\right]} \tag{3.36b}$$

point by point till convergence occurs. In order to accelerate the calculation, the pressure corrections are iterated using

$$P'_{i,j,k} = \frac{-\omega_o(D)_{i,j,k}}{\left[2\delta\tau\left(\frac{1}{\delta X^2}+\frac{1}{\delta Y^2}+\frac{1}{\delta Z^2}\right)\right]} \tag{3.37}$$

where ω_o is the overrelaxation factor. A value of $\omega_o = 1.7$ is commonly used. After calculating $P'_{i,j,k}$, the pressure in the cell (i,j,k) is adjusted as

$$P^{n+1}_{i,j,k} \rightarrow P^n_{i,j,k} + P'_{i,j,k} \tag{3.38}$$

Now the pressure in each cell has been corrected so that the velocity divergence in each cell vanishes. The velocity field is also corrected using the pressure correction equations. All the problems attempted in this thesis are steady state. Thus although the algorithm used is time

accurate, it was used only in a 'false transient' way-time-stepping to a steady state solution from arbitrary initial conditions. There is one more important aspect of this scheme. If only velocity boundary conditions are applied, this method avoids the application of pressure boundary conditions. This feature, typical of the modified MAC method has been discussed in greater detail by Peyret and Taylor (1983).

3.4.2 Solution of the Energy Equation

After evaluating the steady state velocities, the energy equation is solved with a Successive Over-Relaxation technique to determine the temperature field. The procedure adopted for this is presented in this section. The steady state energy equation, neglecting the dissipation term, may be written in the following conservative form as

$$\frac{\partial U\theta}{\partial X}+\frac{\partial V\theta}{\partial Y}+\frac{\partial W\theta}{\partial Z} = \frac{\nabla^2\theta}{Pe} \tag{3.39}$$

Equation (3.39) may be rewritten as

$$\nabla^2\theta = Pe\,[CONVT]^m_{i,j,k} \tag{3.40}$$

where, $[CONVT]_{i,j,k}$ is the discretized covective terms on the left hand side of equation (3.39) and m stands for the iterative counter. To start with we can assume any guess value of θ throughout the flow field . The velocities U, V, and W are known from the solution of momentum equation and hence equation (3.39) is now a linear equation. Using the guess values of θ and known correct values of U, V, and W the left hand side of equation (3.40) is evaluated. A weighted average scheme is

adopted for discretisation of the convective terms. After discretising and evaluating the right hand side of equation (3.40) we obtain a Poisson equation for temperature with a source term on the right hand side. Now, we can follow a SOR technique for solving equation (3.40). Consider a discretized equation as

$$\frac{\theta_{i+1,j,k}-2\theta_{i,j,k}+\theta_{i-1,j,k}}{(\delta X)^2}+\frac{\theta_{i,j+1,k}-2\theta_{i,j,k}+\theta_{i,j-1,k}}{(\delta Y)^2}+\frac{\theta_{i,j,k+1}-2\theta_{i,j,k}+\theta_{i,j,k-1}}{(\delta Z)^2}=S^{*m} \quad (3.41)$$

where $S^{*m} \equiv Pe\,[CONVT]^m_{i,j,k}$

This equation is solved by the SOR method with the right hand side being updated after each iterative sweep.

3.4.3 Numerical Stability Considerations

For accuracy the mesh size must be chosen small enough to resolve the expected spatial variations in all dependent variables. Once a mesh has been chosen, the choice of the time increment is governed by two restrictions, namely, the Courant-Friedrichs- Lewy (CFL) condition and the restriction on the basis of grid -Fourier numbers. According to the CFL condition, material can not move through more than one cell in one time step. Therefore the time increment must satisfy the inequality

$$\delta\tau < \min\left\{\frac{\delta X}{|U|},\frac{\delta Y}{|V|},\frac{\delta Z}{|W|}\right\} \quad (3.42)$$

where the minimum is with respect to every cell in the mesh. Typically, $\delta\tau$ is chosen equal to one fourth to one-third of the minimum cell transit time. When the viscous diffusion terms are more important, the

condition necessary to ensure stability is dictated by the restriction on the grid Fourier numbers, which results in

$$\delta\tau < \left[\frac{1}{2\,\mathrm{Re}} \frac{(\delta X)^2 (\delta Y)^2 (\delta Z)^2}{\{(\delta X)^2 (\delta Y)^2 + (\delta Y)^2 (\delta Z)^2 + (\delta Z)^2 (\delta X)^2\}} \right] \qquad (3.43)$$

The final $\delta\tau$ for each increment is the minimum of the $\delta\tau$'s obtained from equations (3.42) and (3.43)

3.5 Numerical Boundary Conditions

For the staggered-grid arrangement, the usual practice is to employ a layer of fictitious cells all around the boundary of the computational domain. The boundary conditions are then implemented by specifying appropriate values for the velocities in these fictitious cells which lie outside the region of real flow. But in the present formulation fictitious cells have not been employed. This has been necessitated by the fact that, in the case of a punched vortex generator fluid flows on both sides of the no-slip surface *ABB'A'* (from which the vortex generator is punched out as shown in Figure 3.5) due to the presence of the stamping. Consequently use of fictitious cells is not possible as the cell would be occupying a region where there is real flow. The procedure used to overcome this difficulty is explained below.

3.5.1 Boundary Conditions for Confining Walls

The present formulation uses the MAC *Predictor- Corrector* method for computing the converged flow field. Velocity boundary conditions are needed while advancing the flow field by explicit time stepping of the

momentum equations in the *predictor* step ; and while evaluating the divergence in each cell, as a part of the *corrector* step to enforce mass conservation in each cell. In the scheme used in the present computation the boundary conditions are directly incorporated in the expressions used for the calculation of divergence as well as in the discretised equations used for time-stepping of the momentum equations. The details of the procedure used are given below.

(a) Velocity boundary conditions for Continuity equation

The divergence of any cell is calculated using the expression

$$D_{i,j,k} = \frac{U_{i,j,k} - U_{i-1,j,k}}{\Delta X} + \frac{V_{i,j,k} - V_{i,j-1,k}}{\Delta Y} + \frac{W_{i,j,k} - W_{i,j,k-1}}{\Delta Z} \qquad (3.44)$$

where i, j, k refer to the location of the cell in the x , y, z directions respectively (Figure 3.8). This expression is used as it is for all the interior cells. The cells along the boundaries are divided into different groups; for all the cells in any given group the same set of boundary conditions apply. The different groups and the corresponding expression for divergence are as follows.

(1) Cells lying just above a horizontal no-slip boundary (such as the surface *ABB'A'* in Figure 3.3)

V(i,j-1,k) = 0 for these cells (Figure 3.9 a) as this V component is located on the no_slip surface. Hence the divergence for these cells is calculated using

$$D_{i,j,k} = \frac{U_{i,j,k} - U_{i-1,j,k}}{\Delta X} + \frac{V_{i,j,k}}{\Delta Y} + \frac{W_{i,j,k} - W_{i,j,k-1}}{\Delta Z} \qquad (3.45)$$

(2) Cells adjacent to an inclined no-slip boundary (such as the surface *BCC'B'* in Figure 3.3)

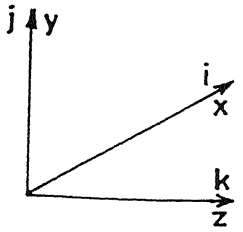

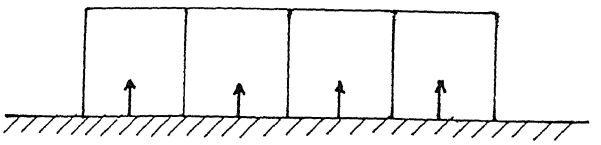

(a)

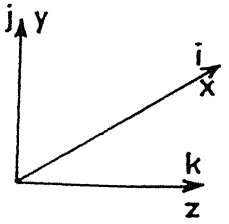

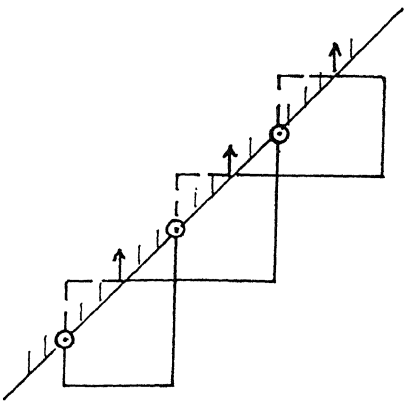

(b)

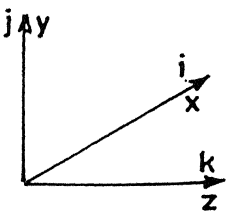

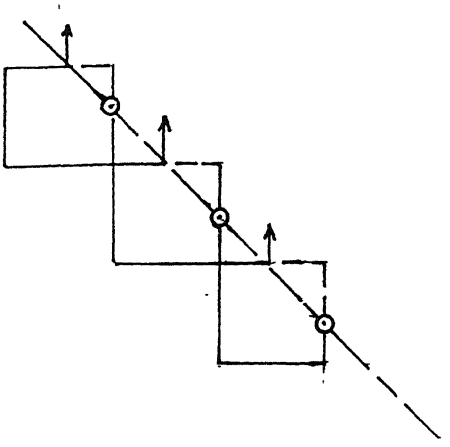

(c)

↑ Is the location of V - Component of velocity

⊙ Is the location of W - Component of velocity

Figure 3.9 Velocity boundary conditions for continuity equation

For these cells we have V(i,j,k) = 0 and W(i,j,k-1) = 0 (Figure 3.9 b). By incorporating these conditions the expression for divergence of these cells becomes

$$D_{i,j,k} = \frac{U_{i,j,k} - U_{i-1,j,k}}{\Delta X} - \frac{V_{i,j-1,k}}{\Delta Y} + \frac{W_{i,j,k}}{\Delta Z} \qquad (3.46)$$

(3) Cells adjacent to an inclined plane of symmetry.(such as the plane $ACC'A'$ in Figure 3.3)

For these cells we have V(i,j,k) = 0 and W(i,j,k) = 0 (Figure 3.9 c) and therefore the expression for divergence becomes

$$D_{i,j,k} = \frac{U_{i,j,k} - U_{i-1,j,k}}{\Delta X} - \frac{V_{i,j-1,k}}{\Delta Y} - \frac{W_{i,j,k-1}}{\Delta Z} \qquad (3.47)$$

(b) Velocity boundary conditions for the Navier-Stokes equation

The same approach is adopted while time-stepping the momentum equations as well. That is, the interior cells are treated separately using the discretised equations of MAC method without any changes. The cells along the boundaries are divided into a number of groups, and the discretised equations are modified to incorporate the boundary conditions applicable to each group. This procedure is repeated for all the groups. The steps involved are as follows.

(1) Identify the stencils of U, V, W components of velocity from the discretised equations of the MAC method.

(2) For a cell adjacent to a boundary surface, identify those velocity components of the stencil which lie on or outside the boundary surface.

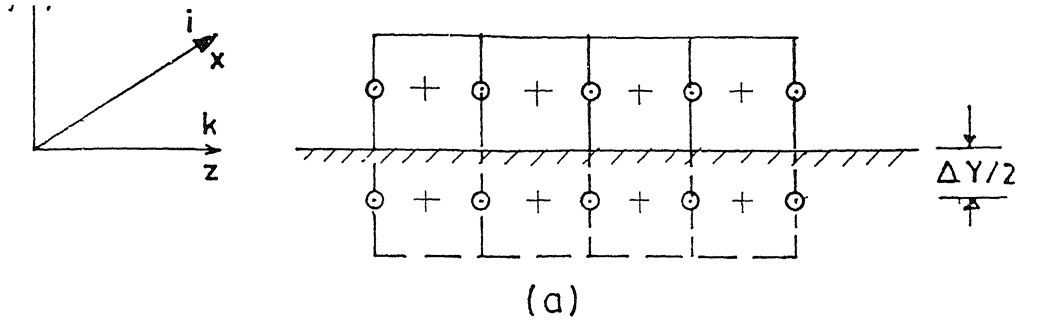

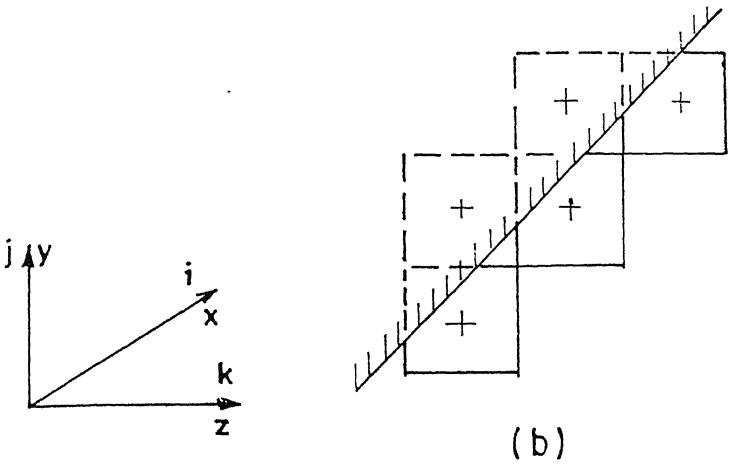

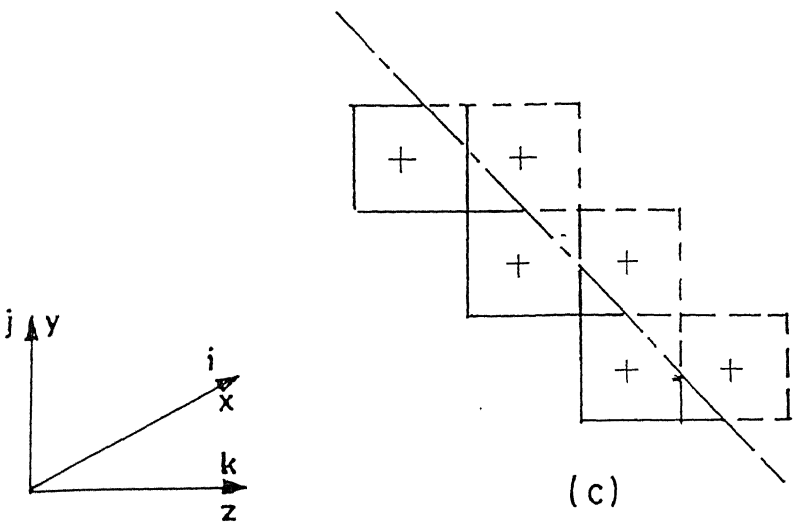

+ Is the location of U-component of velocity

⊙ Is the location of W-component of velocity

Figure 3.10 Velocity boundary conditions for N-S equations.

(3) Specify the appropriate values of these velocity components either directly or in terms of the velocity of an interior cell.

(4) Rewrite the discretised equations incorporating the boundary conditions of the group and use these modified equations for advancing the velocities of that particular group of cells.

Step no (3) of the above procedure involves the specification of velocity components lying outside the computational domain. The various cases which arise are explained below.

(1) Cells lying just above a horizontal no-slip boundary:

For these cells the velocity components U(i,j-1,k) and W(i,j-1,k) are located below the channel wall at a distance $\Delta Y/2$ (Figure 3.10 a).

By setting

$$U(i,j-1,k) = -U(i,j,k) \tag{3.48}$$

the condition U = 0 on the no-slip surface is implemented.. Similarly by setting

$$W(i,j-1,k) = -W(i,j,k) \tag{3.49}$$

the condition W = 0 on the no-slip surface is implemented.

(2) Cells adjacent to an inclined no-slip boundary:

For these cells the velocity components U(i,j,k-1) are located outside the flow domain on the other side of the channel wall (Figure 3.10b). By setting

$$U(i,j,k-1) = -U(i,j,k) \tag{3.50}$$

the no-slip boundary condition U = 0 is implemented along the inclined channel wall.

(3) Cells adjacent to an inclined plane of symmetry:

For these cells the velocity component U(i,j,k+1) lies outside the computational domain (Figure 3.10c). The condition of symmetry is enforced by setting

$$U(i,j,k+1) = (U(i,j-1,k) + U(i,j,k-1))/2 \qquad 3.51)$$

(c) Thermal boundary conditions for the energy equation

In the staggered grid arrangement used (Figure 3.7) there are no temperature points lying directly on any of the boundaries. Hence the value of temperature on the boundaries can not be directly specified. Instead the temperatures of cells lying just outside the computational domain are specified in such a manner that the required thermal boundary condition is enforced. The details of the different cell groups and their respective thermal boundary conditions are as follows.

Case 1. Uniform wall temperature.

(1) Cells just above a horizontal channel wall at temperature T_w

For these cells θ(i,j-1,k) lies just outside the boundary at a distance of ΔY/2 (Figure 3.11a). The boundary condition $\theta_w = 1$ is enforced by specifying

$$\theta(i,j-1,k) = 2 - \theta(i,j,k) \qquad (3.52)$$

This equation is derived by assuming a linear variation of temperature across the channel wall.

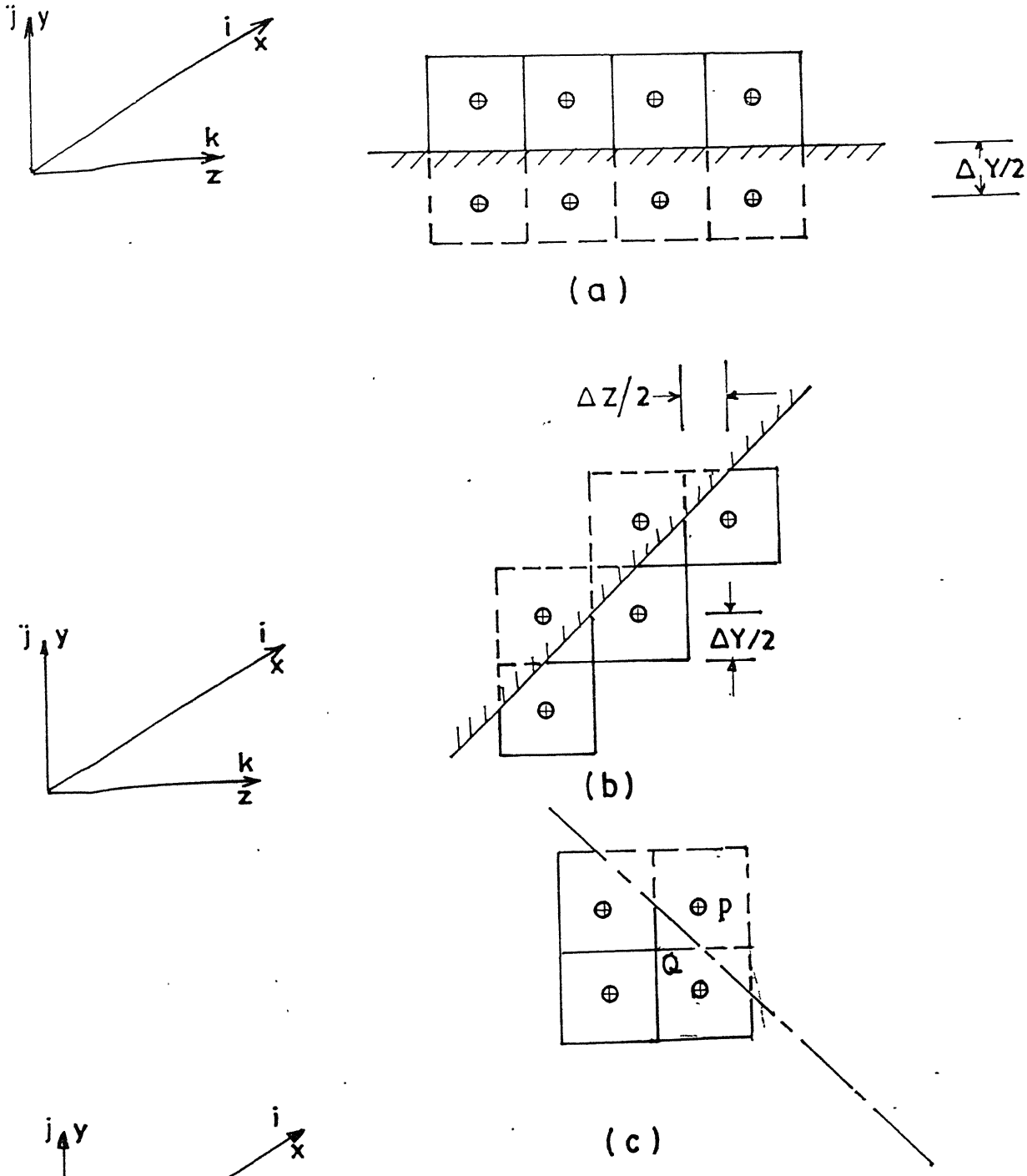

⊕ Is the location of temperature

Figure 3.11 Temperature boundary conditions for energy equat

This equation is derived by assuming a linear variation of temperature across the channel wall.

(2)Cells along an inclined channel wall at temperature T_w

For these cells θ (i,j,k-1) is located outside the flow domain (Figure 3.11b).

The condition $\theta_w = 1$ is enforced by specifying

$$\theta(i,j-1,k) = 2 - \theta(i,j,k) \tag{3.53}$$

This equation has been derived assuming a linear variation of temperature across the boundary.

(3) Cells adjacent to an inclined plane of symmetry:

For these cells $\theta(i,j+1,k)$ lies outside the computational domain and it must be specified in terms of the temperatures at the interior points. This is done as explained below. In Figure 3.11c the points P and Q must have the same temperature because they are equidistant from the plane of symmetry but lie on opposite sides of this plane. Whereas the point P is the location of $\theta(i,j+1,k)$ the point Q does not coincide with any temperature location. However the point Q lies exactly midway between the locations of $\theta(i,j+1,k-1)$ and $\theta(i,j,k)$. Therefore we have

$$\theta(i,j+1,k) = 0.5 *(\theta(i,j,k) + \theta(i,j+1,k-1)) \tag{3.54}$$

as the thermal boundary condition.

Case (2) Uniform wall heat flux:

(1) Cells along a horizontal channel wall.

For these cells $\theta(i,j-1,k)$ lies outside the flow domain. This can be specified as follows.

The boundary condition q_w = constant reduces to

$$\left(\frac{d\theta}{dY}\right)_{Y=0} = -1 \qquad (3.55)$$

for a horizontal wall losing heat in the positive Y direction. Using the discretisation

$$\left(\frac{d\theta}{dY}\right) = \frac{\theta(i,j,k)-\theta(i,j-1,k)}{\Delta Y} \qquad (3.56)$$

we get

$$\theta(i,j-1,k) = \theta(i,j,k) - \Delta Y \qquad (3.57)$$

(2) Cells along inclined channel wall:

For these cells θ(i,j,k-1) lies outside the flow domain and is specified as given below.

$$\theta(i,j,k-1) = \theta(i,j,k)+\theta(i,j-1,k-1)+\sqrt{2}\Delta Y \qquad (3.58)$$

3.5.2 Boundary conditions for vortex generator

A special effort is required to numerically implement the boundary conditions on the surface of the vortex generator. This section describes the procedure used for the same.

3.5.2.1 Velocity boundary conditions

The dimensions of the staggered grid are chosen according to the following relations

$$tan\beta = \frac{\Delta Y}{\Delta X}$$ in the case of the delta wing

$$= \frac{\Delta Z}{\Delta X}$$ in the case of delta winglet.

β being the angle of attack of the vortex generator. With this choice the plane of the delta wing passes through a set of U and V-velocity locations as shown in Figure 3.12; and the plane of the delta winglet passes through a set of U and W-velocity locations as shown in Figure 3.13. All these velocities are set to zero because the plane of the vortex generator is a no-slip surface..In the case of the delta wing the plane of the wing lies mid-way between pairs of adjacent W-velocity locations as shown in Figure 3.14. Hence at the time of advancing these W-velocities in the *predictor* step the W-velocity component lying on one side of the wing surface is set equal in magnitude and opposite in direction to its value on the other side. This is equivalent to setting the value of W-component of velocity on the wing surface equal to zero. In other words, by this procedure the no-slip boundary condition for the surface of the delta wing gets implemented. The same technique is adopted for the delta winglet as well, the only difference being that the plane of the winglet lies mid-way between pairs of adjacent V-velocity locations.

3.5.2.2 Temperature boundary conditions

The performance of the vortex generator is evaluated for two different temperature boundary conditions viz., (1) constant wall temperature and (2) Uniform wall heat flux. In the case of uniform wall heat flux the surface of the obstacle is not treated as a source of heat and thus no boundary condition is called for. In the case of uniform wall temperature the plane of the vortex generator passes mid-way between pairs of

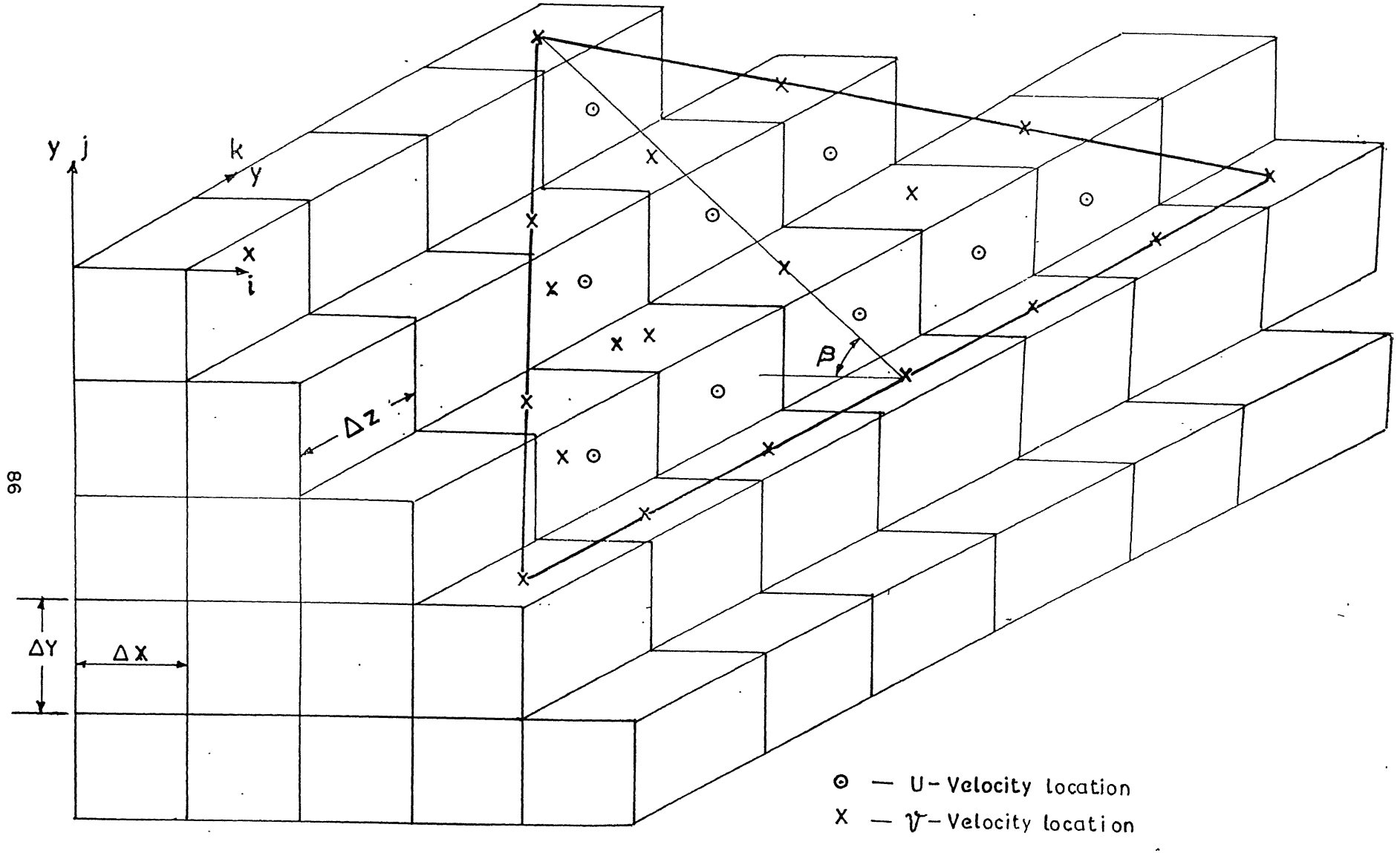

Figure 3.12 Velocity locations on the delta wing surface

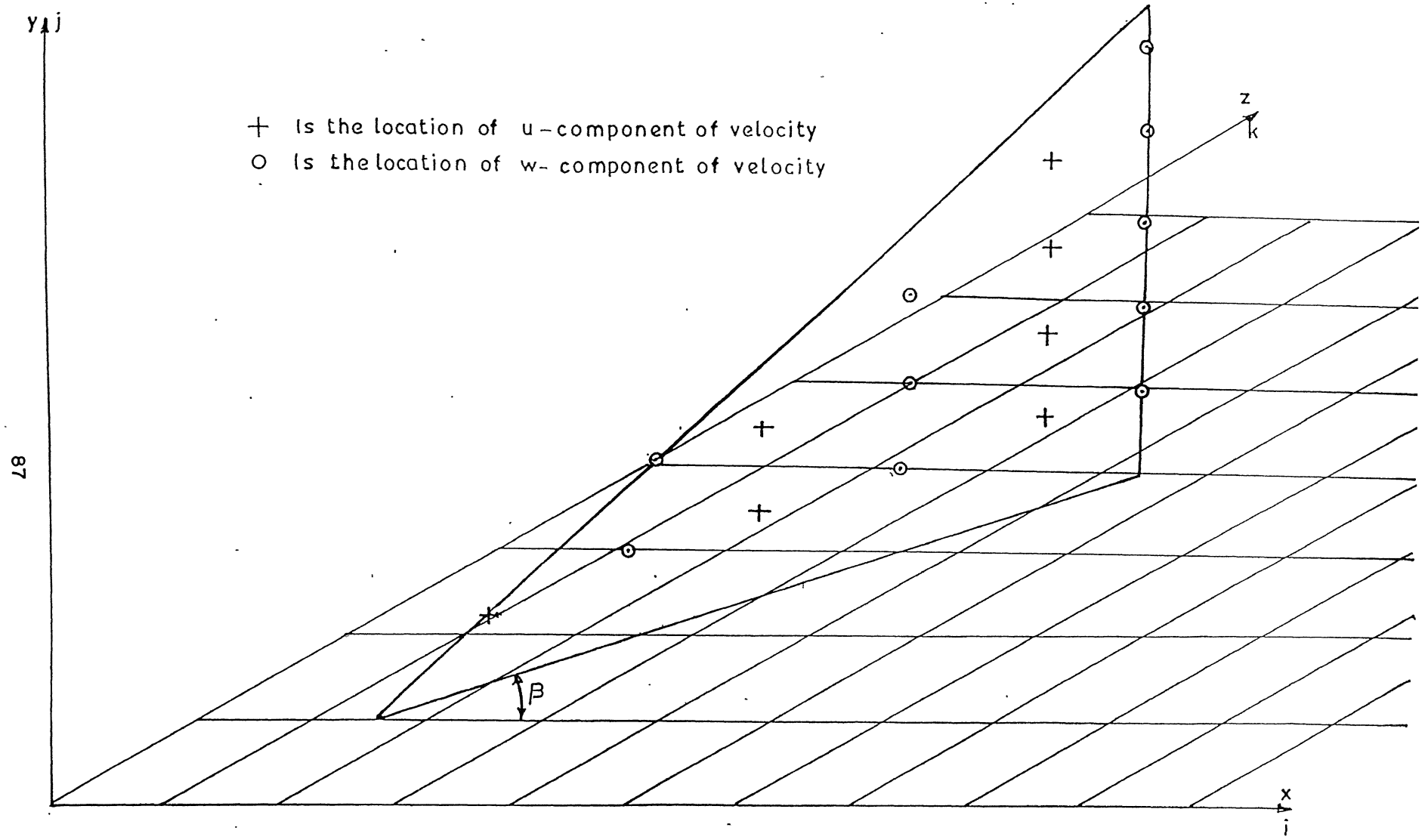

Figure 3.13 Velocity locations on the delta winglet surface

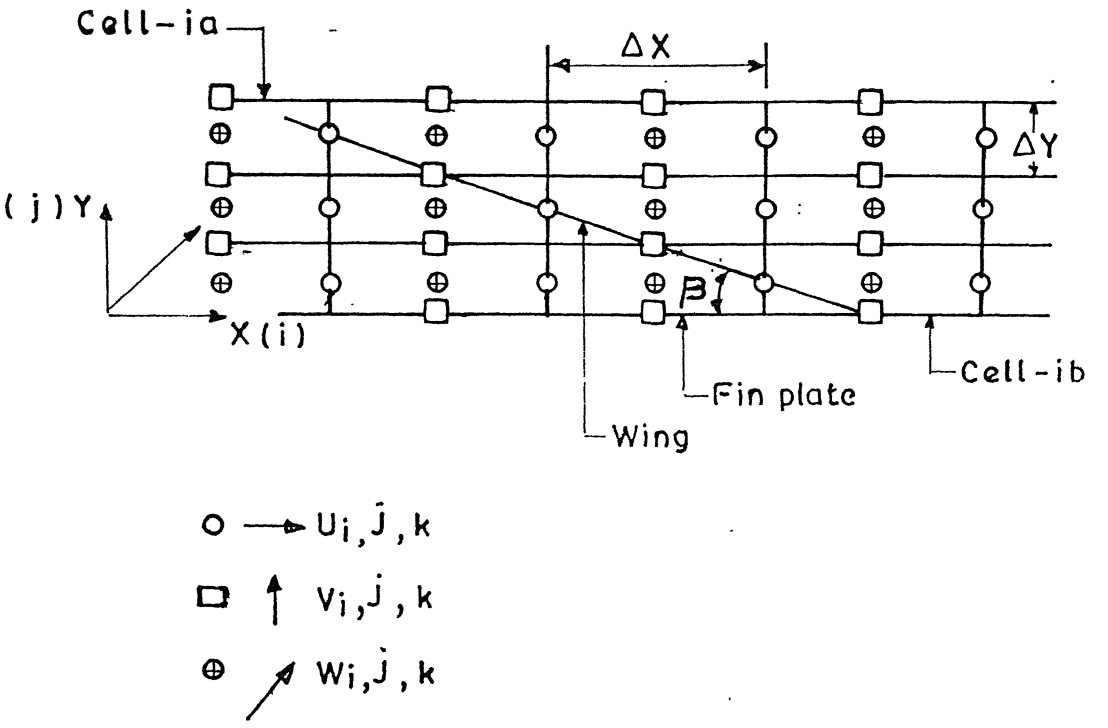

Figure 3.14 Relative location of velocity components and delta wing on X-Y plane

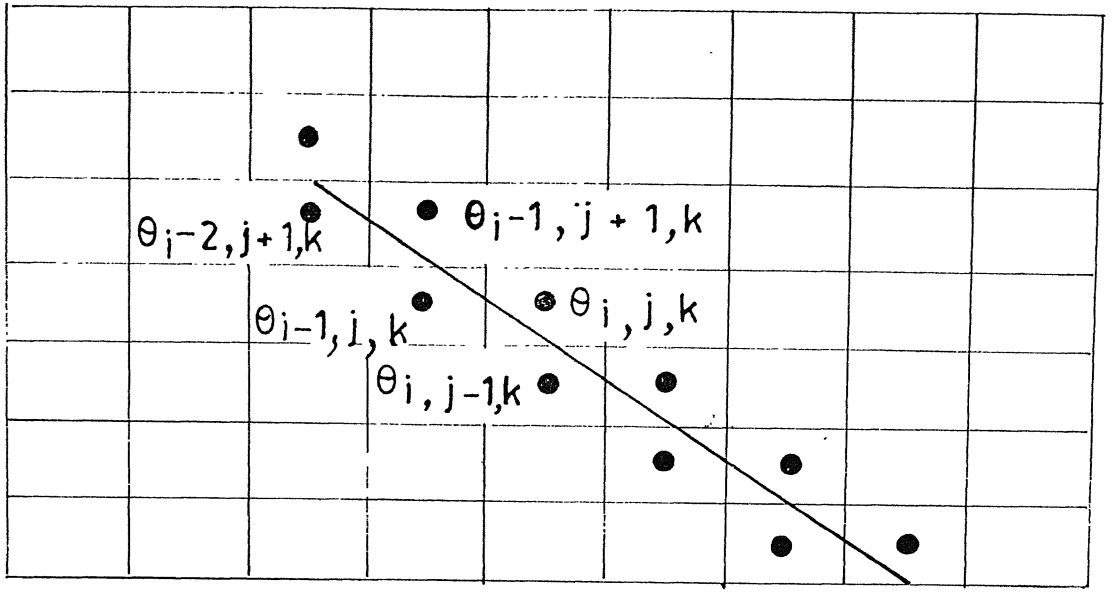

Figure 3.15 Thermal boundary conditions for the delta wing.

adjacent temperature locations as shown in Figure 3.15. The condition $\theta_w = 1$ along the surface of the vortex generator is enforced by setting the sum of the temperatures lying on opposite sides of this surface equal to 2. For example while computing $\theta_{i,j,k}$ the temperature locations which lie on the other side of the plane of the delta wing are specified as

$$\theta_{i,j-1,k} = 2 - \theta_{i,j,k} \tag{3.59}$$

$$\theta_{i-1,j,k} = 2 - \theta_{i,j,k} \tag{3.60}$$

This procedure is adopted for computing all the temperatures lying next to the surface of the vortex generator.

3.6 Spatial Grid Independence

Computations have been carried out for three different grids, viz., (1) 30× 10 ×20; (2) 60 × 20 ×40 ; and (3) 90 ×30 × 60. The grids are specified in the x, y, z directions respectively. The difference between the extrapolated grid-independent average Nusselt number and the average Nusselt number obtained for 60 × 20 × 40 grid mesh is less than 4 percent. Finally, all the computations were performed using a 60 × 20 × 40 grid-mesh. Computations were performed on a DEC-Alpha 255 (233 MHz) workstation.

3.7 Comparision of Results based on Model Problem

The discretization scheme used for computation was tested on a model problem of flow in a lid-driven square cavity. The computational domain consists of a two dimensional lid-driven square cavity with no slip and impervious boundary conditions at the bottom and side walls except at the top, where u is non zero constant and equal to ULID. In the governing equations the velocities have been non dimensionalised with respect to ULID. All lengths have been scaled with respect to the cavity height H and the Reynolds number is defined as Re = (ULID.H)/ν. Figure 3.16 shows the variation of U velocity along the vertical mid plane for this problem. The result is compared with the computational results of Ghia et.al (1982). It may be mentioned that Ghia et.al. adopted a 129 x 129 mesh with multigrid technique. However, the present computation on a 51 x 51 grid shows good agreement with the results of Ghia et al. as seen in Figure 3.16. The minimum U-velocity position and the variation of U-velocity match well.

The problem of flow over a delta wing placed inside a rectangular channel was also solved using this code. Figures 3.17, 3.18 and 3.19 show the results of this computation. Figure 3.17 (a) (b) and (c) show the generation of vortices and their movement in the downstream. Figure 3.17 (a) shows the presence of vortical structure over three different horizontal planes. The secondary flow on several cross-stream planes are shown in Figure 3.17(b). Velocity vectors on three different longitudinal sections (x-y planes) are shown in Figure 3.17 (c).

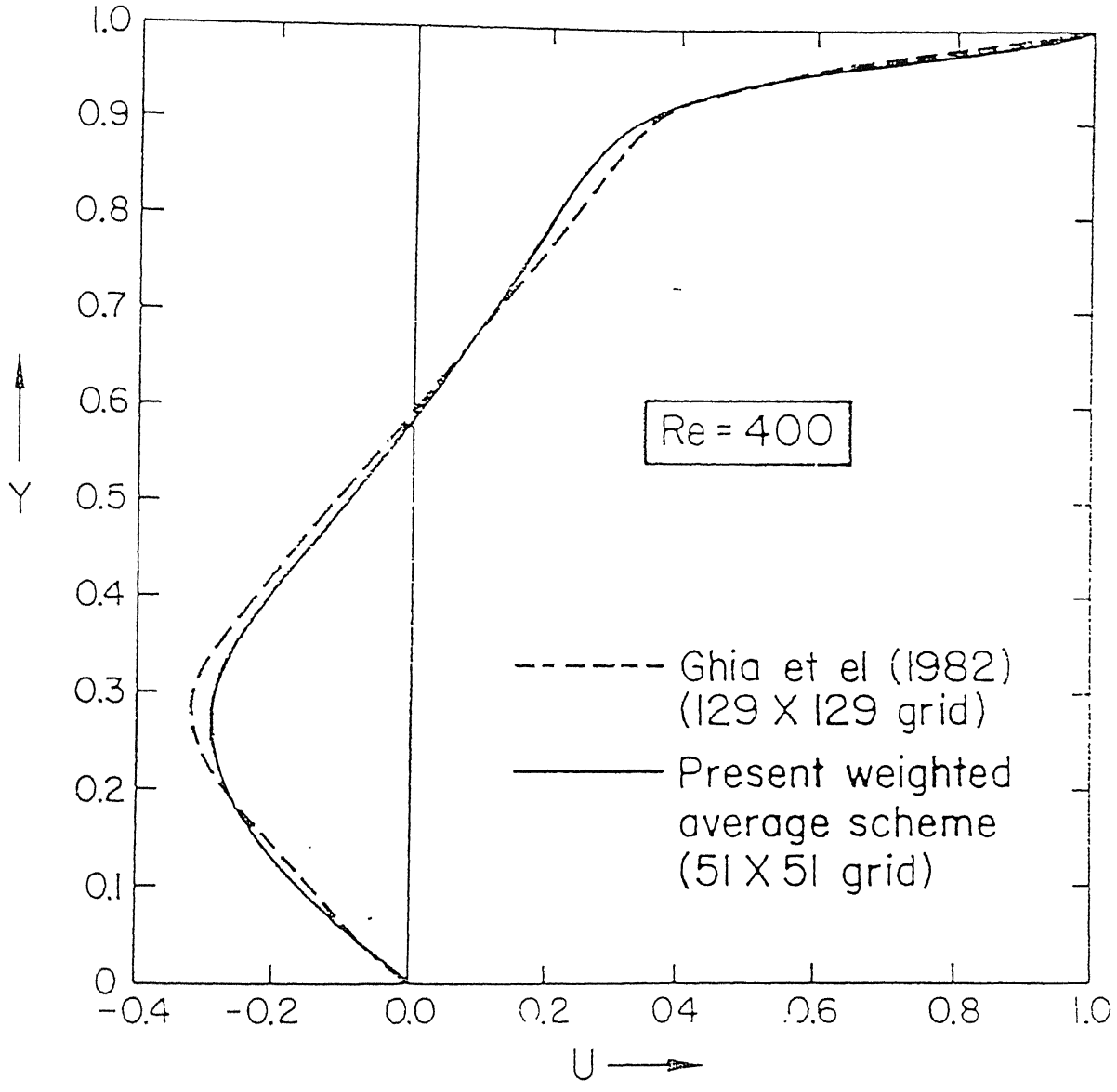

igure 3.16 Variation of U velocity along the vertical midplane for the lid driven flow in a square cavity

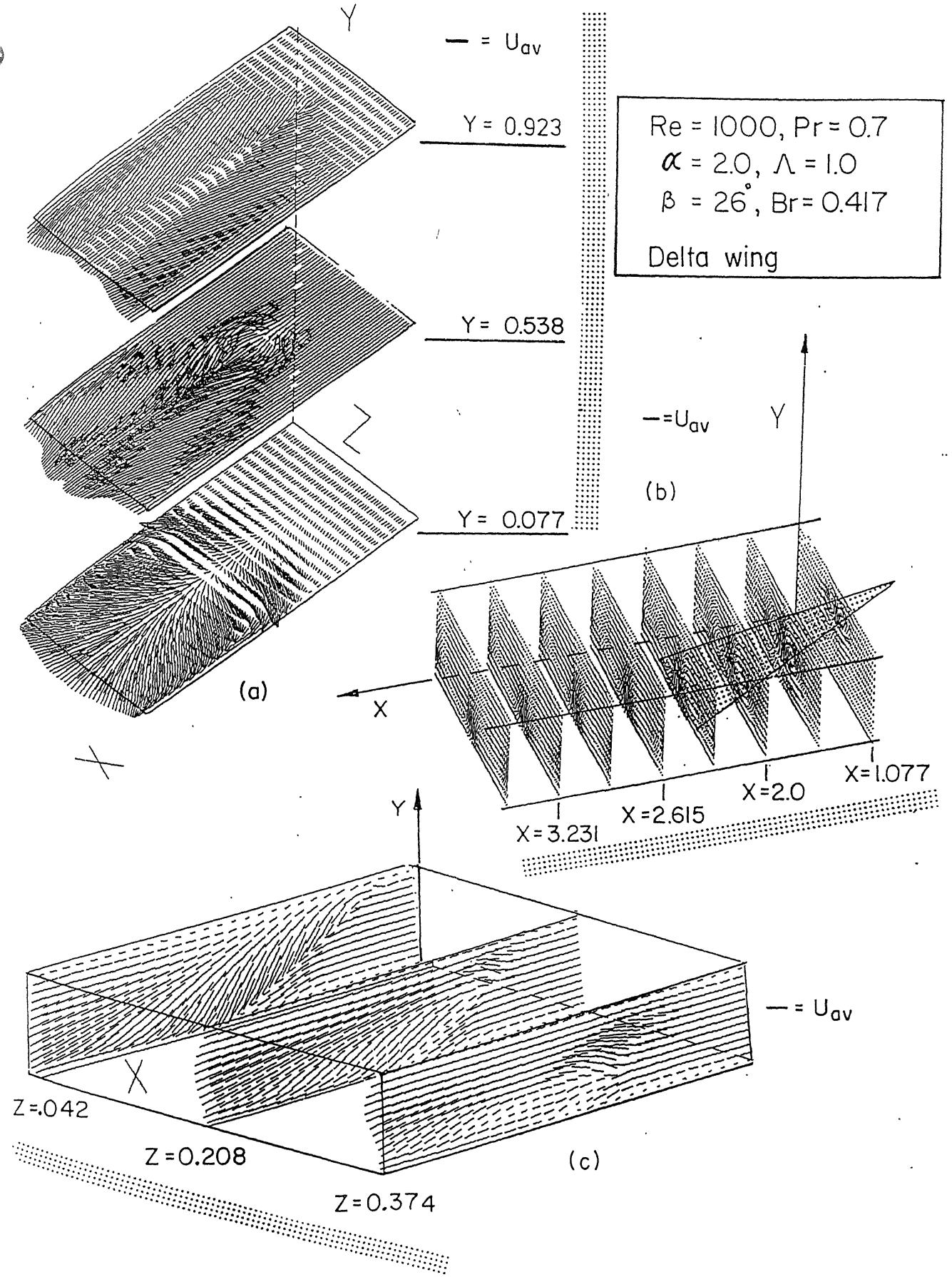

Figure 3.17 Vortex structure generated by a delta wing

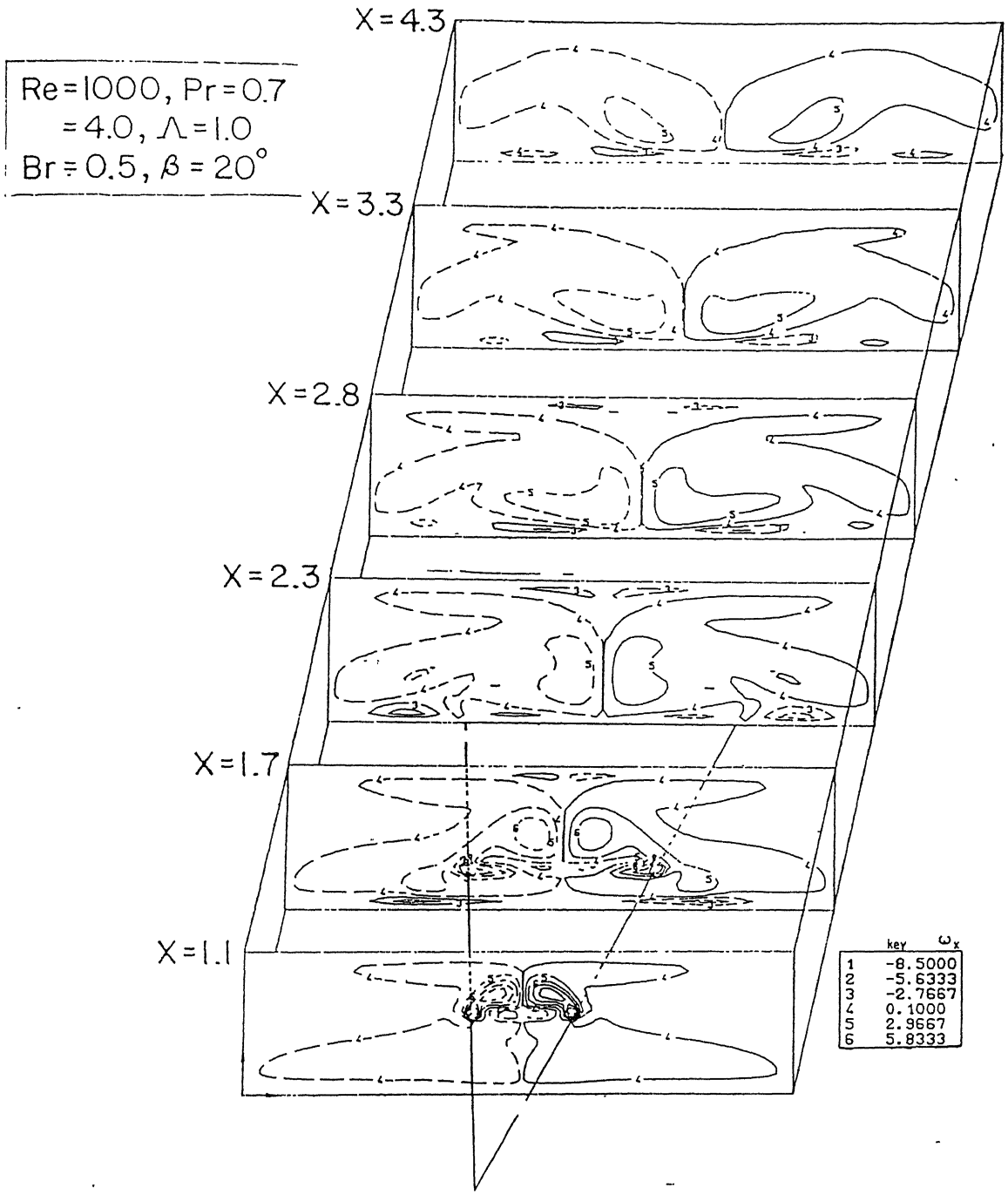

Figure 3.18 Contours of normalized vorticity

Figure 3.18 shows the normalised vorticity contours in a channel for a built-in delta wing with an angle of attack of 20°. The dotted lines indicate negative vorticity. Peak vorticity occurs at the vortex centres. The constant axial velocity lines at two different locations downstream of a delta wing ($\beta = 15^{\circ}$)inside a channel have been shown in Figure 3.19. The counter-rotating vortices lead to a thinning of the velocity boundary layer in the downwash region. The thickening of the boundary layers at the symmetry-planes is also evident from this figure.

Re = 1000

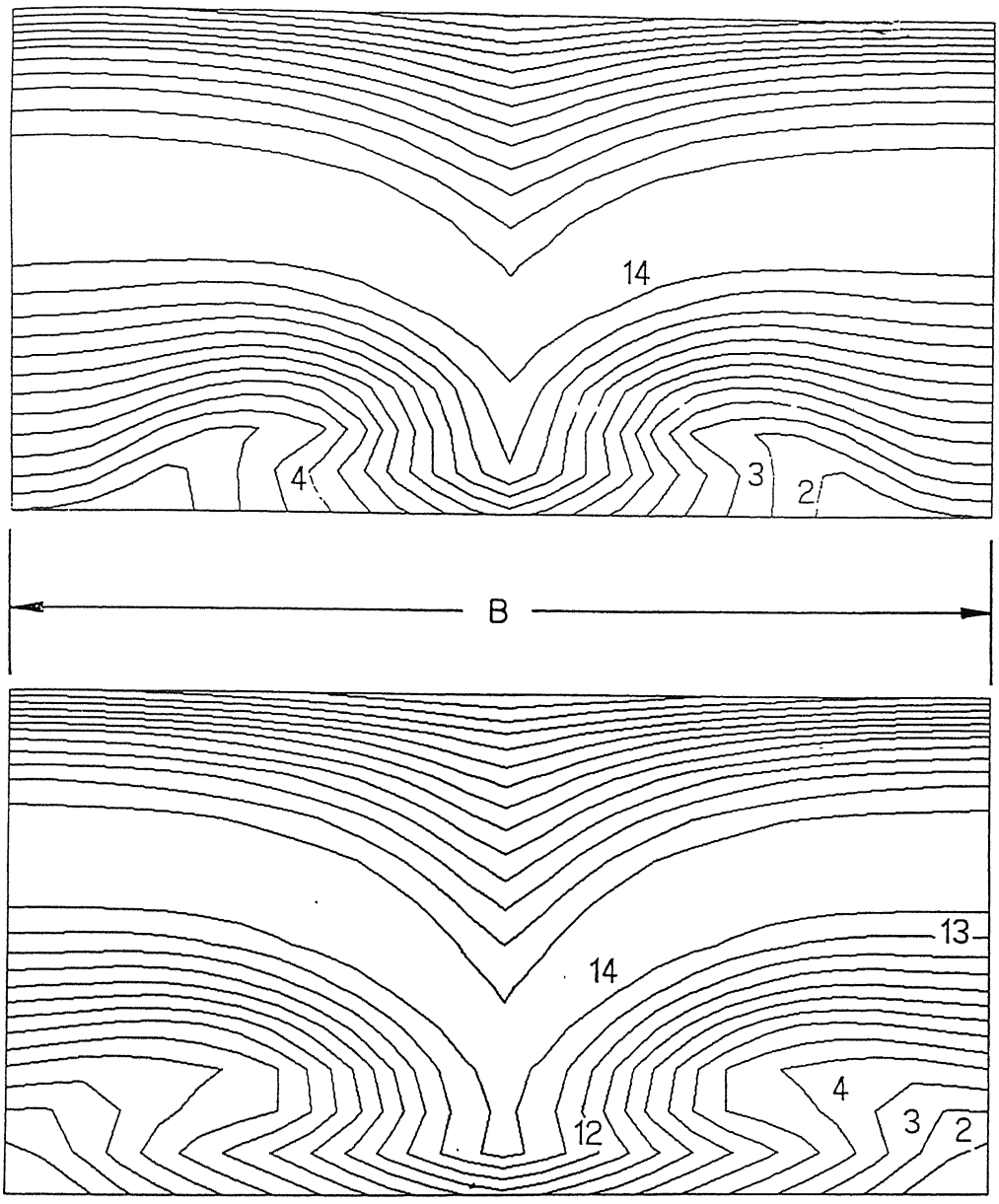

1. .22987643
2. .32957286
3. .42926928
4. .52896571
5. .62866217
6. .72835857
7. .82805502
8. .92775148
9. 1.02744790
10. 1.12714430
11. 1.22684070
12. 1.32653710
13. 1.42623360
14. 1.52593000

(a)

1. .29431856
2. .38809714
3. .48187569
4. .57565427
5. .66943288
6. .76321137
7. .85698998
8. .95076853
9. 1.04454700
10. 1.13832560
11. 1.23210430
12. 1.32588260
13. 1.41966120
14. 1.51343980

(b)

$\Lambda = 1.0, \beta = 15, \alpha = 2.0$, Br = 0.357

(Figure 3.19)

Isolines for axial velocity at two different cross-stream planes (a) 0.58 wing-chord downstream and (b) 1.74 wing-chord downstream of a delta wing.

Chapter 4

Performance of the Delta Winglet

4.1 Introduction

The velocity and temperature fields in a triangular channel with a built-in delta winglet have been obtained in the form of numerical solutions to the governing equations, using the MAC algorithm. The computations were done for different thermal boundary conditions, different angles of attack and different Reynolds numbers. It is however necessary to express the performance of the winglet in terms of quantities in which the heat exchanger designer will be primarily interested viz.,

(1) the levels of heat transfer enhancement, and (2) the associated increase in pumping power. This chapter presents the procedure used for evaluating these quantities. Performance parameters such as the spanwise averaged Nusselt number and the normalised wall temperature are defined, in terms of which the heat transfer in the bare channel (a channel without any vortex generator) is compared with that in a channel having a delta winglet.

4.2 Vortex formation by delta winglet

It is instructive to study the flow structure in a triangular channel with a delta winglet as it reveals some new aspects of the physics of flow over a vortex generator. The secondary flow at different sections along and behind the winglet, for a Reynolds number of 100 and an angle of attack of 15^0, are shown in Figures 4.1 and 4.2. The symbol X in these figures stands for the distance in units of H ('H' being the characteristic length dimension) from the duct entrance. The winglet extends from X = 2.639 to X = 3.694. It is seen that the vortex strength increases along the length of the winglet and decreases gradually downstream of the winglet.

Figure 4.3 shows the velocity field at various sections normal to the duct axis for the case of flow through a bare duct, i.e., a duct without the winglet, for a Reynolds number of 20. It is observed that at sections next to the inlet, fluid moves away from the no-slip boundaries BC and AB (on the left and bottom) towards the duct axis of symmetry AC (on the right). This can be explained as follows. At the entrance to the duct we have a uniform U-velocity profile. (the V and W components of velocity are zero at the entrance). But the fully developed U-velocity profile is roughly parabolic with the maximum value occurring at the centre as seen in Figure 4.4.. For this change in the U-velocity profile, from a constant profile at the inlet to a parabolic profile at a downstream section, mass must shift away from the walls of the duct towards its axis and the line of symmetry AC. What is seen in Figure 4.4 is precisely such shifting of mass.

Figure 4.5 shows the secondary flow at various sections along the duct having an attached winglet at an angle of attack of 15^0 for a low Reynolds number of 20. If we compare the secondary flow at section X = 3.43 with that at X = 5.01, it appears as if the sense of rotation of the vortices has changed from counterclockwise to clockwise. Actually, as a

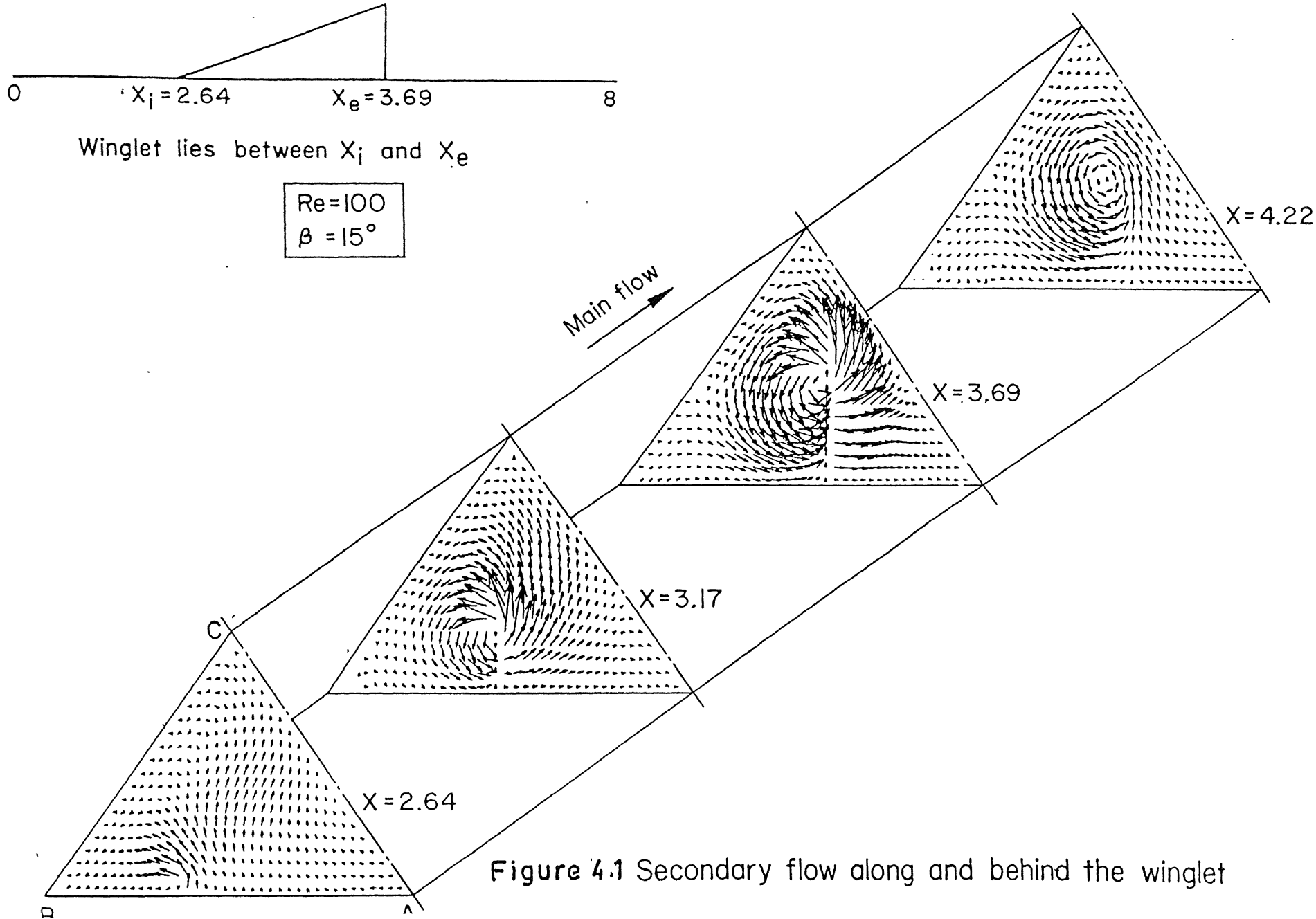

Figure 4.1 Secondary flow along and behind the winglet

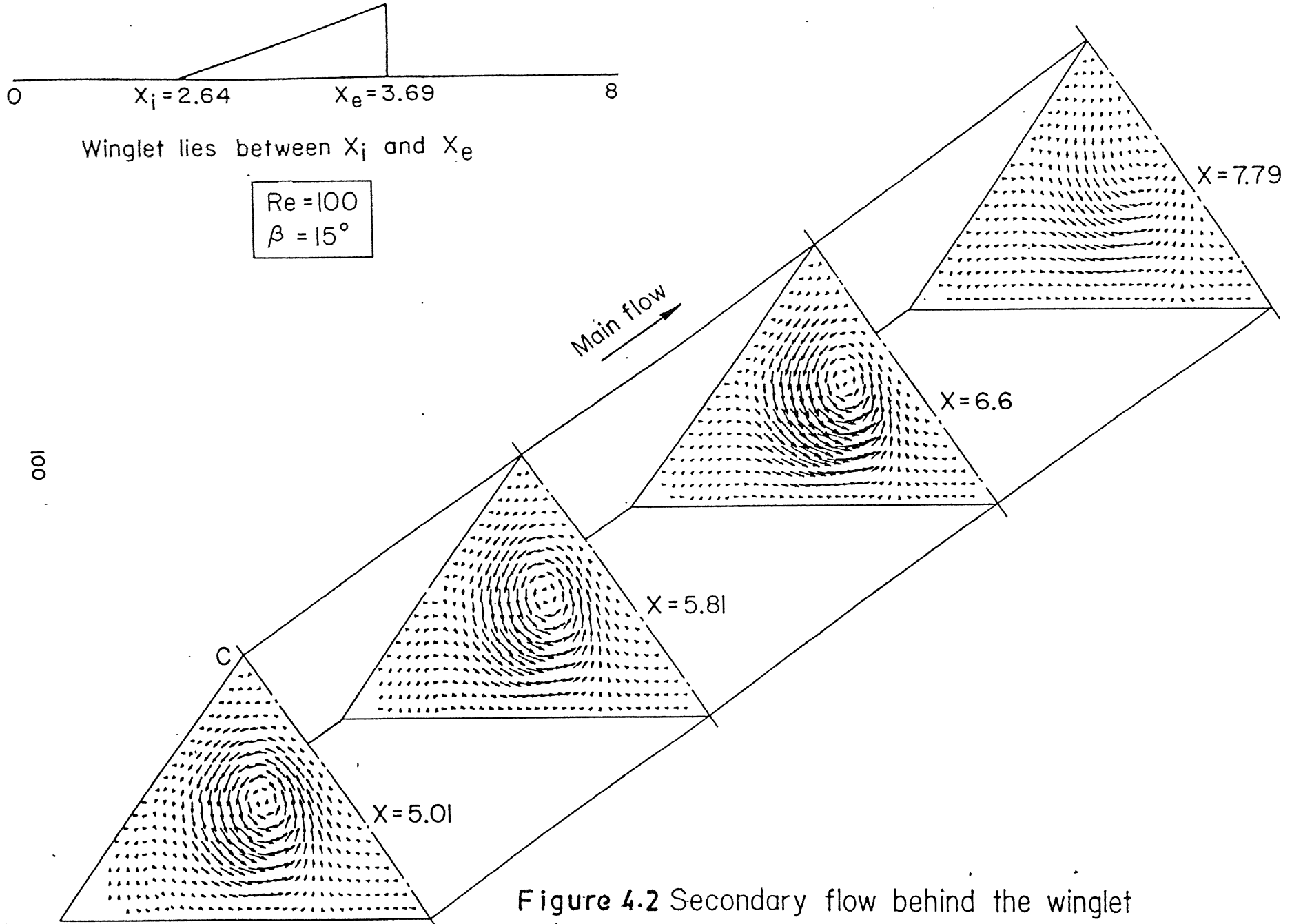

Figure 4.2 Secondary flow behind the winglet

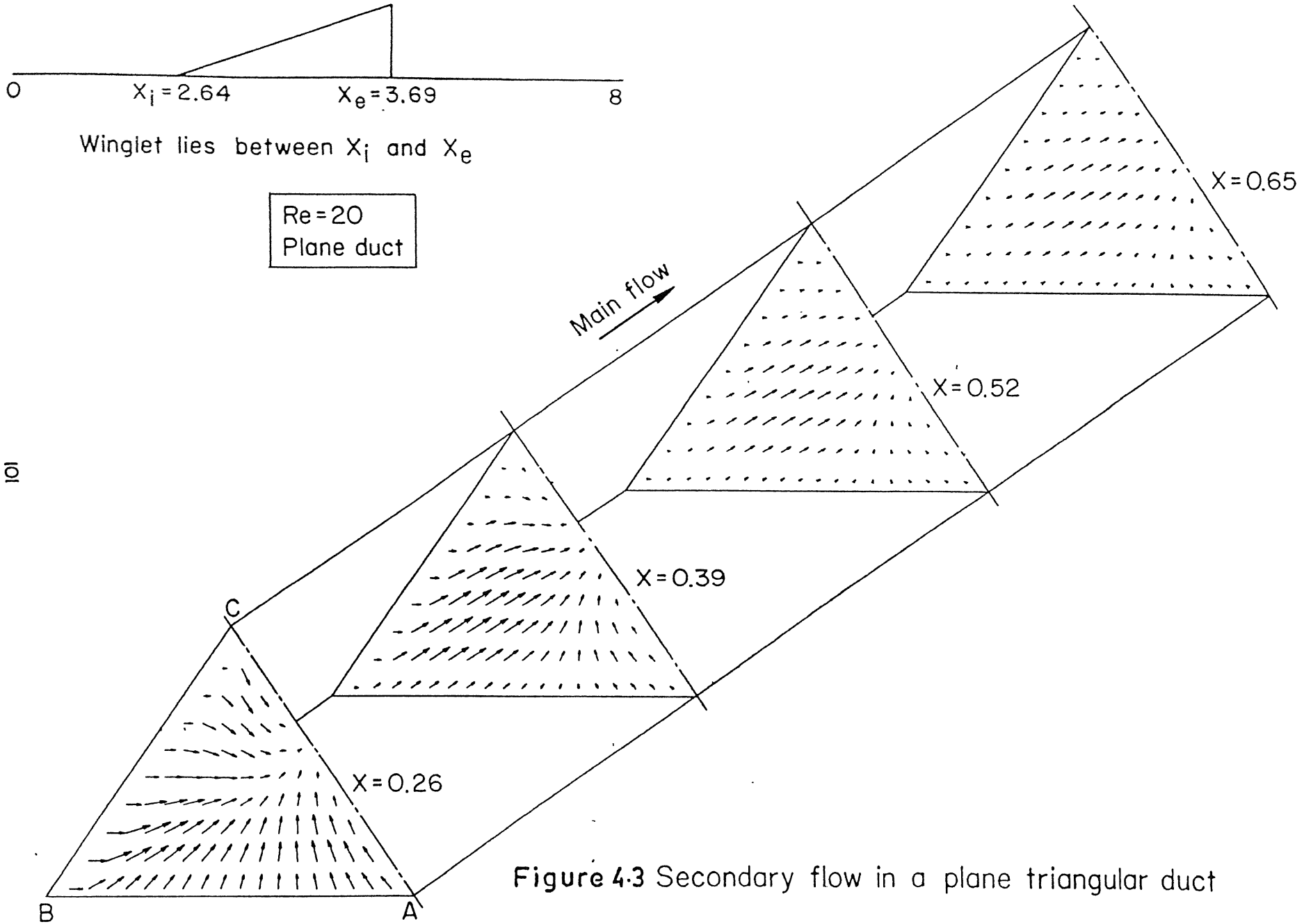

Figure 4.3 Secondary flow in a plane triangular duct

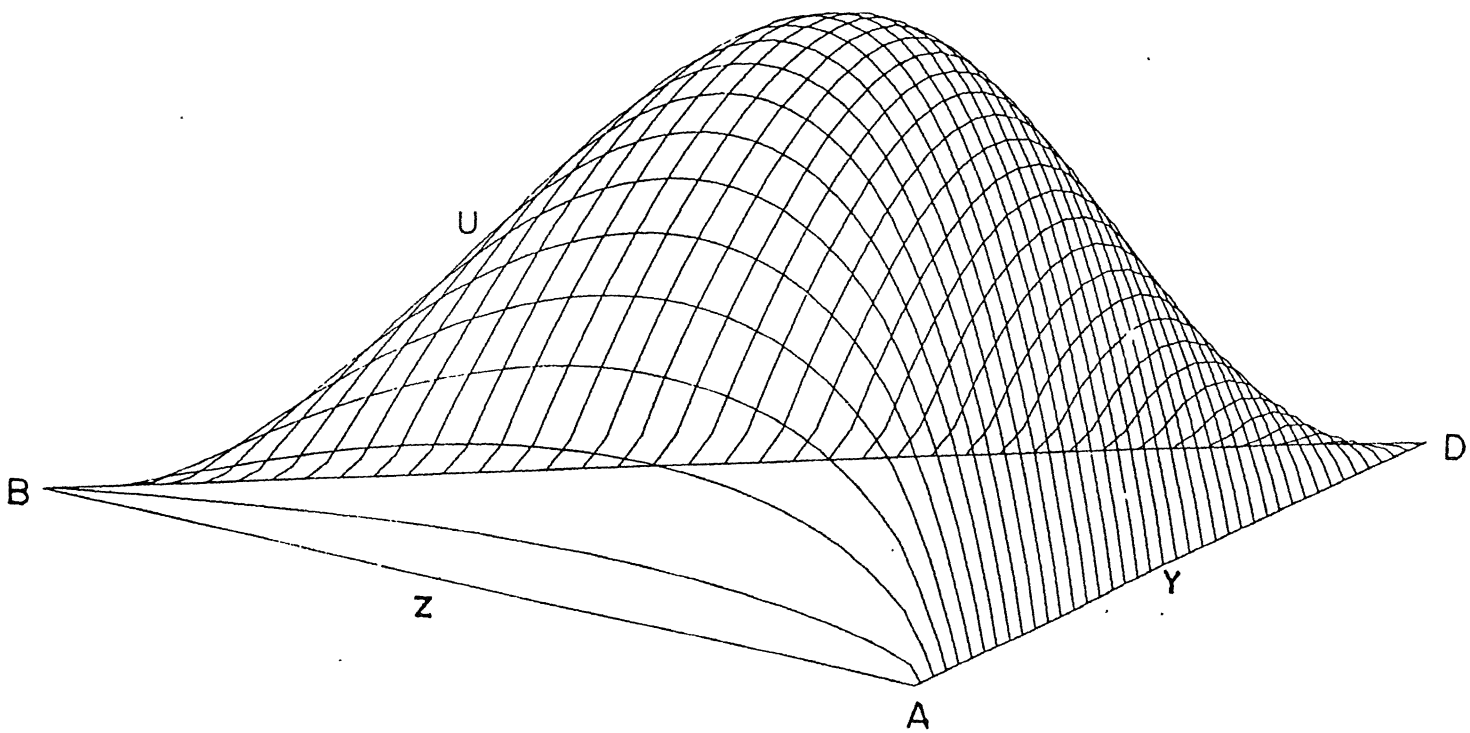

Figure 4.4 Fully developed velocity profile in the triangular duct.

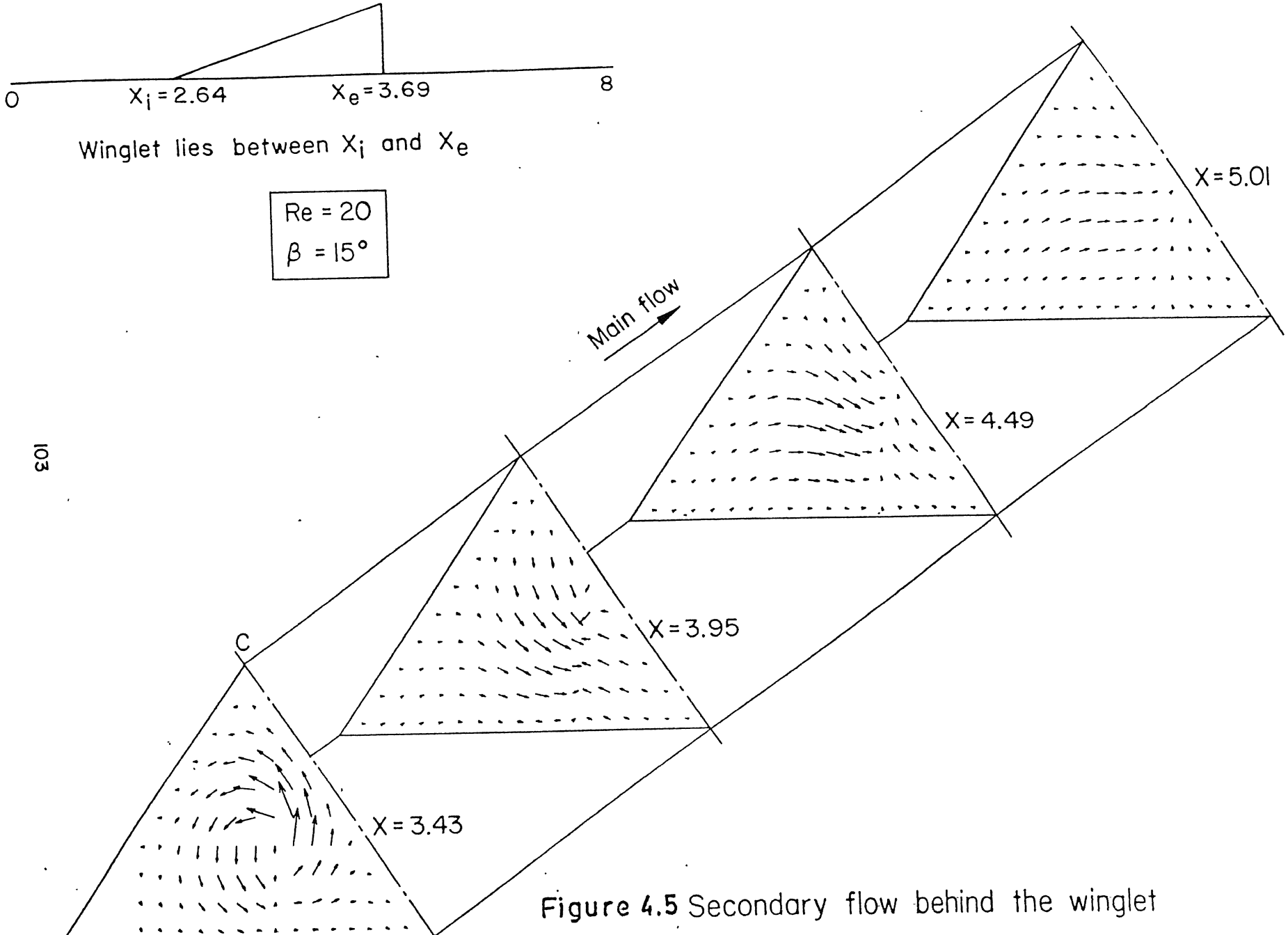

Figure 4.5 Secondary flow behind the winglet

closer study shows, no such switching is taking place behind the winglet. At the section X = 5.01, which lies downstream of the winglet, there is flow from the duct walls towards the duct axis, which is the adjustment due to the no-slip walls as explained earlier. This flow overwhelms the now-weak vortex and creates an illusion of a switch in the sense of the vorticity. In order to confirm this interpretation, the orientation of the winglet was changed and the flow field was recomputed. Again the apparent switching was observed between the sections at X = 3.43 and X = 5.01, this time from clockwise to anti-clockwise.

At higher Reynolds numbers the vortices generated by the winglet are much stronger and hence the apparent switching is not observed within the duct length. But it was also observed using a longer duct for a higher Reynolds number. The secondary flow pattern in the case of the winglet with stamping is shown in Figures 4.6 and 4.7. The gradual development of a vortex along the length of the winglet is clearly seen in these figures. At the section X = 4.75, as shown in Figure 4.7, it is observed that the counterclockwise rotating vortex in the upper half of the duct has induced a weak clockwise rotating vortex in the lower half as a result of flow across the stamping.

4.3 Heat Transfer

In order to evaluate the performance of the winglet the following parameters are computed. The bulk temperature of the fluid, is defined as

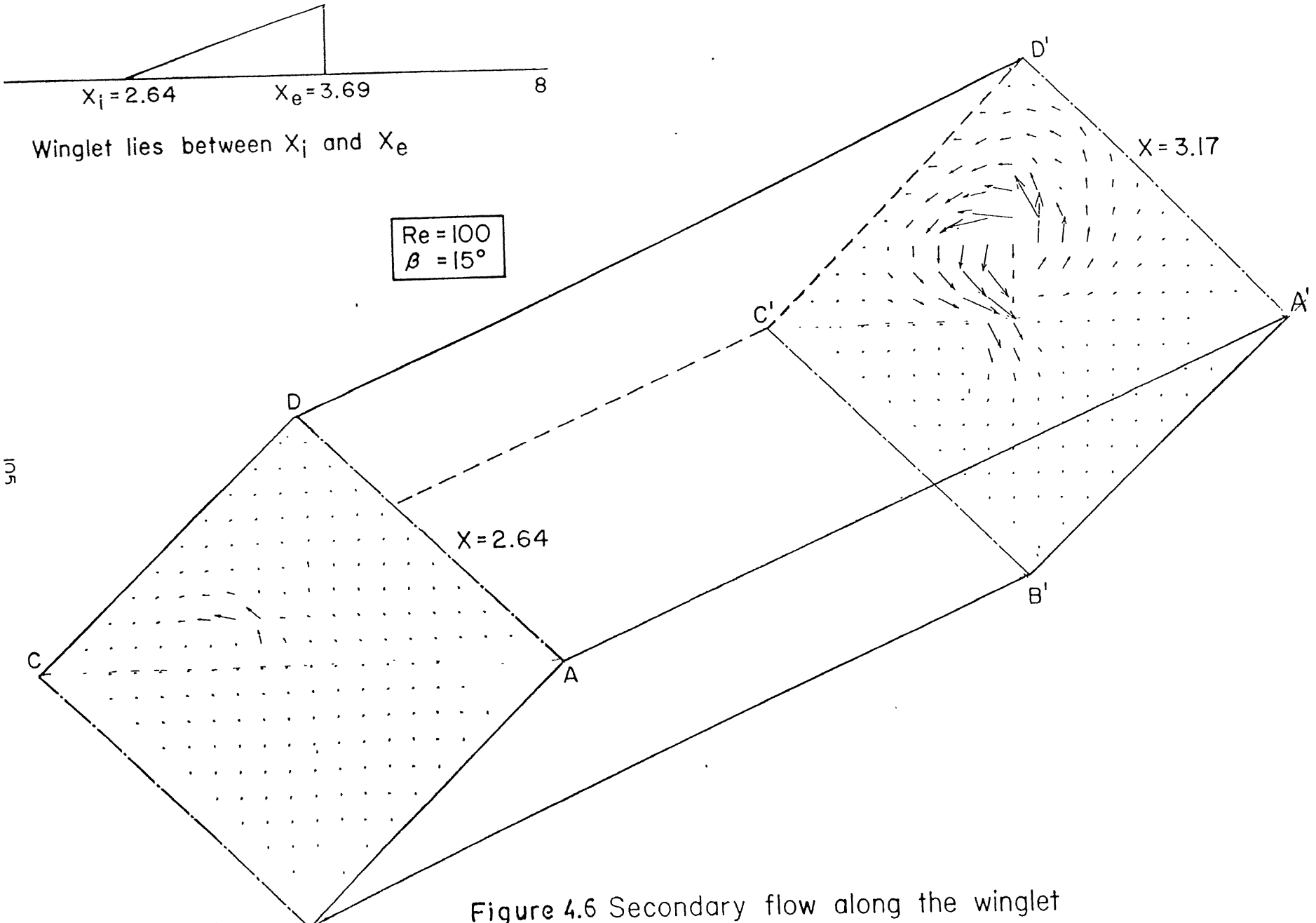

Figure 4.6 Secondary flow along the winglet

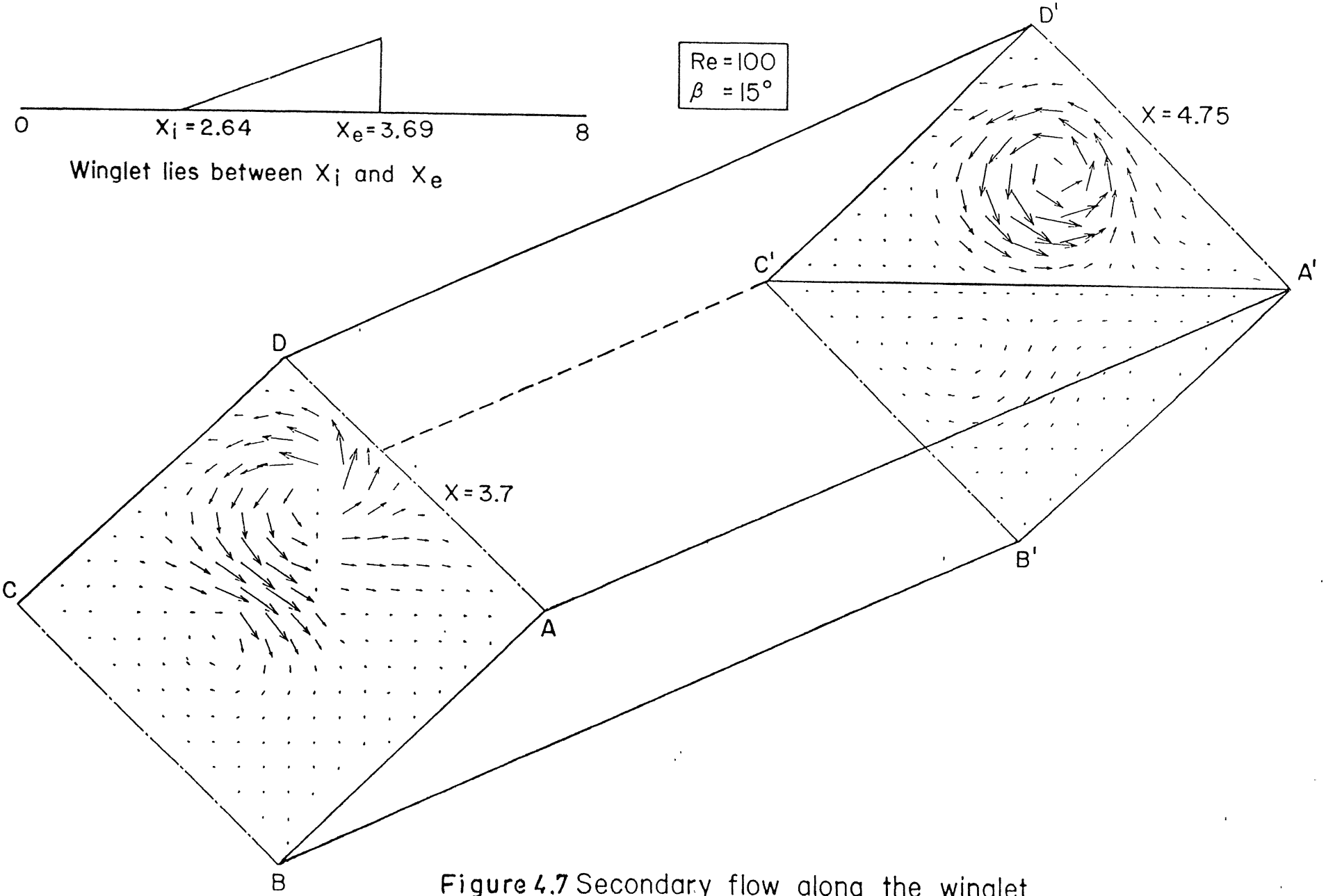

Figure 4.7 Secondary flow along the winglet

$$\theta_b(x) = \frac{\left(\int_{A_c} |U|\,\theta\, dA_c\right)}{\left(\int_{A_c} |U|\, dA_c\right)} \tag{4.1}$$

where, A_c is the area of cross section. It is computed using

$$\theta_b(x) = \frac{\left(\sum U\theta\right)}{\left(\sum U\right)} \tag{4.2}$$

where the summation is done across the cross section of the duct. Whereas the bulk temperature of the fluid is a measure of its thermal energy, the efficacy of the heat transfer process is characterised by the Nusselt number. The appropriate expression for computing the local Nusselt number can be derived as under.

Case (1) Isothermal walls.

By definition,

$$Nu = (h.L)/k \tag{4.3}$$

'L' being the characteristic length dimension. (L = H, the distance between adjacent plates of the heat exchanger in the present problem.) The wall heat flux is given by

$$q'' = -k\left(\frac{\partial T}{\partial y}\right) = h.\left(T_w - T_b\right) \tag{4.4}$$

where T_w = wall temperature (C); and T_b = bulk temperature of the fluid (C).

From equations (4.3) and (4.4) we can write

$$Nu = \left(\frac{H}{T_h - T_w}\right)\left(\frac{\partial T}{\partial y}\right) \tag{4.5}$$

Invoking the length and temperature scales of the problem we get

$$\frac{\partial T}{\partial y} = \left(\frac{T_w - T_\infty}{H}\right)\left(\frac{\partial \theta}{\partial Y}\right) \tag{4.6}$$

Therefore the local Nusselt number is given by

$$Nu = \frac{\left(\partial\theta/\partial Y\right)}{\left(\theta_h - \theta_w\right)} \qquad \text{(isothermal walls)} \tag{4.7}$$

at any point along the walls where θ_b is the bulk temperature at the section and θ_w is the wall temperature.

Case (2). Uniform wall heat flux

In this case the dimensionless temperature is defined as

$$\theta = \frac{T - T_\infty}{\left(q_w H/k\right)} \tag{4.8}$$

Proceeding as before we get

$$Nu = \frac{hL}{k}; \quad q_w = h\left(T_w - T_b\right) \tag{4.9}$$

or

$$Nu = \frac{q_w}{\left(T_w - T_h\right)}\left(\frac{H}{k}\right) \tag{4.10}$$

and from eq. (4.8) we get

$$Nu = \left(\theta_w - \theta_b\right)^{-1} \qquad \text{(uniform wall heat flux)} \qquad (4.11)$$

The spanwise average Nusselt number $\overline{Nu_{sa}}$ is given by

$$\overline{Nu_{sa}} = \frac{H}{kP} \frac{\left(\int_P q_w \, dP\right)}{\left(T_b(x) - T_w(x)\right)} \qquad (4.12))$$

where P is the perimeter of the channel cross section, dP is a line element along the periphery, H is the characteristic length dimension and k is the thermal conductivity of the fluid. It is computed by averaging the local Nusselt number all around the periphery of the duct at each section.

4.3.1 Isothermal walls

(a) Performance of the winglet without stamping

It is well known that at the entrance (X < 2.0) the Nusselt number is very high due to the large temperature difference between the incoming fluid and the channel walls .The thermal boundary layer is also very thin in this region. The actual effect of the winglet is revealed at the portion of the duct downstream of the winglet. To put the enhancement effect in the right perspective, all figures focus on the portion of the duct behind the winglet. Figures 4.8 and 4.9 show the variation of bulk temperature and the distribution of combined spanwise average Nusselt number respectively for a Reynolds number of 100 for different angles of attack for the case of isothermal walls. At any section behind the winglet the bulk temperature is higher when the winglet is used. This is a direct measure of the enhanced heat transfer due to the delta winglet. Further, the bulk temperature increases with increasing angle of attack because

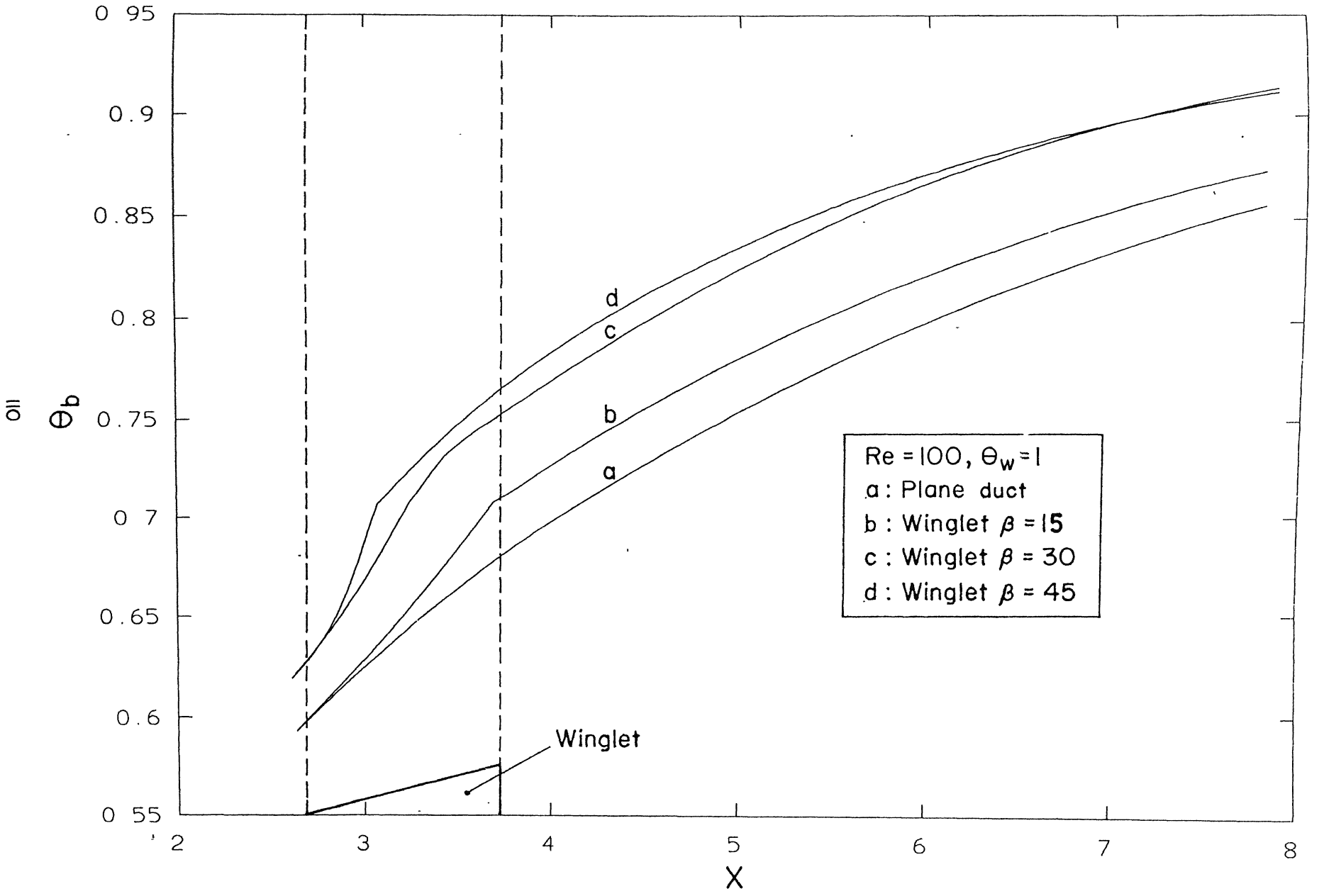

Figure 4.8 Variation of bulk temperature in the channel

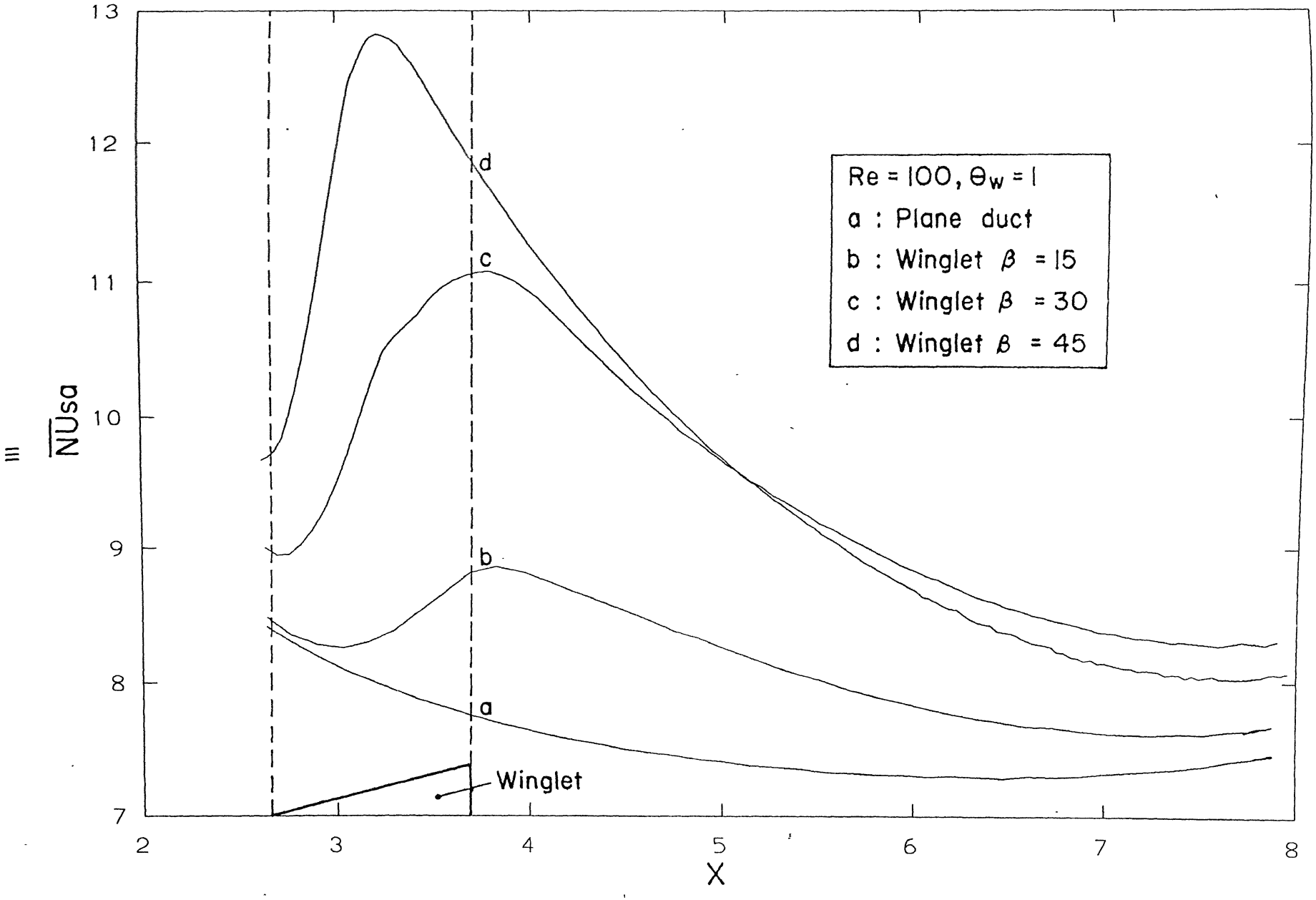

Figure 4.9 Distribution of combined spanwise average Nusselt number in the channel

the strength of the vortices generated by the winglet increases with β (though there is a proportionate increase in the pumping power).

Figure 4.9 shows that the combined spanwise average Nusselt number increases steadily along the vortex generator length and then decreases. The heat transfer enhancement effect of the winglet is clearly evident. The ultimate objective of using vortex generators is to design a more compact heat exchanger. A measure of the compactness achievable by the use of delta winglets can be had by comparing the lengths of the channel required to attain the same exit bulk temperature. The necessary exchanger length for attaining an exit bulk temperature of, say, 0.8 is shown in the following table.

Table 1: Percentage Reduction in length of the exchanger

Geometry	Exchanger length	% Reduction
Plane duct	6.1	-
Duct with Winglet ($\beta = 15^0$)	5.85	4.0
Duct with Winglet ($\beta = 30^0$)	5.1	16.4
Duct with Winglet ($\beta = 45^0$)	4.9	19.67

It can be seen that using a single pair of delta winglets, a substantial (upto 20 percent) decrease in the channel length (exchanger length) can be achieved.

The variation of bulk temperature and the distribution of combined spanwise average Nusselt number in the channel for a Reynolds number of 200 are shown in Figures 4.10 and 4.11 respectively. The trends are identical to those for Re = 100. Results for a Reynolds number of 200 are compared with those of 100 in Figures 4.12 and 4.13.. These figures reveal the fact that while higher Nusselt numbers are achieved with higher Reynolds numbers, the exit bulk temperature decreases with

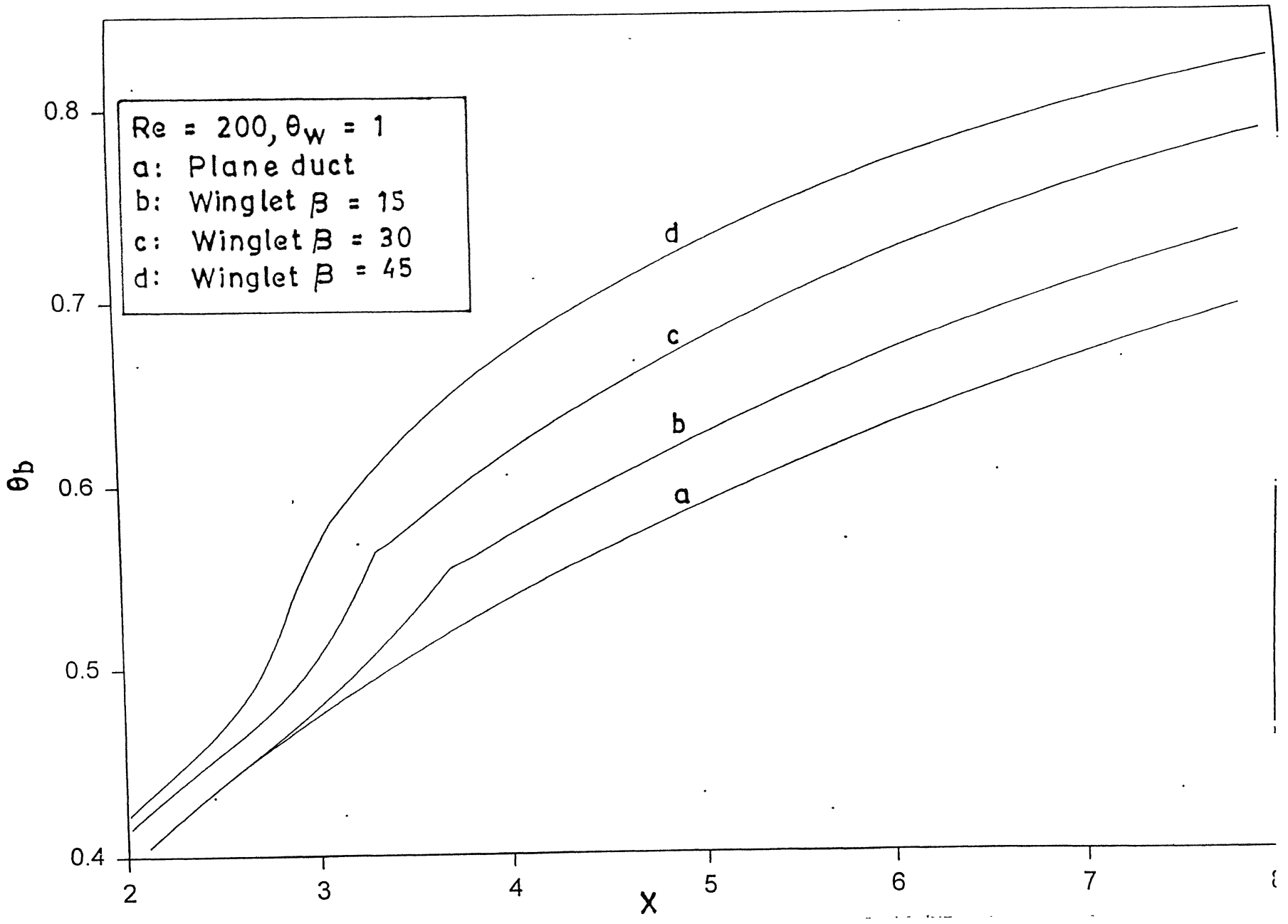

Fig 4.10 Variation of bulk temperature in the channel

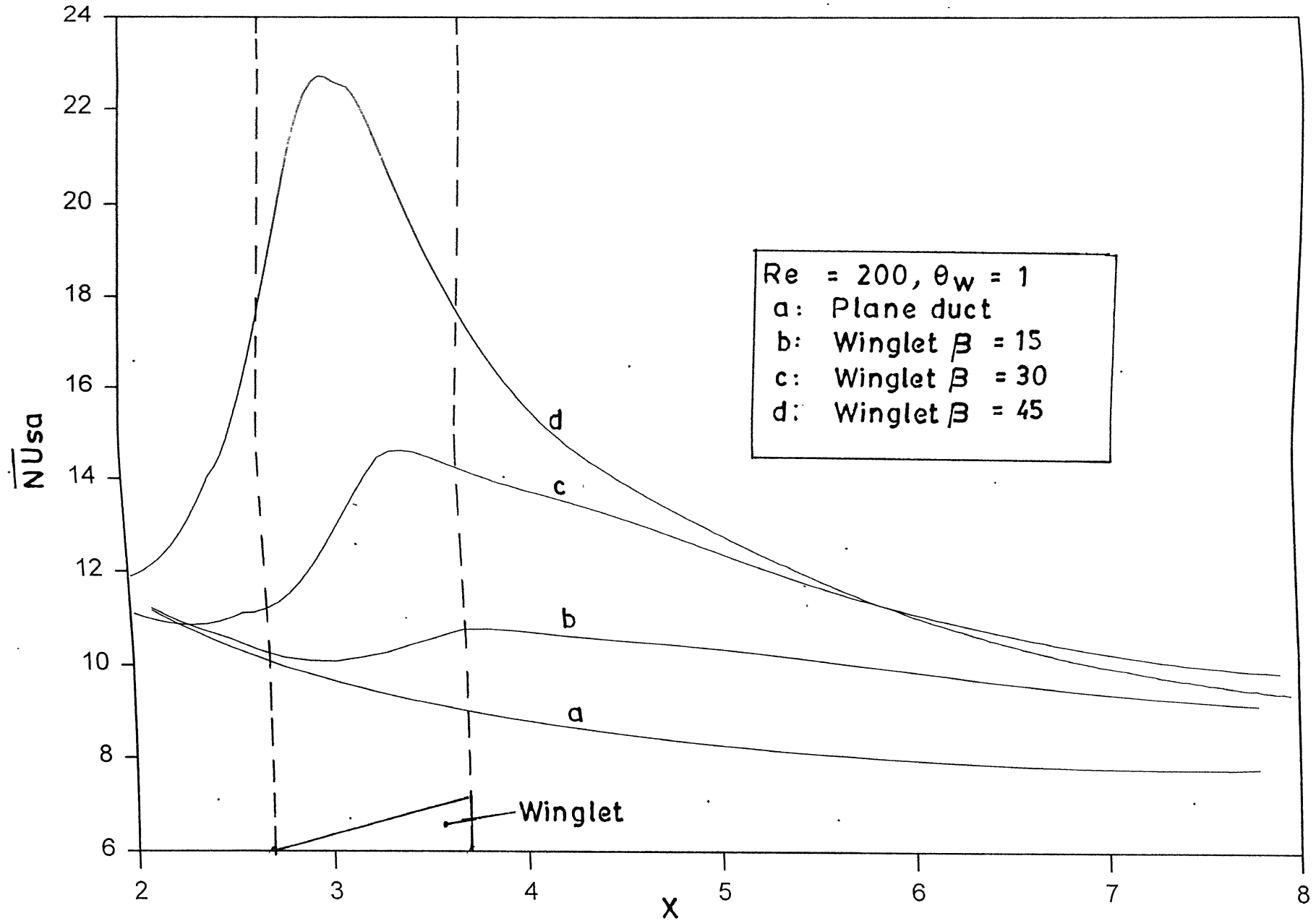

Figure 4.11 Distribution of combined spanwise average Nusselt number in the channel

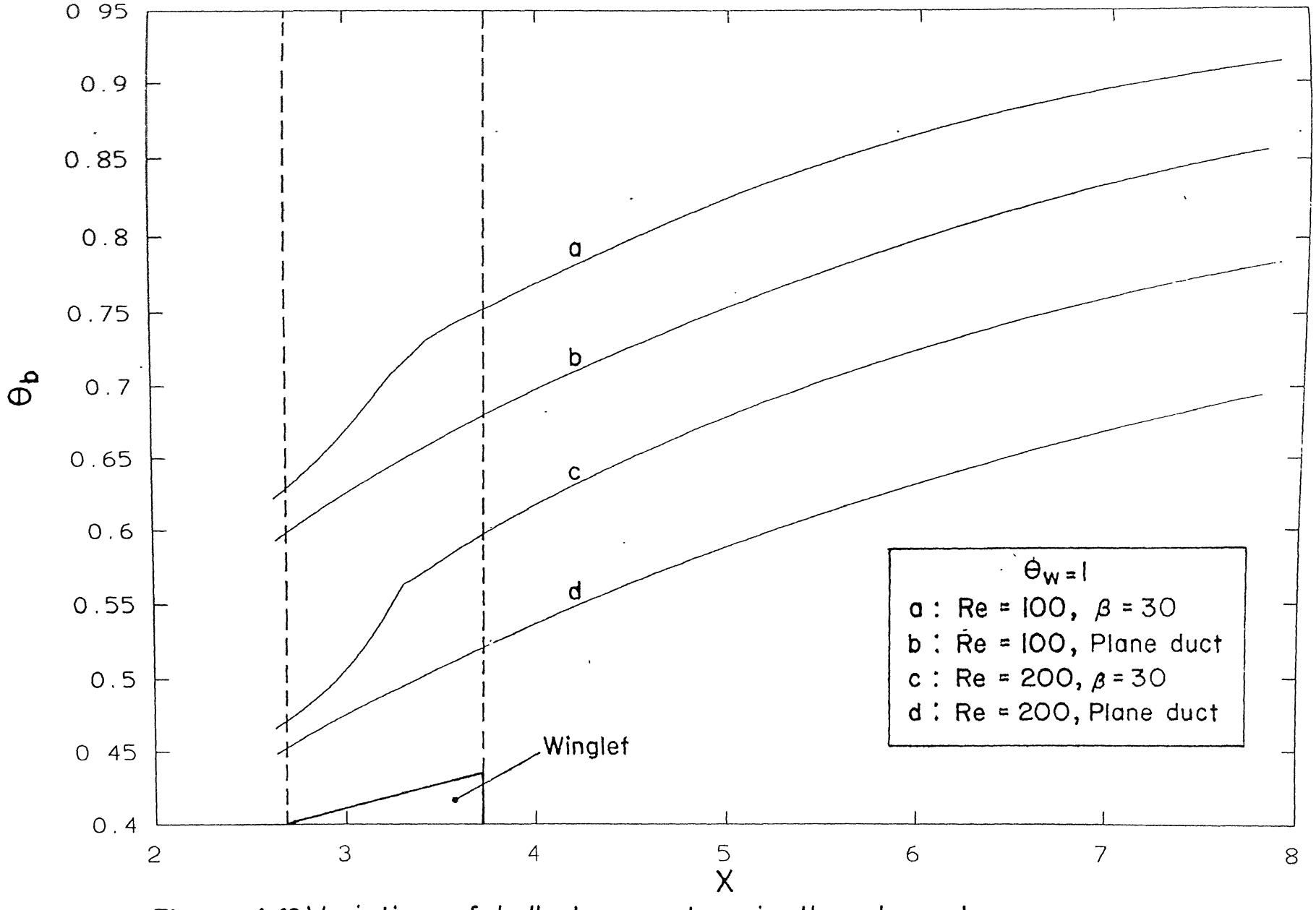

Figure 4.12 Variation of bulk temperature in the channel

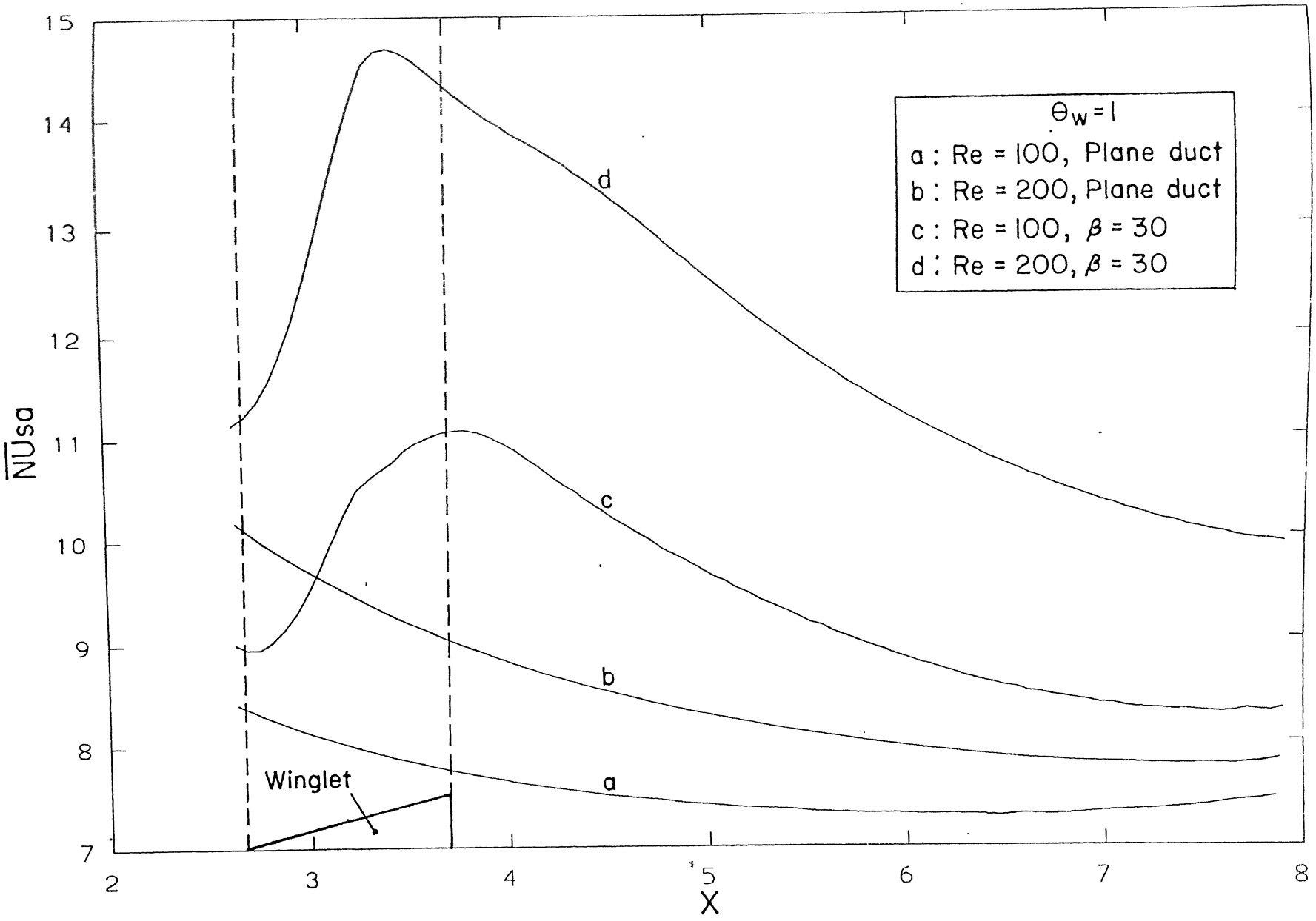

Figure 4.13 Distribution of combined spanwise average Nusselt number in the channel

increasing Reynolds number. This is to be expected because a higher Reynolds number also implies a great fluid mass flow rate in the duct. At the exit of the channel the combined spanwise average Nusselt number, for Re = 200 is 20 percent higher than that for Re = 100. The angle of attack is 30^0 for both the above cases.

In practice the plate surface of plate-fin heat exchangers is provided with a series of winglets placed one behind the other. This will result in repeated interruption in the growth of the thermal boundary layer and a further reduction in the resistance to heat transfer. As a preliminary step in modelling such a geometry the performance of two winglets placed one behind the other with the same angle of attack (15^0) and for a Reynolds number of 100 has been computed as shown in Figures 4.14 and 4.15. It is obvious from these figures that two winglets placed one behind the other leads to a much higher enhancement rate than a single winglet.

(b) Performance of the winglet with stamping

It has already been described that the easiest way to manufacture winglets on the flat surfaces is to punch out the triangular-shaped slender bodies from the flat surfaces. This punching operation leaves a hole underneath each winglet and the hole is called stamping. In this section we shall discuss the heat transfer performance of a triangular duct in the presence of a winglet and a stamping. Figures 4.16 and 4.17 show the results of the case of a triangular duct with a punched winglet in the presence of the stamping for a Reynolds number of 100. The overall Nusselt number of the stamped winglet is somewhat inferior to that of the attached winglet. This is due to the weakening of the vortices caused by the cross flow from the upper half of the duct to its lower half in the presence of the stamping. However when we compare the heat exchanger channel length required to obtain an exit bulk temperature of 0.8 there is only a slight difference between the cases of a stamped winglet and an attached winglet. Thus the loss in performance due to

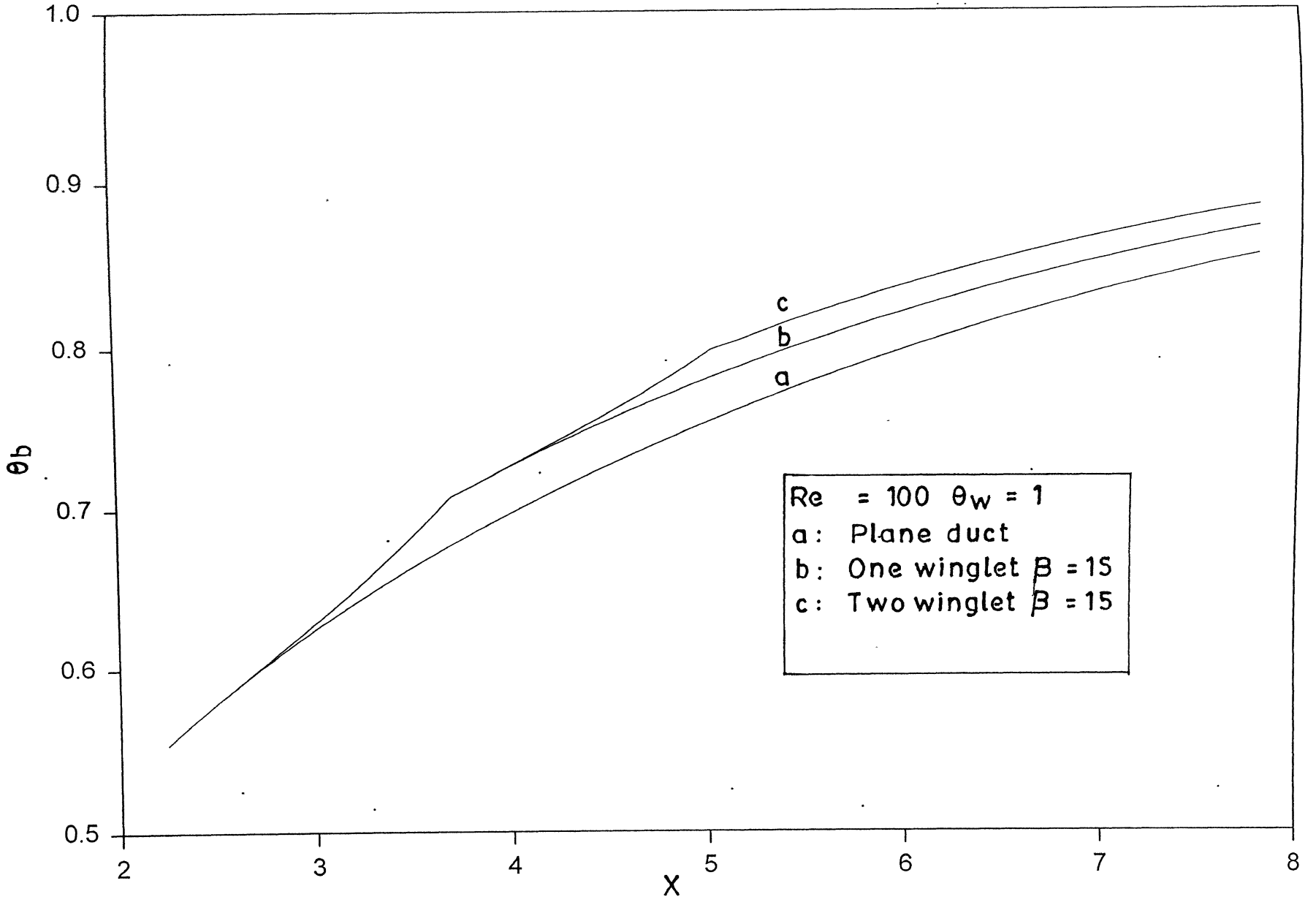

Figure 4.14 Variation of bulk temperature: single vs double winglets

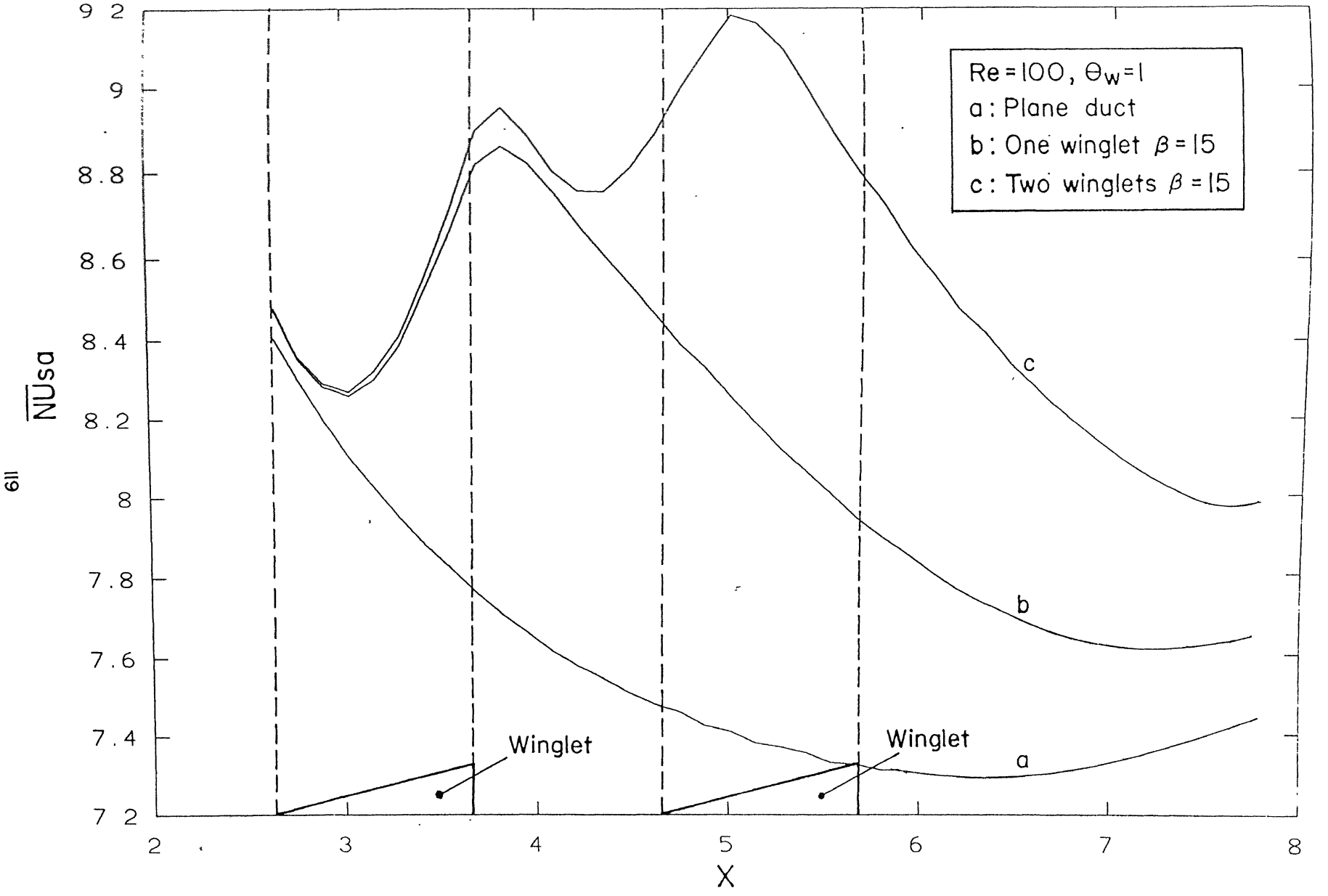

Figure 4.15 Distribution of combined spanwise average Nusselt number in the channel

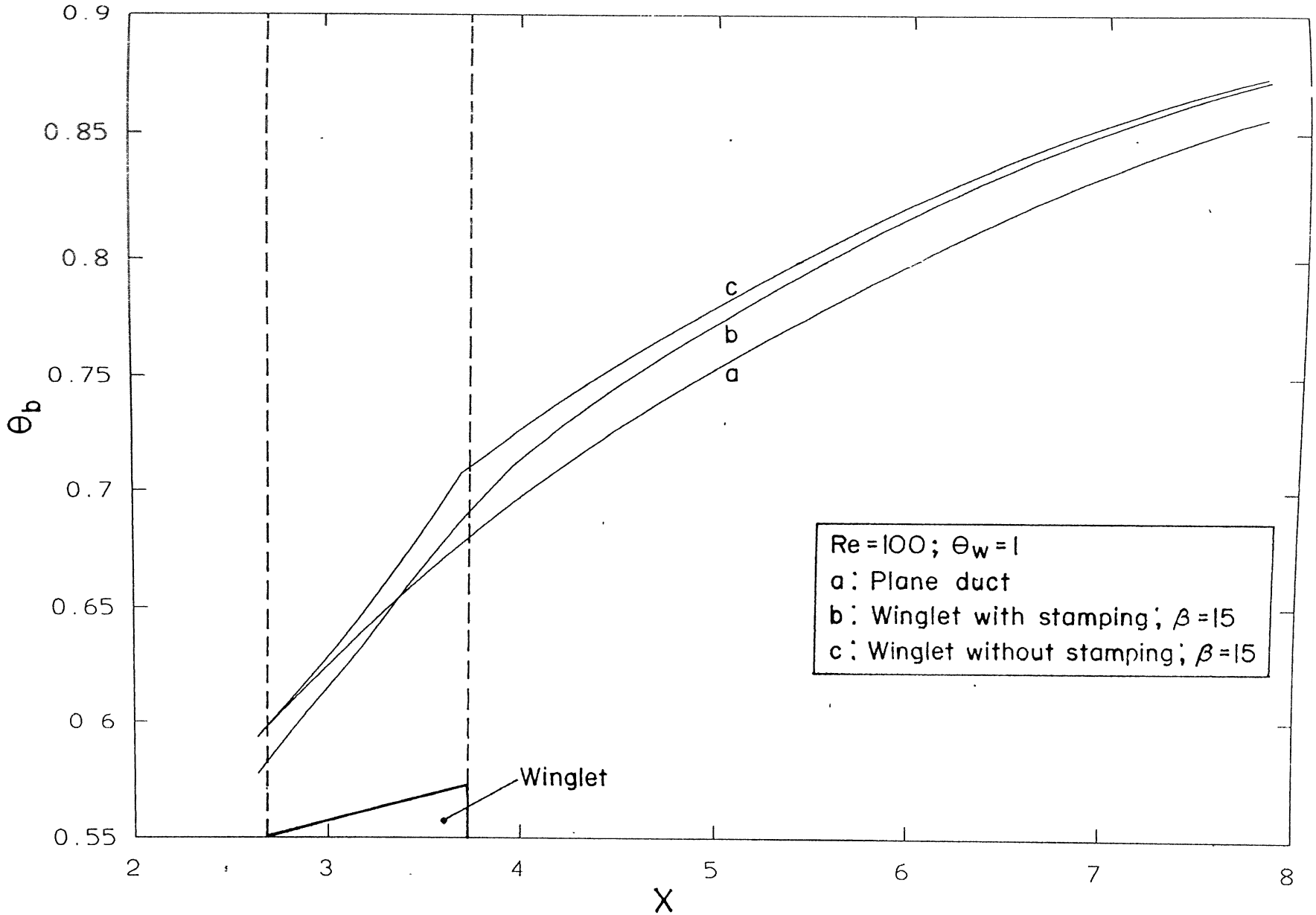

Figure 4.16 Variation of bulk temperature in the channel

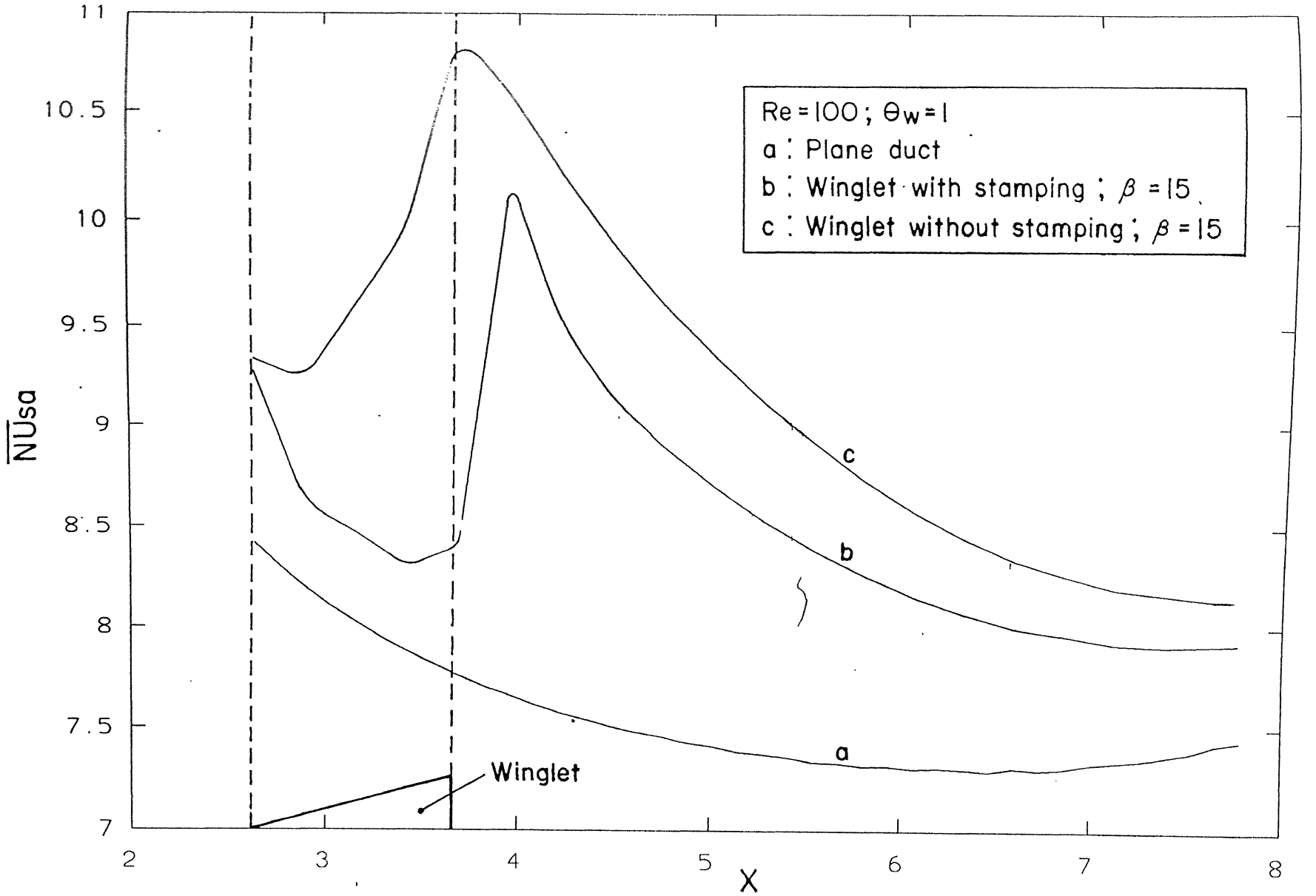

Figure 4.17 Distribution of combined spanwise average Nusselt number in the channel

the presence of the stamping is almost negligible and is easily outweighed by the ease of manufacture of the stamped winglets.

4.3.2 Uniform Wall Heat Flux

We now consider the case of constant wall heat flux. In this case, the bulk temperature variation is identical for the plane channel and the channel with a winglet, because the same amount of heat energy is supplied to the fluid in each case. When the wall heat flux is constant an appropriate way of evaluating the performance of the winglet is to compare the temperature difference driving the heat transfer. When the winglet is present, the boundary layer thickness is reduced due to the swirling motion of the fluid and consequently a lower wall temperature is sufficient to transfer a given amount of heat. So as to express the effect of the winglet in quantitative terms we define a normalised wall temperature as

$$\theta_{normalised} = \frac{\left(\theta_w - \theta_b\right)}{\theta_b} \tag{4.13}$$

Figures 4.18 and 4.19 show the variation of the normalised wall temperature for different angles of attack of the winglet for the Reynolds number values of 100 and 200 respectively. It can be seen that the winglet can reduce the normalised wall temperature by 20 percent. The higher normalised values closer to the inlet are due to the lower values of θ which appears in the denominator of equation (4.13)

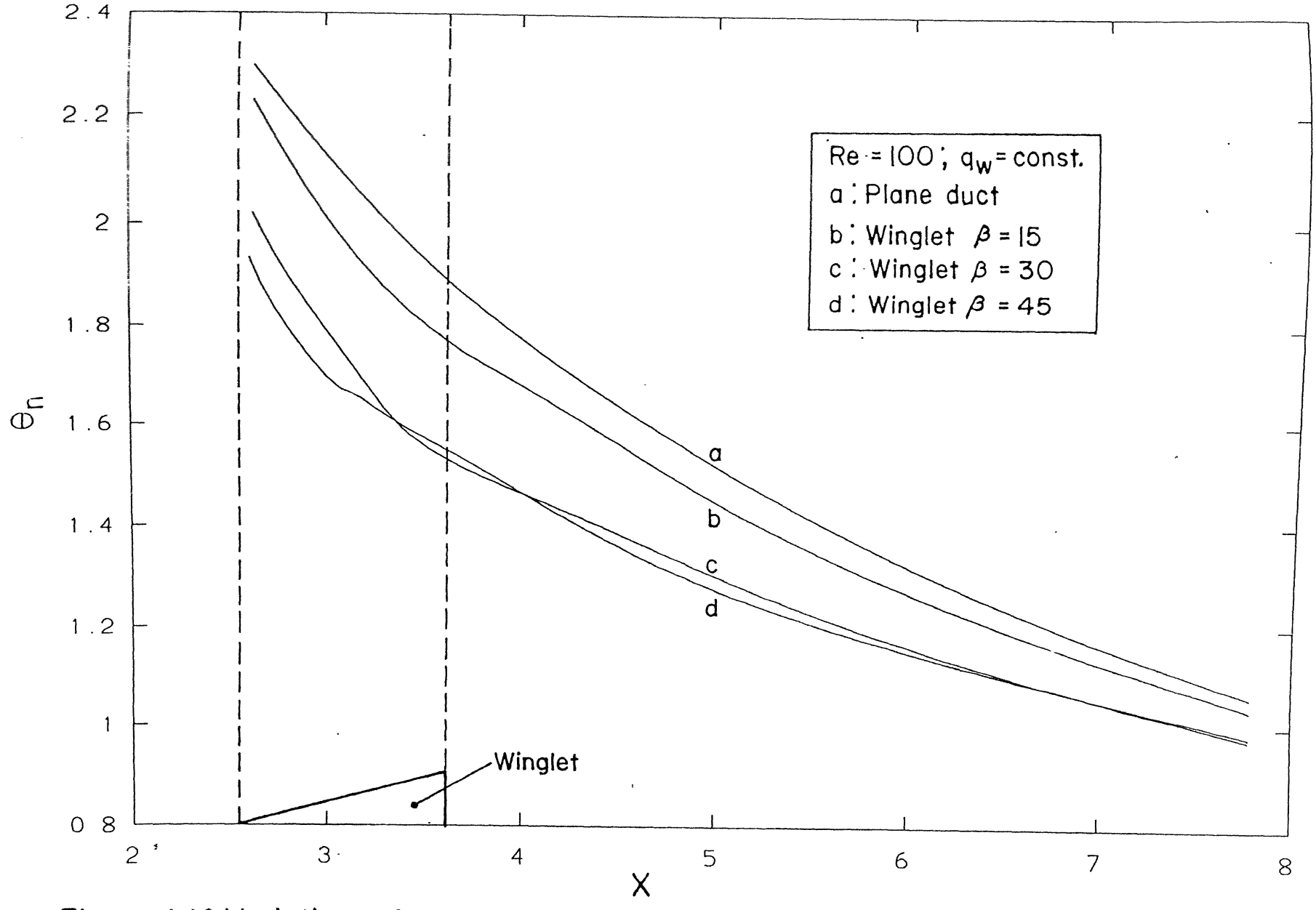

Figure 4.18 Variation of normalised wall temperature in the channel

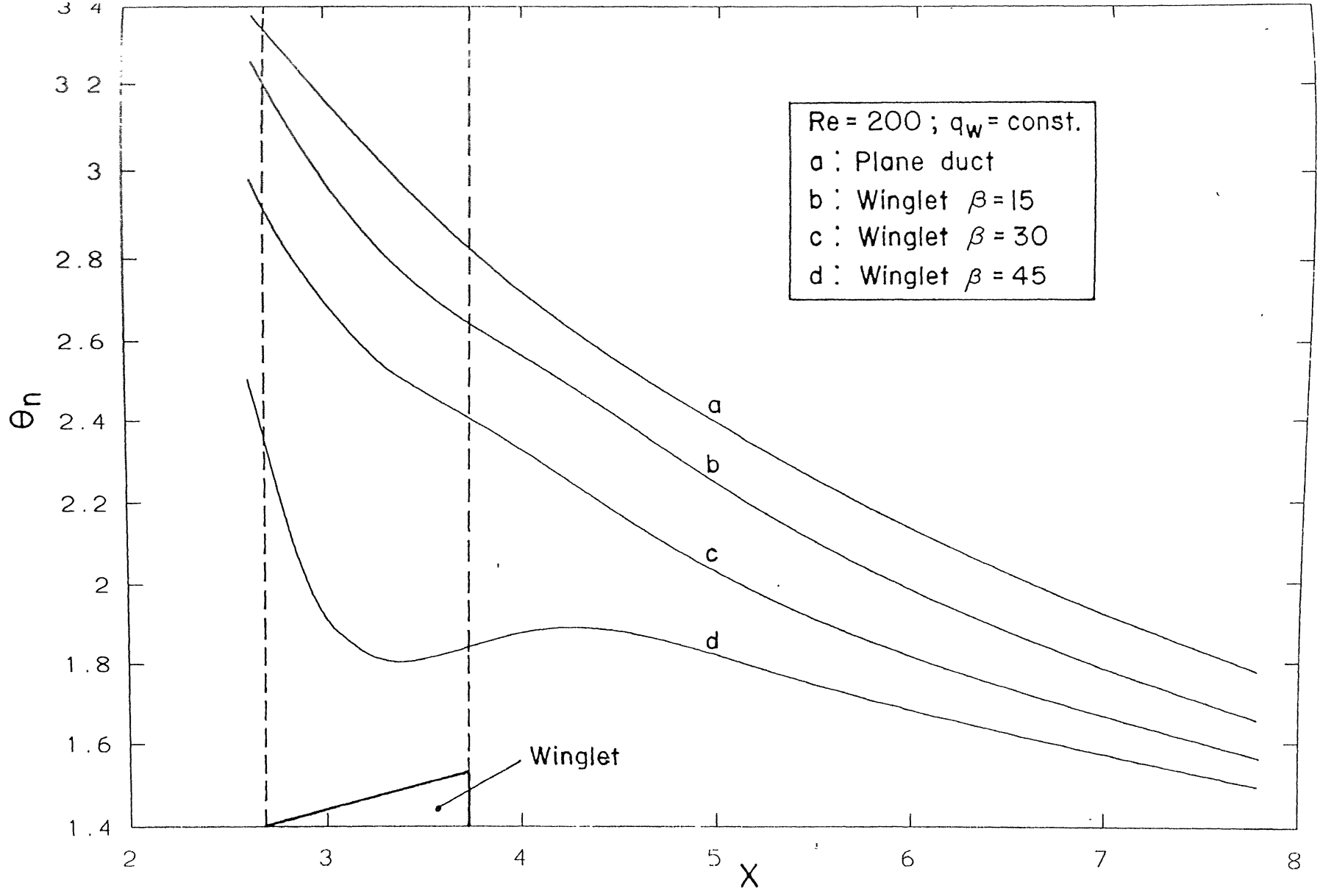

Figure 4.19 Variation of normalised wall temperature in the channel

4.4 Pressure Loss Penalty

Table-2 shows the variation of average pressure drop in the triangular duct and in the duct with winglet for varying angles of attack. It is evident that the pressure drop is maximum (5.01) for an angle of attack of 45 ^{0}.

Table: 2 Pressure Drop in the Duct (with and without winglet)

Geometry	Angle of attack	ΔP (non-dimensional)
Plane duct	-	3.75
Plane duct with winglet	(15^0)	4.1
Plane duct with winglet	(30^0)	4.91
Plane duct with winglet	(45^0)	5.01

Figure 4.20 shows the streamwise variation of pressure drop in the triangular channel for a Reynolds number of 100 for different angles of attack of the winglet.The average pressure at any section was determined from the integral value of pressure at that section.

4.5 Concluding Remarks

While the heat transfer rate is enhanced due to the winglet leading to a more compact heat exchanger there is an associated increase in the pumping power. It can be seen that about 20-25 percent enhancement of heat transfer can be achieved at the expense of a moderate pressure drop. The enhancement of heat transfer is also dependent on the angle of attack of the delta winglet. In conclusion it can be said that the

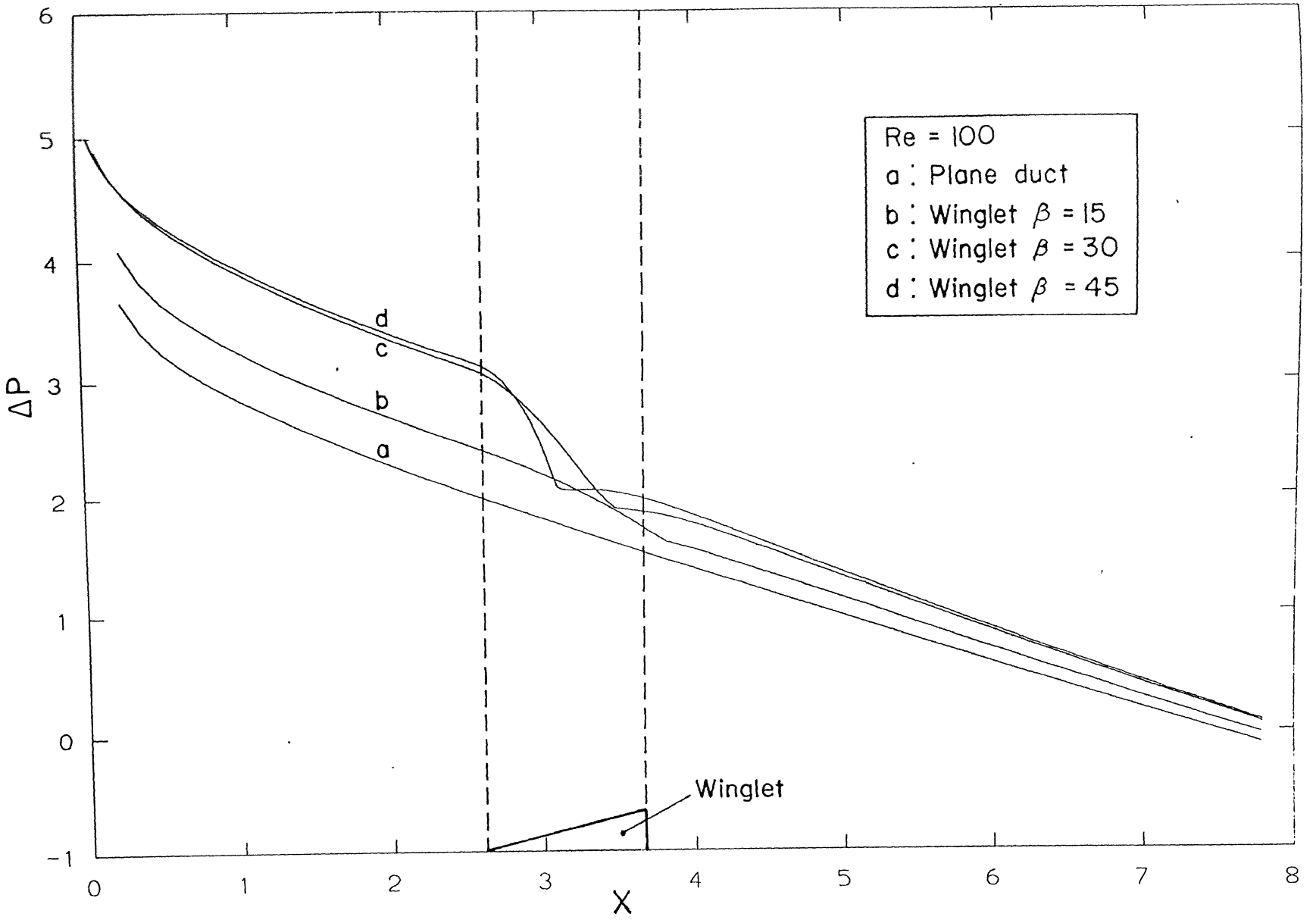

Figure 4.20 Variation of average pressure in the channel

triangular fins with mounted delta winglets (secondary fins) have a lot of promise as the inserts (protrusions) within the flow passages created by the two neighbouring plates in a plate-fin heat exchanger. The delta winglets can also be punched out to facilitate the manufacturing process. Under such a situation, stampings are formed on the duct wall. The flow structure becomes more complex but nearly the same amount of enhancement in heat transfer is brought about.

Chapter 5

Performance of the Delta Wing

5.1 Introduction

Based on the mechanism of vortex generation, there are two types of vortex generators, namely longitudinal vortex generators such as delta wings, delta winglets and rectangular wings; and transverse vortex generators such as surface mounted ribs and corrugations. For the applications of heat transfer enhancement, the superiority of longitudinal vortex generators has been confirmed both theoretically and experimentally. The present work evaluates the performance of the delta wings and delta winglets as secondary fins on the triangular inserts placed between the plates of plate-fin heat exchangers. The results of the computation for the delta wings are presented in this chapter. An effort has been made to compare the performance of the two as well.

5.2 Vortex formation by the delta wing

Figure 5.1 compares the secondary flow pattern behind the delta wing with that behind the delta winglet at the same cross-section of the

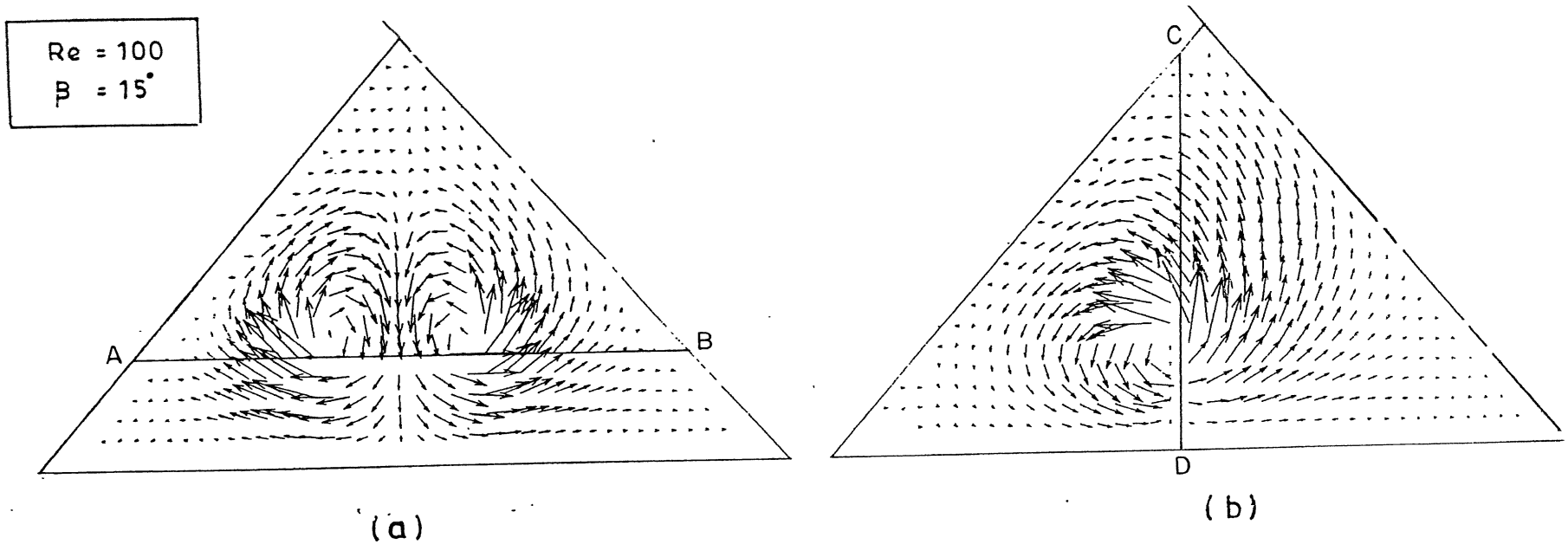

Figure 5.1 Comparison of secondary flow pattern (a) Delta wing; (b) Delta winglet

triangular channel. The angle of attack in both cases is 15° and the Reynolds number is 100. The difference in the vortical structure can be explained in the following way. In the case of the delta wing the secondary flow is caused by the movement of the fluid from below the surface of the wing to the space above it. Whereas, in the case of the delta winglet the secondary flow is due to the passage of fluid from the right of the winglet to its left. In other words, the pressure side and the suction side are separated by the horizontal line AB for a delta wing (AB is the line along which a transverse plane cuts the delta wing) and by the vertical line CD for the winglet (CD is the line along which a transverse plane cuts the delta winglet).

In the case of a delta wing, the induced spiralling motion takes the fluid from the underside of the wake, swirls it around the upper side and then impinges on the attached plate. The spiralling motion is initiated symmetrically from the two side edges of the wing facing the incoming flow and this flow structure is called common-flow-down (Pauley and Eaton, 1988). Many practical configurations utilise uniformly spaced arrays of small delta winglets (often used for controlling the flow over aircraft wings). The flow structure in such a situation is called co-rotating (Pauley and Eaton,1988). A single delta winglet creates one main-vortex system due to the pressure difference between the suction surface and the pressure surface. In addition, the corner vortices are also formed (Figure 5.2).

Figures 5.3 and 5.4 depict the secondary flow at different sections of the channel along and behind the delta wing. The vortex strength increases along the length of the delta wing and then in the downstream of the wing there is a gradual reduction in the vortex strength. This pattern was also observed in the case of a delta winglet (Figures 4.1 and 4.2)

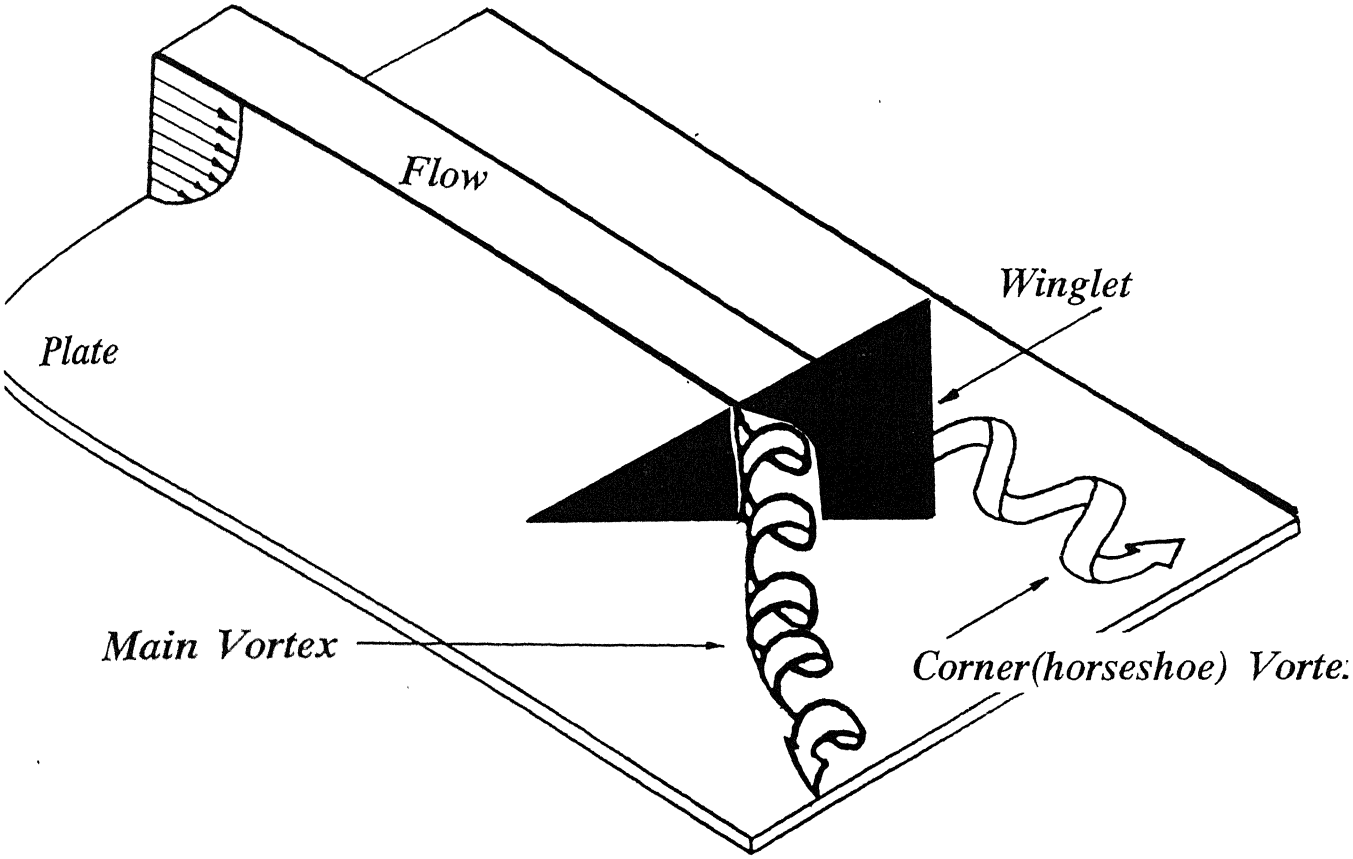

Fig.5.2 Formation of vortices by a delta winglet
[after Biswas et. al. (1995)]

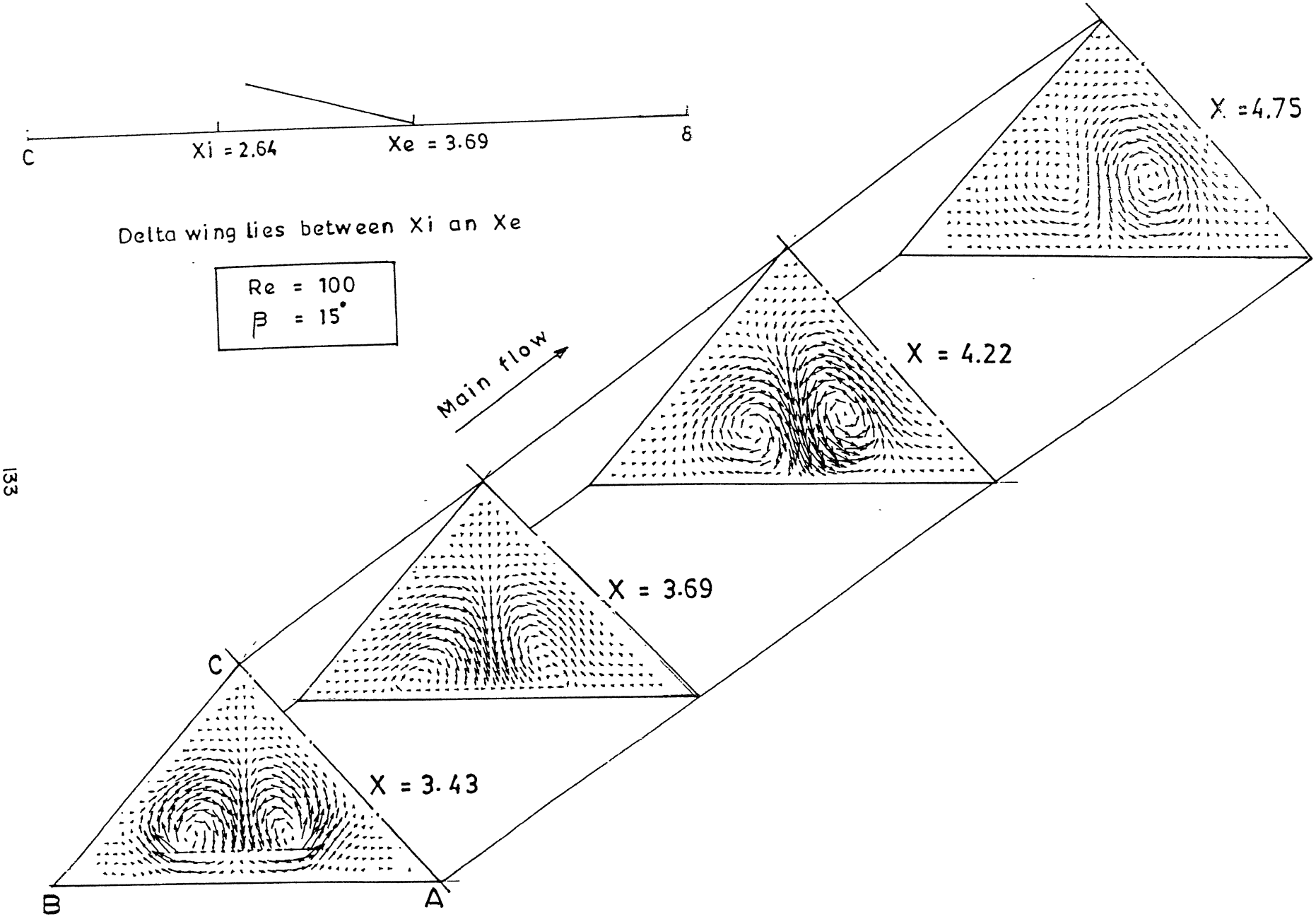

Figure 5.4 Flow along and behind the delta wing

5.3 Heat Transfer

5.3.1 Isothermal walls

The performance parameters used to express the heat transfer enhancement of the vortex generator , such as the bulk temperature and the combined spanwise average Nusselt number have been defined in chapter-4. The variation of these quantities for a channel having a delta wing, when the walls of the channel are maintained at a uniform temperature are discussed in this section. Figures 5.5 and 5.6 show the variation of bulk temperature and the distribution of combined spanwise average Nusselt number respectively for a Reynolds number of 100 for different angles of attack. The enhancement in heat transfer caused by the delta wing can be seen in the form of a higher bulk temperature (as compared to the case of a plane duct without any vortex generator) at any section behind the delta wing. Figure 5.5 reveals that the higher the value of the angle of attack, the greater is the increase in the bulk temperature. This trend is similar to what was observed in the case of a delta winglet.

Figure 5.6 shows that there is a marked increase in the combined spanwise average Nusselt number behind the delta wing and downstream of the wing the Nusselt number tapers off gradually. As was done in the case of the delta winglet, the heat transfer enhancement effect of the delta wing can be quantified in terms of the reduction in size of the heat exchanger that can be accomplished using the delta wing. The length of the heat exchanger required for attaining an exit bulk temperature of, say, 0.8 is shown in the following table.

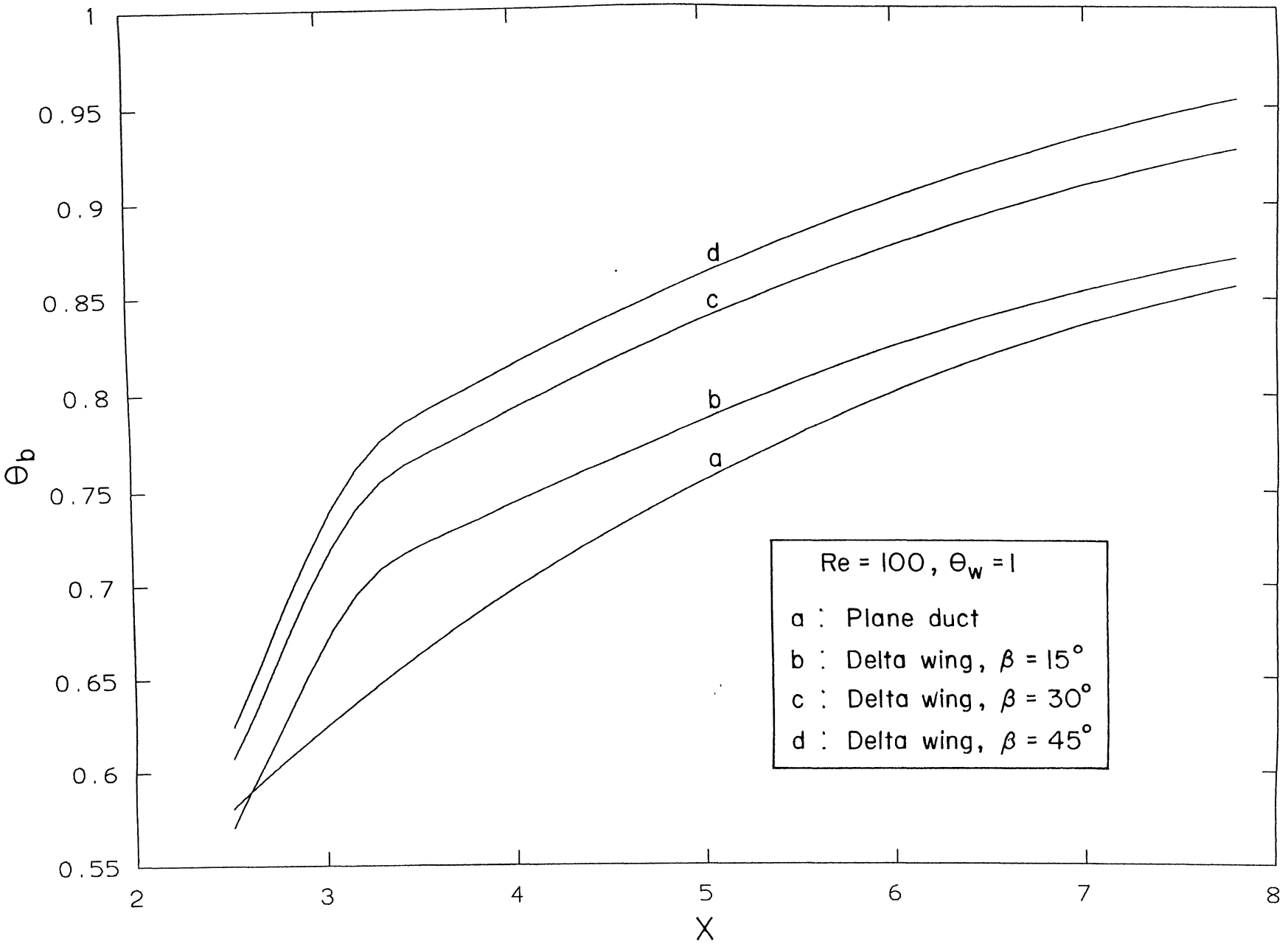

Fig 5.5 Variation of bulk temperature in the channel

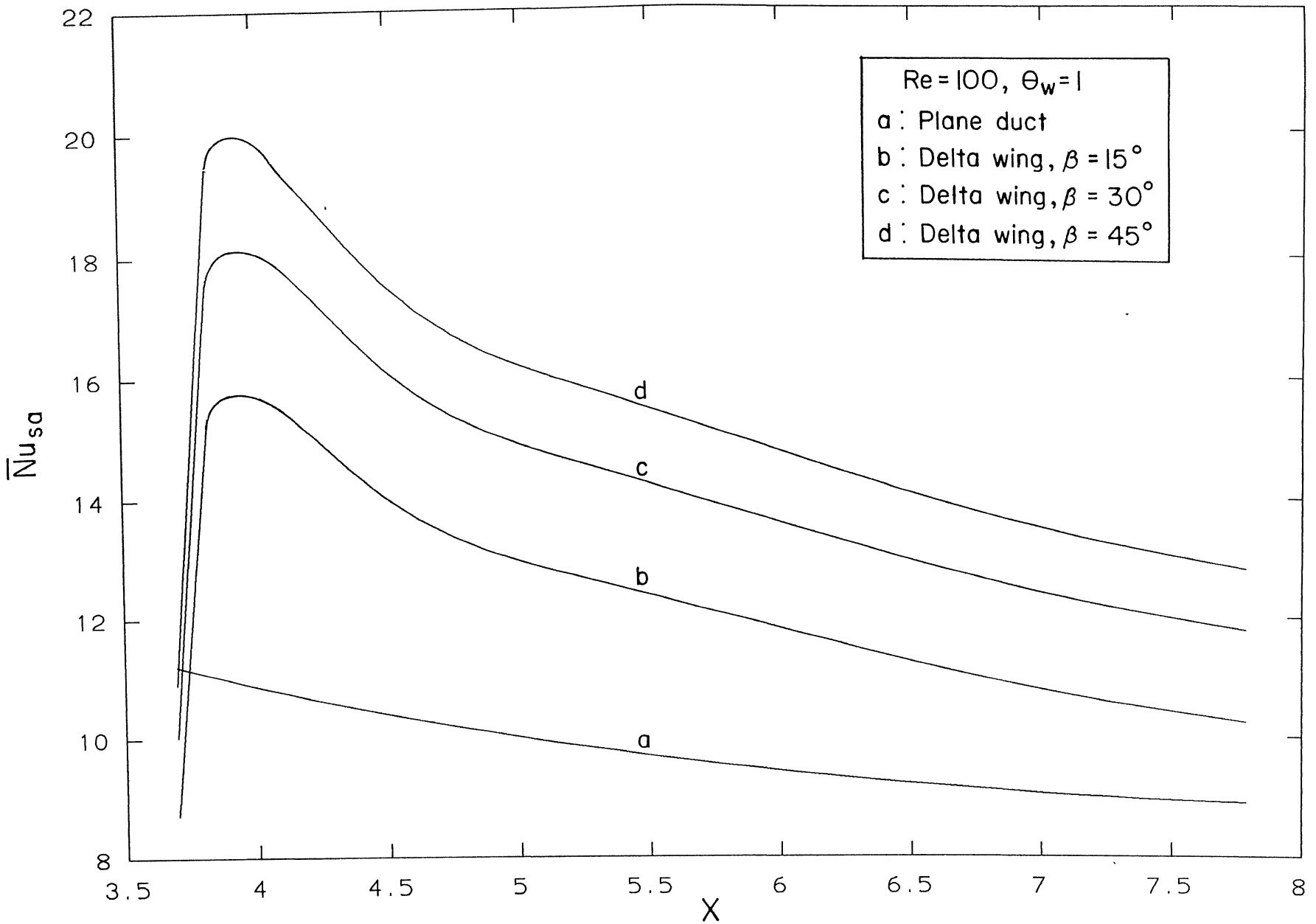

Fig. 5.6 Distribution of combined spanwise average Nusselt number

Table 1: Percentage Reduction in length of the exchanger

Geometry	Exchanger length	% Reduction
Plane duct	6.1	-
Duct with Wing ($\beta = 15^0$)	5.5	9.8
Duct with Wing ($\beta = 30^0$)	4.25	30.3
Duct with Wing ($\beta = 45^0$)	3.81	37.7

The maximum reduction in length of 37.7 % corresponds to an angle of attack of 45^o. It is clear that a high level of compactness is achievable using the delta wing.

The variation of bulk temperature and the distribution of combined spanwise average Nusselt number in the channel for a Reynolds number of 200 are shown in Figures 5.7 and 5.8 respectively. The trends are identical to those for Re = 100. Results for a Reynolds number of 200 are compared with those of 100 in Figures 5.9 and 5.10. These figures reveal the fact that while higher Nusselt numbers are achieved with higher Reynolds numbers, the exit bulk temperature decreases with increasing Reynolds number. This is due to the fact that as the Reynolds number is increased there is a proportionate increase in the mass flow rate of the fluid in the channel. At the exit of the channel the combined spanwise average Nusselt number, for Re = 200 is 28 percent higher than that for Re = 100. The angle of attack is 30^0 for both the above cases.

As was done in the case of the delta winglet, the enhancement level that can be achieved by using two delta wings one behind the other was also computed for an angle of attack of 30^o and a Reynolds number of 100. The results of this computation are shown in Figures 5.11 and 5.12. It is evident from these figures that as the number of delta wings is increased a corresponding increase in the heat transfer enhancement is achieved. This is quite expected because the second delta wing serves to

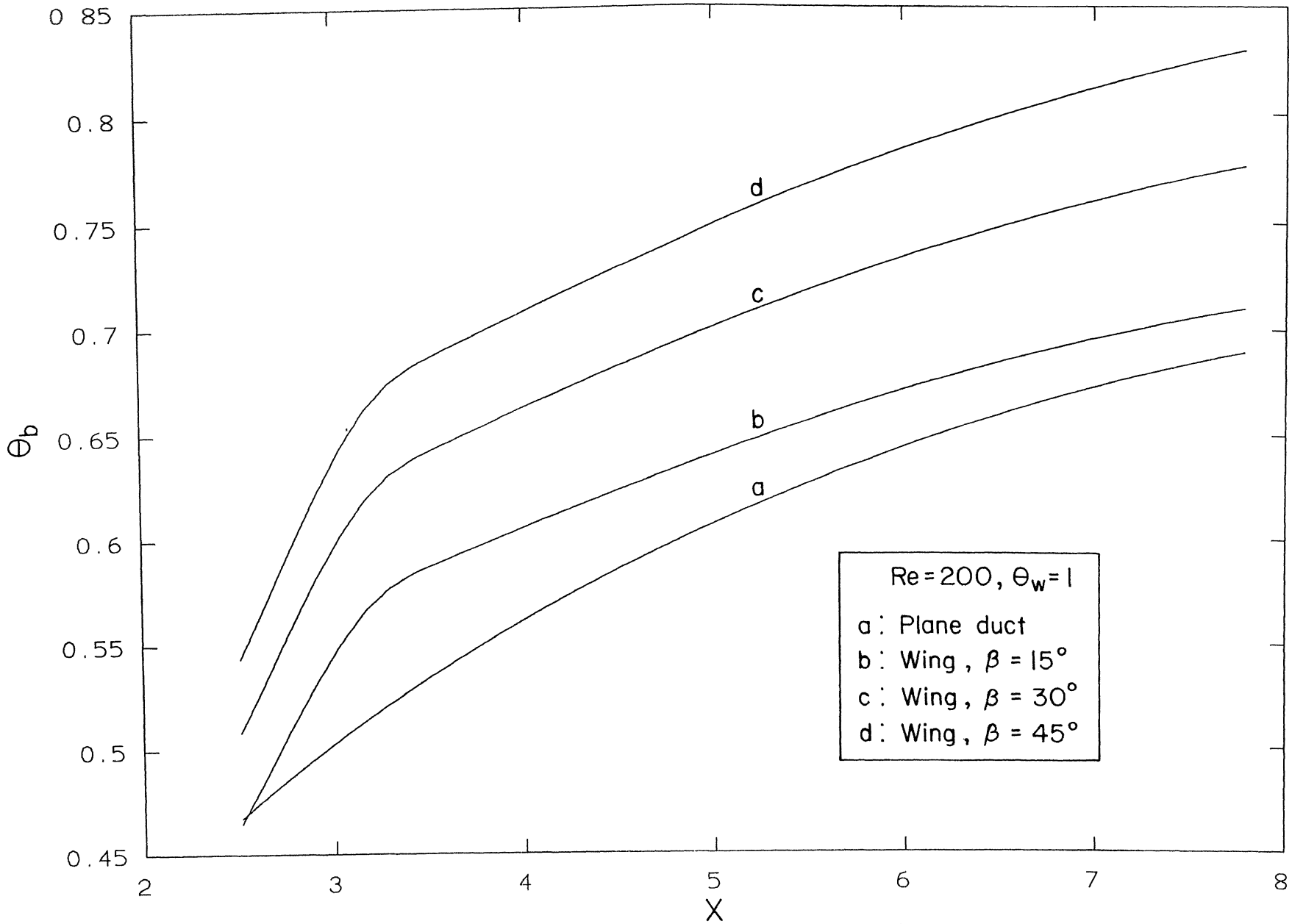

Fig.5.7 Variation of bulk temperature in the channel

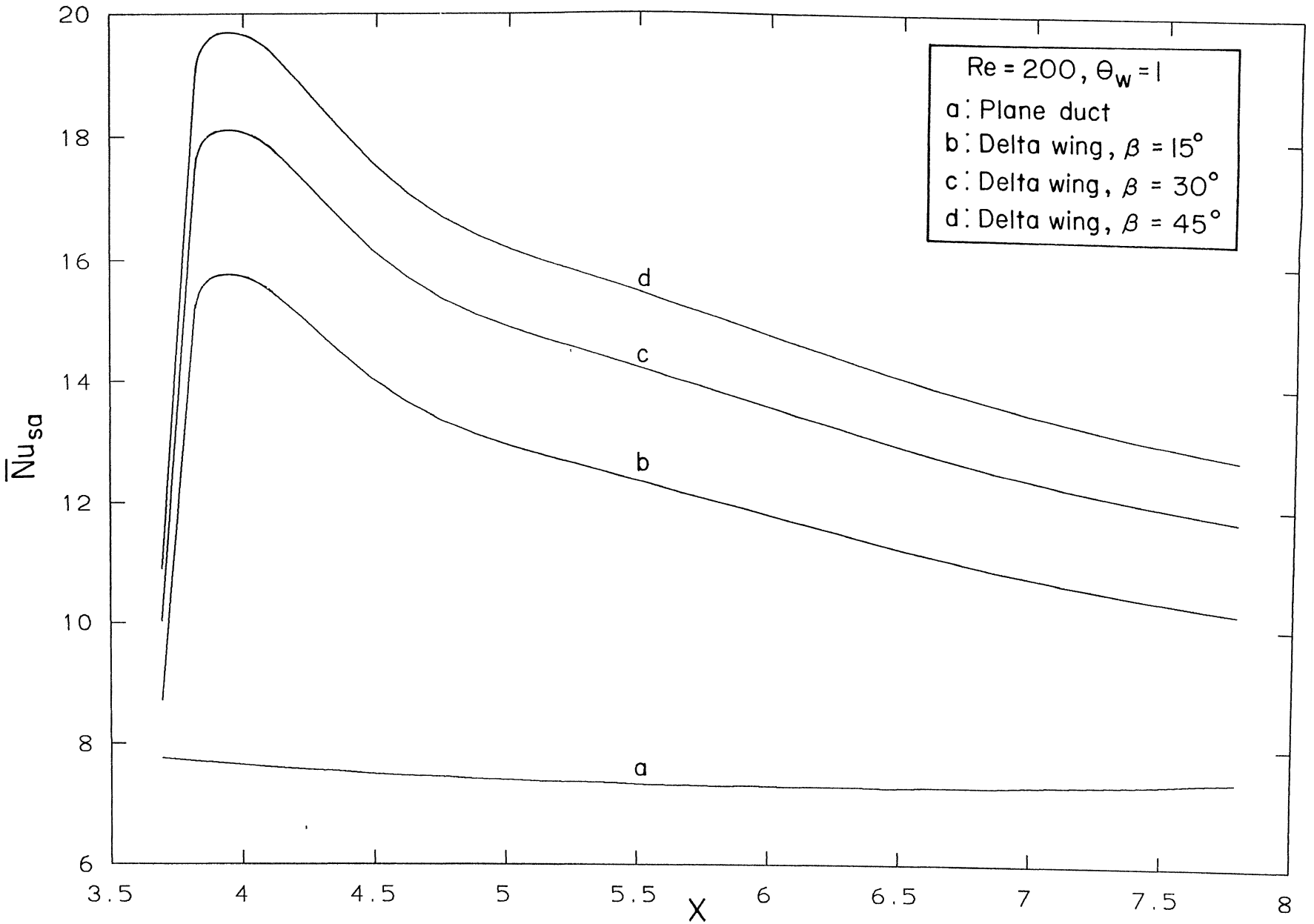

Fig.5.8 Distribution of combined spanwise average Nusselt number

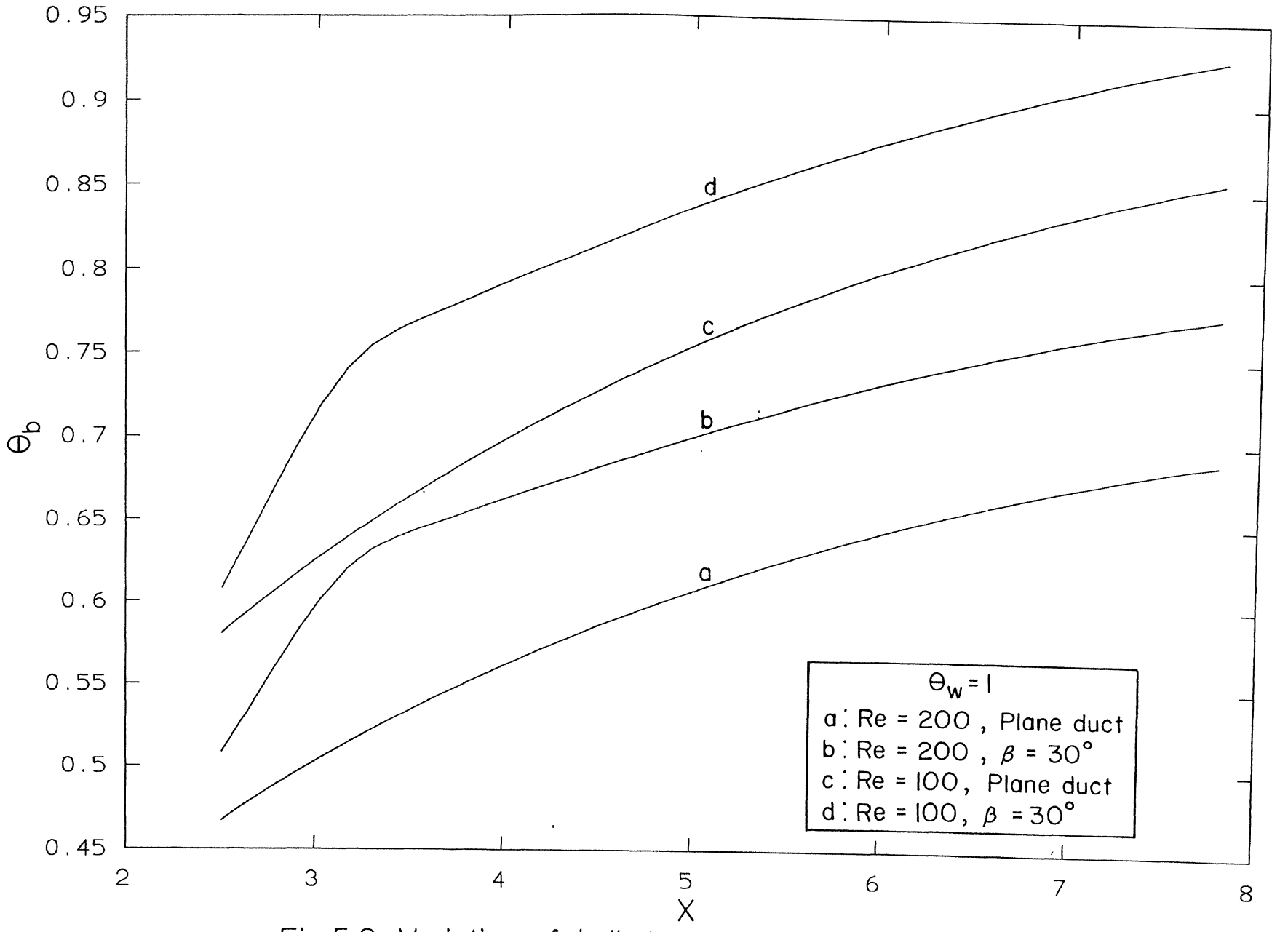

Fig.5.9 Variation of bulk temperature in the channel

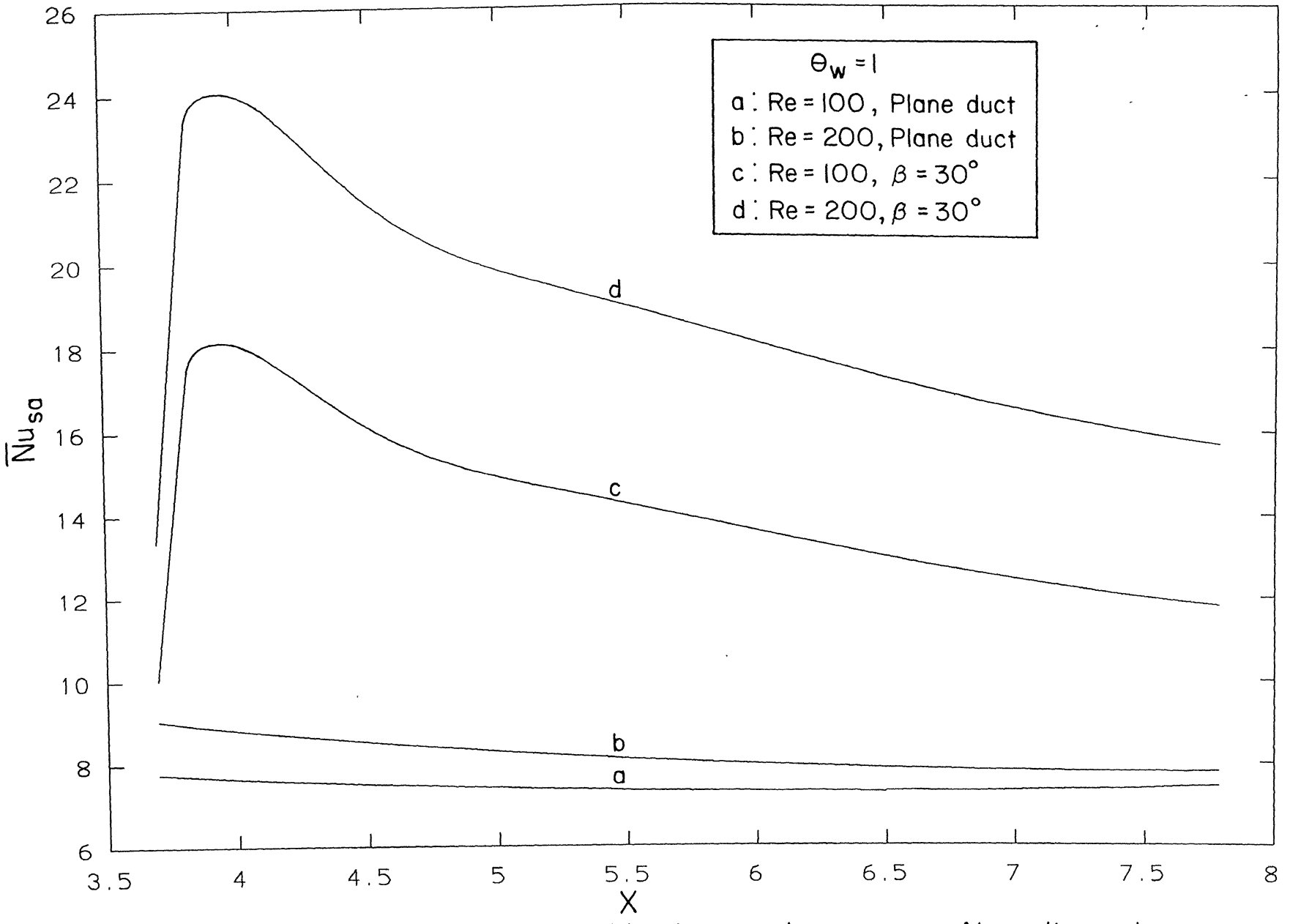

Fig.5.10 Distribution of combined spanwise average Nusselt number

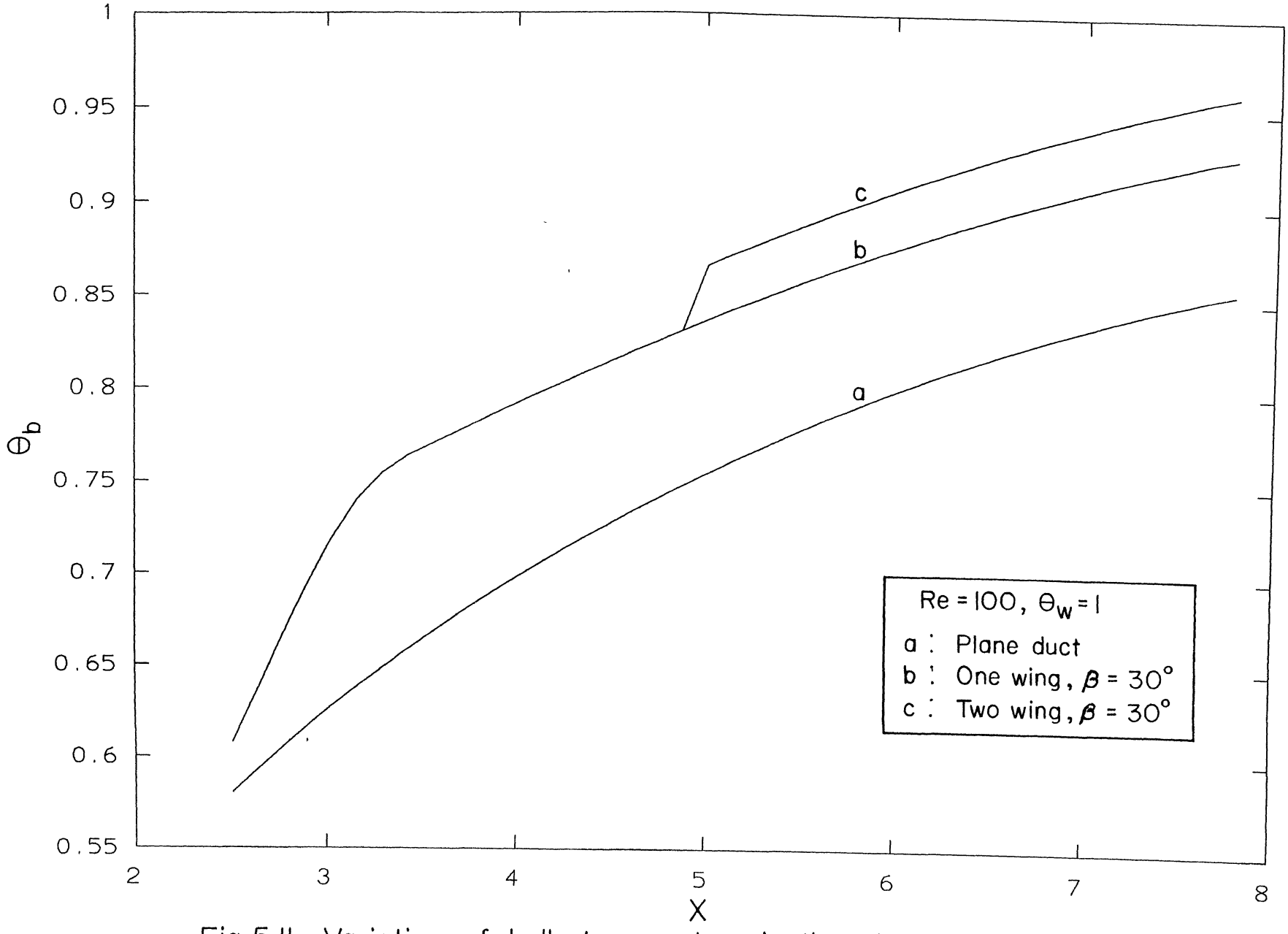

Fig.5.11 Variation of bulk temperature in the channel

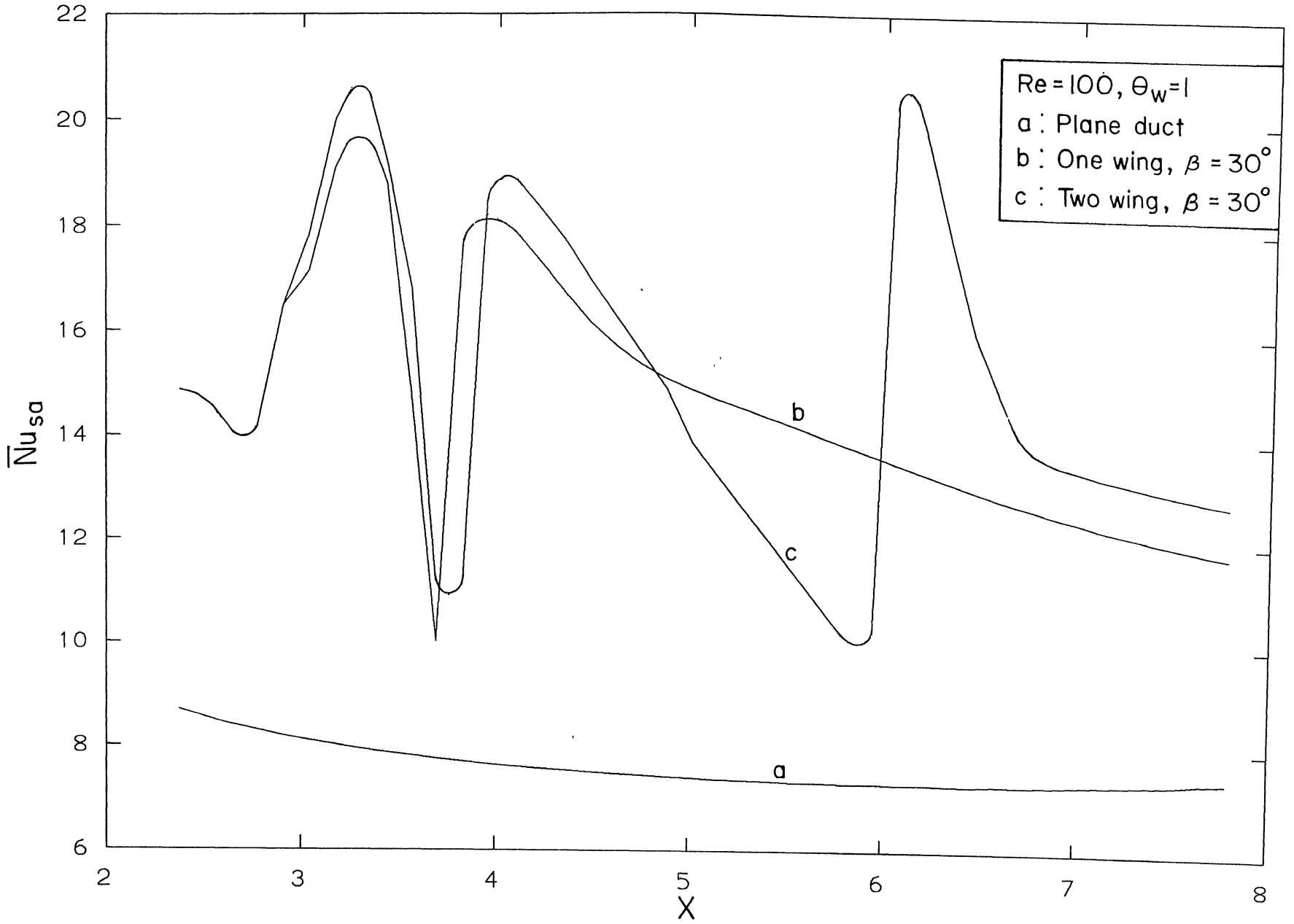

Fig.5.12 Distribution of combined spanwise average Nusselt number

interrupt the growth of the thermal boundary layer as a new longitudinal vortex-pair is formed by the second delta wing.

5.3.2 Uniform Wall Heat Flux

In the case of constant wall heat flux along the channel walls the enhancement effect of the vortex generator is quantified in terms of the normalised wall temperature as explained in chapter 4. Figures 5.13 and 5.14 show the variation of the normalised wall temperature for different angles of attack of the delta wing for the Reynolds number values of 100 and 200 respectively. The lower values of normalised wall temperature when the delta wing is used indicate that for transferring a given quantity of heat, a lower wall temperature would suffice and that justifies the utility of a delta wing.

5.4 Performance Comparison

Though the delta wing and the delta winglet are similar, in the sense that both are triangular surfaces they differ in the manner in which they are mounted. Consequently the pattern of the secondary flow generated by each is different and this aspect has been discussed in section 5.2. Another difference between the wing and the winglet is that the winglet has a free trailing edge, whereas the trailing edge of the wing is attached to the plate. Comparison of their performance in enhancing the heat transfer is presented in this section. The variation in bulk temperature along the channel is compared for the cases of the delta wing and the delta winglet for the same angle of attack in Figure 5.15. The delta wing yields a higher level of enhancement as compared to the

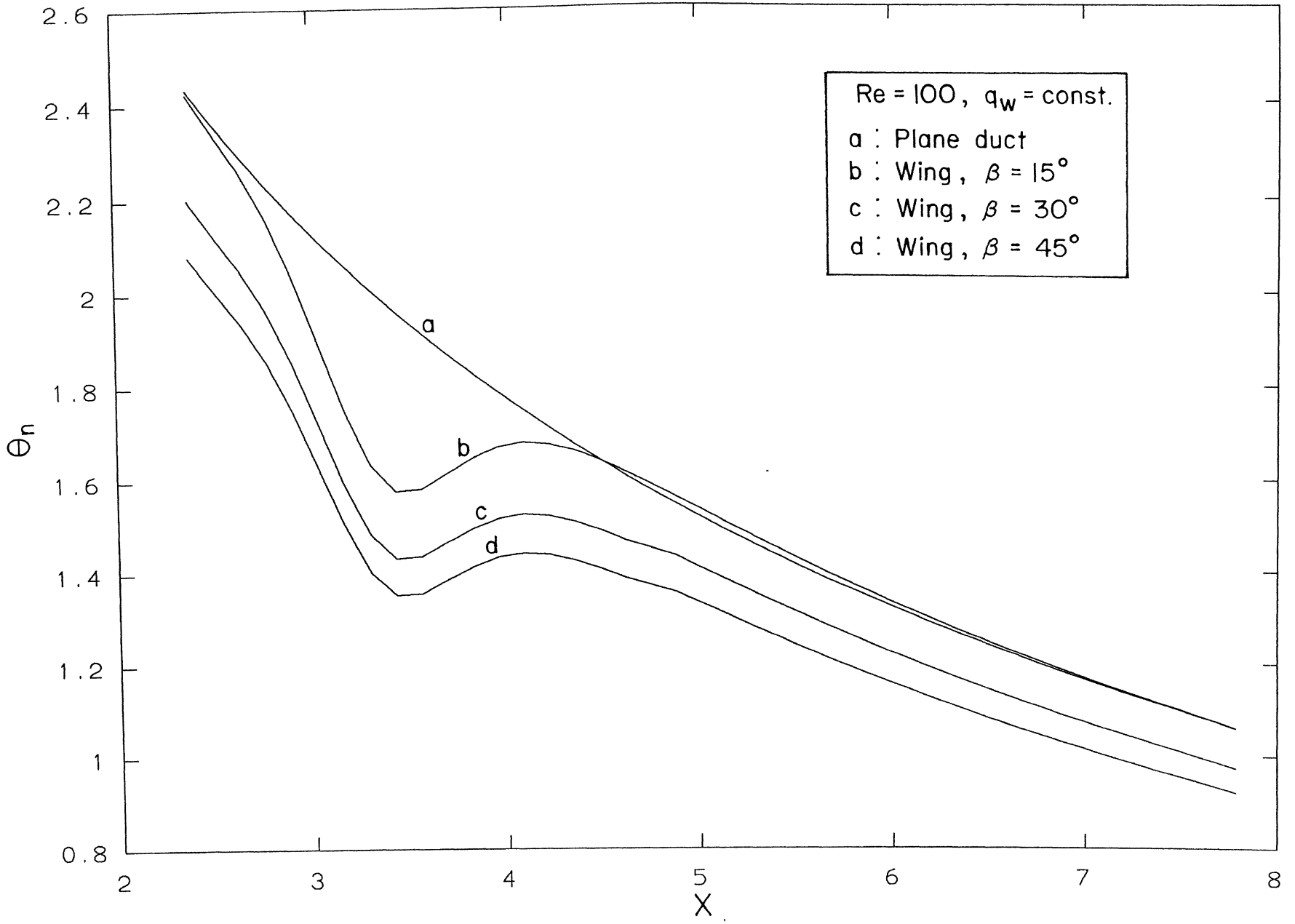

Fig.5.13 Variation of normalised wall temperature

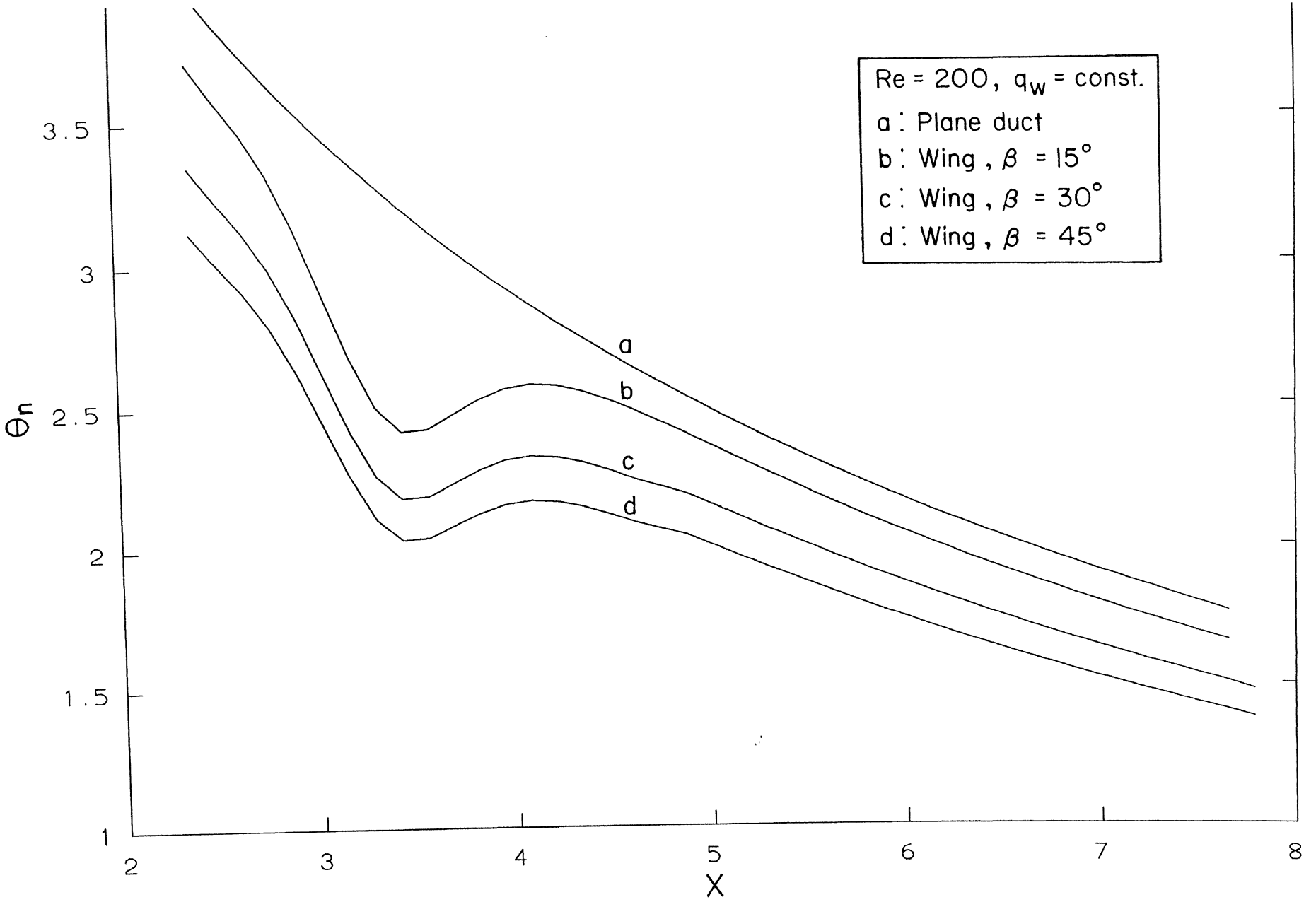

Fig.5.14 Variation of normalised wall temperature

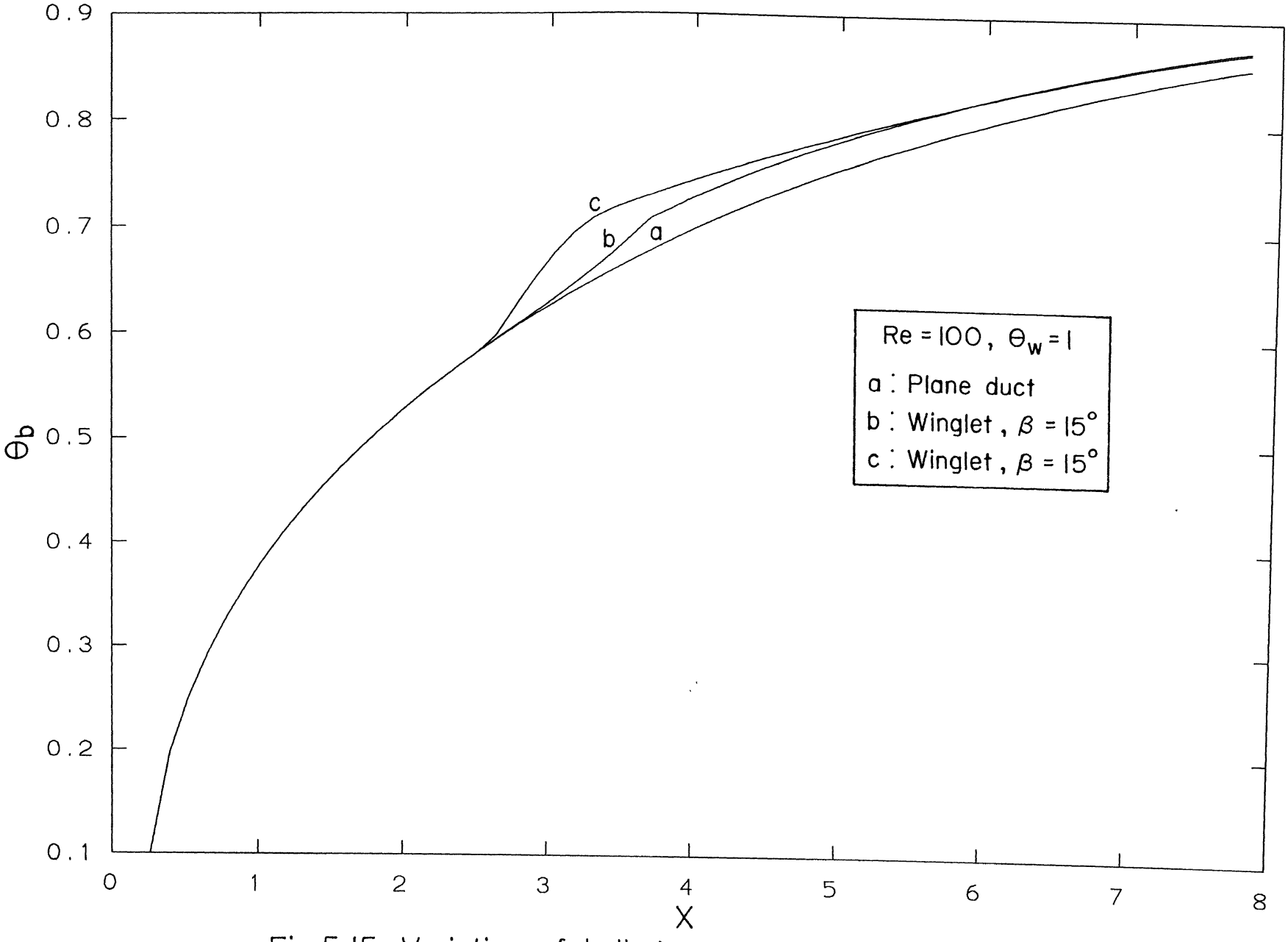

Fig.5.15 Variation of bulk temperature in the channel

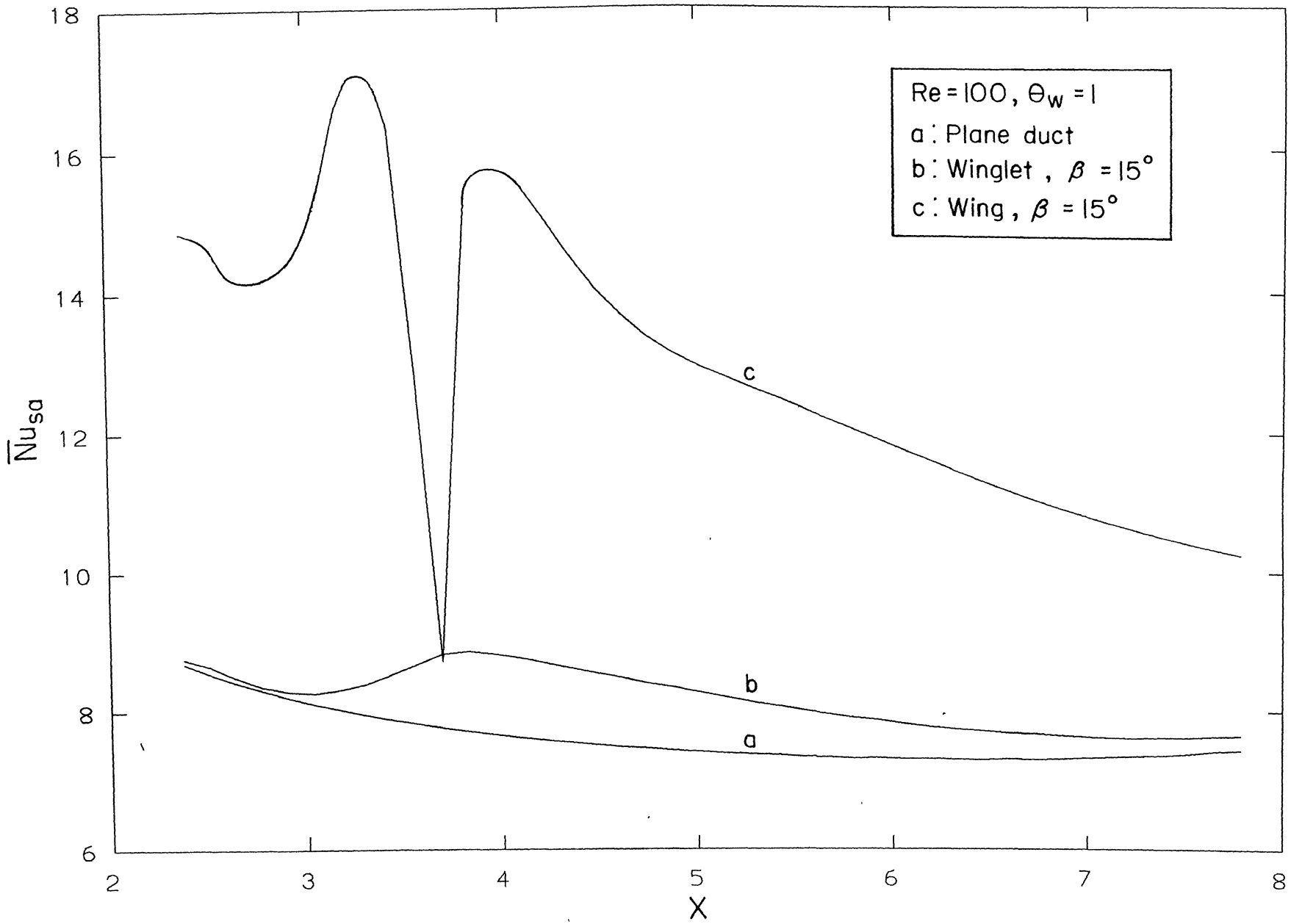

Fig. 5.16 Distribution of combined spanwise average Nusselt number

delta winglet. The same trend is seen in Figure 5.16 as well wherein the combined spanwise average Nusselt numbers are compared. These results agree with the findings of Biswas. *et al* (1994) for a rectangular channel. Though the delta wing performs better than the winglet in terms of heat transfer enhancement, the associated increase in pumping power is also more for the delta wing. Figure 5.17 shows the streamwise distribution of pressure drop in the channel for the wing and winglet and compares them with the pressure drop distribution in a plane triangular duct.

5.5 Pressure Loss Penalty

Table-2 shows the overall pressure drop in the triangular duct and in the duct with delta wing for varying angles of attack. It is evident that the pressure drop is maximum for an angle of attack of 45 ^{0}.

Table: 2 Pressure Drop in the Duct (with and without delta wing)

Geometry	Angle of attack	ΔP (non-dimensional)
Plane duct	-	3.75
Plane duct with wing	(15^0)	4.21
Plane duct with wing	(30^0)	5.15
Plane duct with wing	(45^0)	5.97

Figure 5.18 shows the streamwise variation of pressure drop over the length of the triangular channel for a Reynolds number of 100 for different angles of attack of the delta wing. Increasing the angle of attack has the effect of increasing vortex strength, which in turn increases the resistance to flow and consequently a higher pressure drop is brought

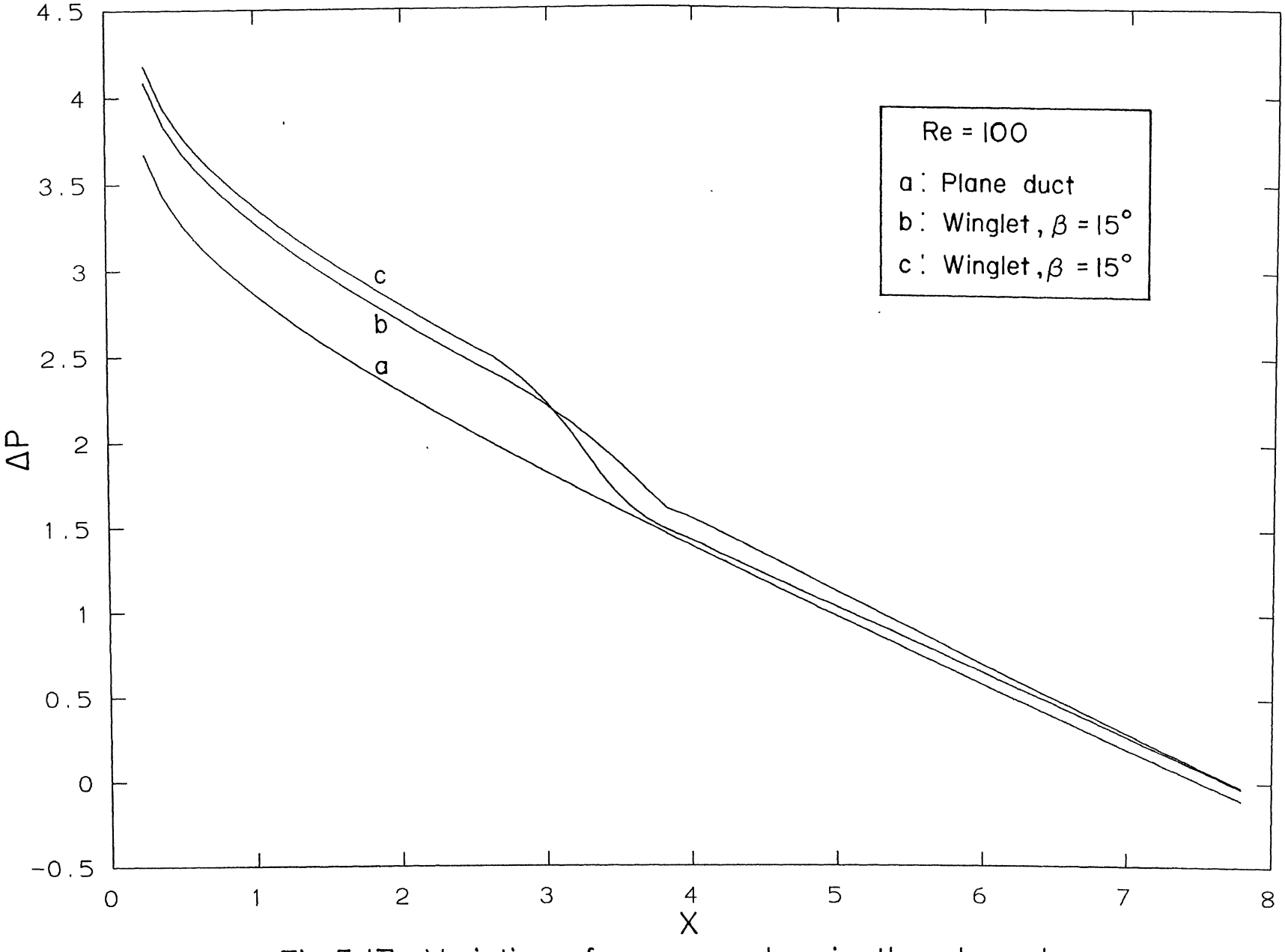

Fig. 5.17 Variation of pressure drop in the channel

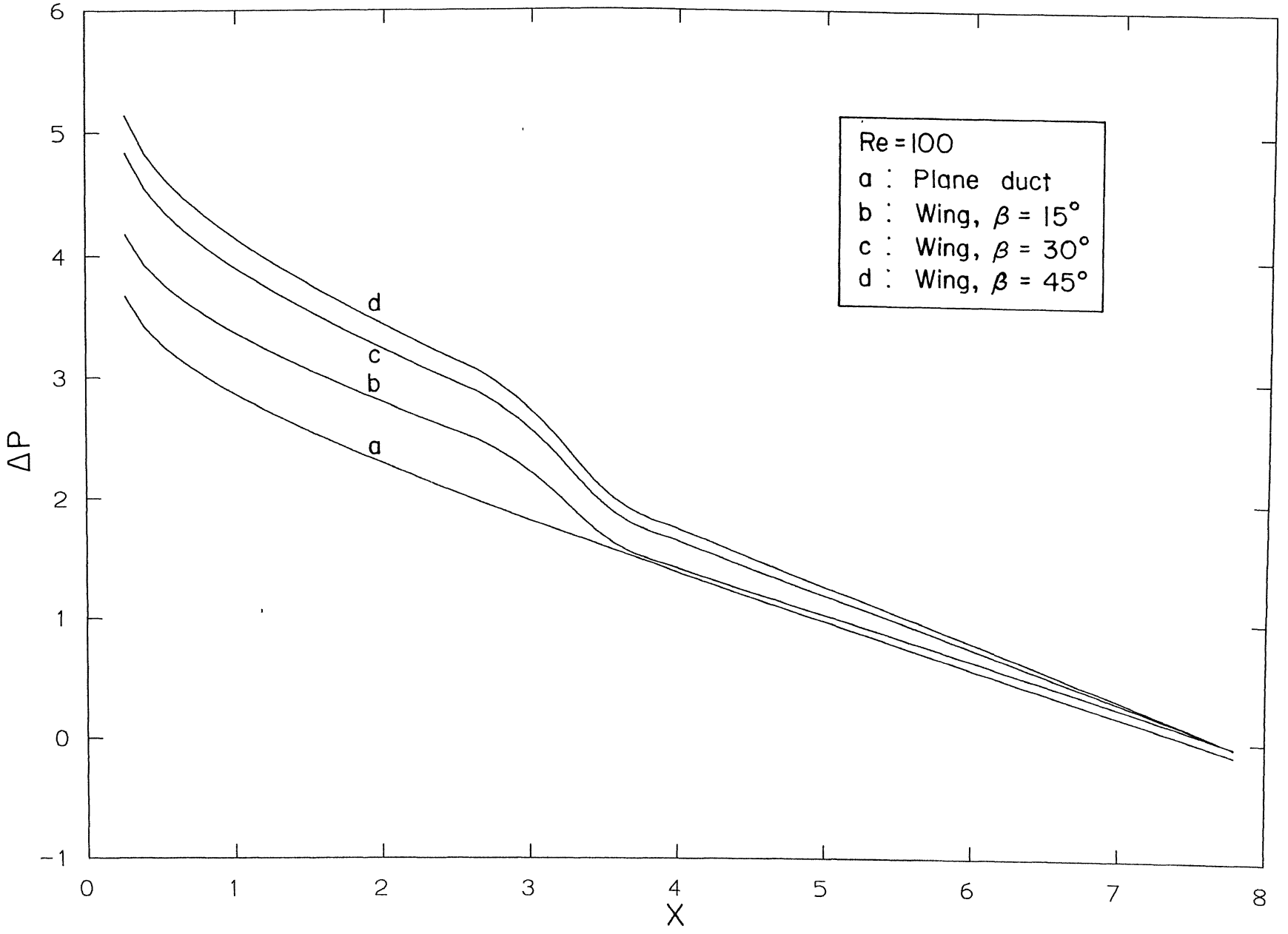

Fig.5.18 Variation of pressure drop in the channel

about. While calculating the pressure drop distribution, the exit pressure was subtracted from the average pressure at any cross-section. It may also be mentioned that the average pressure at any section was determined from the integral value of pressure at that section.

5.6 Concluding Remarks

The vortical structure formed by a delta wing is different from what is formed by a delta winglet . However, the performance curves of both these vortex generators show identical trends. In comparison to the delta winglet the delta wing yields a higher transport enhancement.

Chapter 6

Conclusions

6.1 Major Findings

The potential use of longitudinal vortex generators in the form of delta wings and delta winglets has long been established through experimental investigations as well as numerical computations. The simplest way to manufacture these vortex generators is to punch these out of the parent heat transfer surface. However these punched vortex generators can not be directly introduced on the plate surfaces of plate-fin heat exchangers as that would lead to physical mixing of the cold and hot fluids. This difficulty can be circumvented by using triangular inserts (between the plates) provided with punched vortex generators on their slant surfaces. Such vortex generators may be termed as secondary fins.

The performance of such a combination of primary and secondary fins has been computed in the present investigation. The results are quite encouraging, that is, a substantial enhancement in heat transfer can be achieved using the proposed fin design and the associated increase in the pumping power required is rather not significant. It is clear that delta wings and delta winglets are ideal alternatives for use in the design of enhanced heat exchanger surfaces. The combination of triangular inserts, carrying these vortex generators on their slant surfaces is strongly recommended for the plate-fin heat exchangers. Between the two, the delta wing is more effective in enhancing the heat

transfer and this trend agrees with the predictions of earlier computations in a rectangular channel. A closer study of the secondary flow pattern reveals some interesting aspects of flow in the wake of a vortex generator.

6.2 Scope for Further Work

In the present computations, two different thermal boundary conditions have been considered, viz., (1) Isothermal walls and (2) Constant heat flux along the walls. Both the boundary conditions represent idealised situations. A more accurate model would be to consider the finite thickness of the plates and solve the conjugate heat transfer problem. The solution of the conjugate heat transfer problem can be expected to yield more exact predictions.

The computations have been done assuming the flow regime to be laminar. Though turbulent flow is not frequently encountered in plate-fin heat exchangers, in some special applications involving very high velocities the flow regime can become turbulent. Therefore the present study can be extended for the turbulent flows. Using an appropriate turbulence model, the performance of the proposed design can be computed for high Reynolds numbers.

It is heartening to note that the proposed design is already under manufacture by Britannia Heat Transfer Limited, Birmingham. The results of the computations can be validated via a comparison with the actual performance available with the company. Conversely the numerical model can be used to arrive at the optimum design.

Bibliography

Achaichia, A. and Cowell, T. W., 1988, Heat Transfer and Pressure Drop Characterstics of Flat Tube and Louvered Plate Fin Surfaces, *Experimental Thermal and Fluid science.* vol. 1, pp 147-157.

Amon, C. H., and Patera, A.T., 1989, Numerical Calculation of Stable Three-Dimensional Tertiary States in Grooved-Channel Flow, *The Phys. Fluids-A*, vol. 1, No. 12, pp 2005-2009.

Bergles , A.E., 1983, Augmentation of Heat Transfer, Heat Exchanger Design Handbook Hemisphere Publishing Co., Washington DC.

Bergles, A. E., and Joshi, S. D.,1983, Augmentation Techniques for Low Reynolds Number In-Tube Flow, Low Reynolds Number Flow in Heat Exchangers, Hemisphere Publishing Corporation, Washington,

Bergles, A. E., Webb, R. L., Junkhan, G.H., and Jension, M. K., 1980, Bibliography on Augmentation of Convective Heat and Mass Transfer, *Heat Transfer Laboratory*, Department of Mechanical Engineering, Iowa State University, Ames, IA.

Bergles, A.E. 1978, Enhancement of Heat Transfer, Heat Transfer 1978, *Proceedings of the 6th International Heat Transfer Conference,* Vol.6.

Bergles, A.E., 1985 Techniques to Augment Heat Transfer, Handbook of Heat Transfer Applications, McGraw Hill, New York.

Biswas, G., Mitra, N. K. and Fiebig, M., 1989, Computation of Laminar Mixed Convection Flow in a Channel with Wing type Built-in Obstacles, *Journal of Thermophysics and Heat Transfer, (AIAA)*, vol. 3, pp 447-453.

Biswas, G., Laschefski, H., Mitra, N. K., and Fiebig, M., 1990, Numerical Investigation of Mixed Convection Heat Transfer in a Horizontal Channel with a Built-In Square Cylinder, *Numerical Heat Transfer*, Part – A, vol. 18,pp. 173-188.

Biswas, G. and Chattopadhyaya, H., 1992, Heat transfer in a channel with Built-in Wing type vortex generators, *Int. J. of Heat Mass Transfer*, vol. 35, pp 803-814.

Biswas, G., Deb, P. and Biswas, S., 1994, Generation of Longitudinal Streamwise Vortices: A Device for Improving Heat Exchanger Design, *Journal of Heat Transfer (ASME)*, vol. 116, pp 588-597.

Biswas, G., Mitra, N.K. and Fiebig, M., 1994, Heat Transfer Enhancement in Fin-Tube Heat Exchangers by Winglet-Type Vortex Generators, *Int. J. Heat Mass Transfer*, vol.37, pp 283-291.

Biswas, G., Torii, K., Fujii, D., and Nishino, K., 1996 Numerical and Experimental Determination of Flow Structure and Heat Transfer Effects of Longitudinal vortices in a Channel Flow, *Int. J. Heat and Mass Transfer*, vol. 39, pp 3441-3451.

Biswas, G. and Mitra, N. K.,1998, Longitudinal Vortex Generators for Enhancement of Heat Transfer in Heat Exchanger Applications, *Proc. of the 11th International Heat Transfer Conference*, vol. 5, pp 339-344.

Blum, H. A., and Oliver, L. R., 1966, Heat Transfer in Decaying Vortex System, *ASME Paper*, No. 66-WA/HT-62.

Braza, M., Chassaing, P., and Ha-Minh, H., 1986, Numerical Study and Physical Analysis of the Pressure and Velocity Fields in the Near Wake of a Circular Cylinder, J. Fluid Mech., vol.165, pp. 79-130.

Brown, C. E., and Michael , W. H ., 1954, Effect of Leading Edge Separation on the Lift of a Delta Wing, *J. Aero. Sci..*, vol.21, pp 690-694.

Chorin, A. J., 1967, A Numerical Method for Solving Incompressible Viscous Flow Problems, *J. Comp. Phys.*, vol. 2, pp. 12-26.

Date, A. W., 1974, Prediction of Fully-Developed Flow in a Tube Containing a Twisted Tape, *Int. J. Heat Mass Transfer*, vol. 17, pp. 845-859.

Date, A.W., 1973, Flow in Tubes Containing Twisted Tapes, *Heating and Ventilating Engg.*, vol. 47, pp. 240-249.

Deb, P., Biswas, G. and Mitra, N. K., 1995, Heat Transfer and Flow Structure in Laminar and Turbulent Flows in a Rectangular Channel with Longitudinal Vortices, *Int. J. Heat Mass Transfer*, vol. 38, pp 2427-2444.

Delery, J., Horowitz. E., Leuchter, O., and Solignac, J.L. 1984 Fundamental Studies on Vortex flow. *La Recerche Aerospatiale* , No.2, pp. 1-24.

Dong, Y., 1989, 32. Dong , Y., 1989, Experimentelle Untersuchung der Wechselwirkung von Langswirbelerzeugern und Kreiszylindern in Bezug auf Warmeubergang und Stromungsverlust, Doctoral Thesis, Ruhr-Universitat Bochum, Germany.

Edwards, F. J., and Alker, G. J. R., 1974, The improvement of Forced Convection Surface Heat Transfer Using Surface Protrusions in the Form of (a) Cubes and (b) Vortex Generators, *Proceedings of the Fifth Int. Heat Transfer Conference*, Tokyo, vol. 2, pp. 2244-2248.

Eibeck , P. A. and Eaton, J. K., 1987, Heat Transfer Effects of a Longitudinal Vortex Embedded in a turbulent Shear Flow, *Journal of Heat Transfer, (ASME)*, vol 109, pp 16-24.

Eibeck, P.A., and Eaton, J.K., 1986, The Effects of Longitudinal Vortices Embedded in a Turbulent Boundary Layer on Momentum and Thermal Transport, *Proc. 8th IHTC,* Vol. 3, pp. 1115-1120, San Francisco.

Fiebig, M., Kallweit, P. and Mitra, N.K., 1986, Wing Type Vortex Generators for Heat Transfer Enhancement, *Proceedings of the Eighth International Heat Transfer Conference*, San Francisco, vol. 6, pp 2909-2913.

Fiebig, M., Brockmeier, U., Mitra, N. K. and Guntemann, T., 1989,Structure of Velocity and Tempeature Fields in Laminar Channel Flows with Longitudinal Vortex Generators, *Numerical Heat Transfer-Part A*, vol. 15,pp 103-114.

Fiebig, M., Brockmeier, U., Mitra, N.K. and Guntermann, T., 1989, Structure of Velocity and Temperature Fields in Laminar Channel Flows with Longitudinal Vortex Generators, *Numerical Heat Transfer- Part A,* vol.15, pp 281-302.

Fiebig,M.,Dong,Y.and Mitra,N.K.,1990,Warmeubergangserhohungund Widerstandsverringerung durch Laengswirbelerzeuger in Rippenrohren, *Warme und Stoffubertragung*, vol 25, pp 34-44.

Fiebig, M., Kallweit, P., Mitra, N. K., and Tiggelbeck, S., 1991, Heat Transfer Enhancement and Drag by Longitudinal Vortex Generators in

Channel Flow, *Experimental Thermal and Fluid Science*, vol. 4 pp 103-114.

Fiebig, M., Guntermann, Th. and Mitra, N. K., 1995, Numerical Analysis of Heat Transfer and Flow Loss in a Parallel Plate Heat Exchanger Element with Longitudinal Vortex Generators as Fins, *Journal of Heat Transfer (ASME)*, vol. 117, pp 1064-1067.

Fiebig, M., Chen, Y., Grosse-Gorgemann, A., and Mitra , N. K., 1995, Conjugate Heat Transfer of a finned tube Part B: Heat Transfer Augmentation and Avoidance of Heat Transfer Reversal by Longitudinal Vortex Generators, *Numerical Heat Transfer,* Part A, 28, pp 147-155.

Fink, P.T., 1956, Wind-Tunnel Tests on a Slender Delta Wing at High Incidence, *Flugwiss*, vol. 4, pp 247-249.

Gambill, W. R., and Bundy, R. D., 1963, High Heat Flux Heat Transfer Characterstics of Pure Ethylene Glycol in Axial and Swirl Flow, *AIChE Journal*, vol. 9, pp. 55-59.

Garg, V. K., and Maji, P. K., 1987, Flow through a Converging-Diverging Tube with Constant Wall Enthalpy, *Numerical Heat Transfer*, vol. 12,pp. 285-305.

Garimella, S.V., Eibeck, P.A., 1991, Enhancement of Single Phase Convective Heat Transfer From Protruding Elements Using Vortex Generators, *Int. J. Heat Mass Transfer*, vol. 34, pp 2427-2430.

Ghosh Roychowdhary, D., Das, S. K., and Sundararajan, T., 'An Efficient Solution Method for Incompressible Navier-Stokes Equations Using Non-Orthogonal Collocated Grid, *International Journal for Numerical method in Engineering,* Vol. 45, pp. 741-763, 1999.

Grosse-Gorgemann, A., Fiebig, M., and Muller, U., 1993a, High Amplitude Self Excited Velocity Oscillations of the Flow Over Periodically Ribbed Surfaces , *Proc. Eurotherm 32 Heat Transfer in Single Phase Flow,* pp 108-111. Ed. By T. V. Jones, Oxford, U. K.

Grosse-Gorgemann, A., Hahne, W., and Fiebig, M., 1993b, Influence of Rib Height on Oscillations , Heat Transfer and Pressure Drop in Laminar Channel Flow, Proc. Eurotherm 31, Vortices and Heat Transfer , Bochum, Germany, pp 36-41.

Harlow, F. H. and Amsden, A. A., 1970, The SMAC Method: A Numerical Technique for Calculating Incompressible Fluid Flows, Los Alamos Scientific Lab. Rept., LA 4370.

Harlow, F. H. and Welch, J.E., 1965, Numerical Calculation of Time-Dependent Viscous Incompressible Flow of Fluid with Free Surface, *The Phys. of Fluids*, vol 8, pp 2182-2188.

Hirt, C. W. and Cook, J. L., 1972, Calculating Three-Dimensional Flows around Structures and over Rough Terrain, *J. Comput. Phys.*, vol 10, pp 324-340.

Hong, S. W., and Bergles, A. E., 1976, Augmentation of Laminar Flow Heat Transfer by Means of Twisted Tape Inserts, *Journal of Heat Transfer*, vol. 98, pp. 252-256.

Incropera, F. P., and Schutt, J. A., 1985, Numerical Simulation of Laminar Mixed Convection in the Entrance Region of Horizontal Rectangular Ducts, *Numerical Heat Transfer*, vol. 8, pp. 707-729.

Incropera, F. P., Knox, A. L., Maughan, J. R., 1987, Mixed-Concvection Flow and Heat Transfer in the Entry Region of a Horizontal Rectangular Duct, *Journal of Heat Transfer*, vol. 109,pp. 434-439.

Issa, R.I, Gosman, A.D. and Watkins A.P., 1986, The Computation of Compressible and Incompressible Recirculating Flows by a Non-Iterative Implicit Scheme, *J. Comp. Phys.*, vol.62, pp 66-82.

Jang, D.S., Jetli, R., and Acharya, S., 1986, Comparison of PISO, SIMPLER and SIMPLEC Algorithms for the Treatment of the Pressure Velocity Coupling in Steady Flow Problems, *Numerical Heat Transfer*, vol.10, pp. 209-228.

Junkhan, G. H., Bergles A. D., Nirmalan, V., and Ravigururajan, T., 1985, Investigation of Turbulators for Fire Tube Boilers, *Journal of Heat Transfer*, vol. 107, pp. 354-360.

Kakac, S.,Shah, R. K., and Bergles, A. E., 1981, Low Reynolds Number Flow in Heat Exchangers, Hemisphere Publishing Corporation, Washington, pp. 694-720.

Kays, W.M., London, A.L, Compact Heat Exchangers 3rd edition McGraw Hill Book Company 1984.

Kobayashi, M.H., and Pereira, C.F., Calculation of Incompressible Laminar Flows on a Non-Staggered, Non-Orthogonal Grid, Numerical Heat Transfer, Part-B, Vol. 19, pp. 243-262, 1991.

Kreith, F., and Margolis, D., 1959, Heat Transfer and Friction Factor in Turbulent Vortex Flow, *Applied Sciectific Research*, vol. 8, pp 457-473.

Lawford, J. A., 1964, Low Speed Wind Tunnel Experiments on Series of Sharp-Edged Delta Wings, *Part-2, RAE, Rep. Aero. 2954.*

Majumdar, D., and Amon, C. H., 1992, Heat and Momentum Transport in Self- sustained Oscillatory Viscous Flows, *Journal of Heat Transfer,* vol. 114,pp. 866-873.

Majumdar, S., Rodi, W., and Zhu, J., 1992, Three-Dimensional Finite-Volume Method for Incompressible Flows with Complex Boundaries, *J. of Fluids Engg. (ASME)*, vol. 114, pp. 496-503.

Marsden, D. J., Simpson, R. W., Rainbird , W. J., 1958, The Flow over Delta Wing at Low Speeds with Leading Edge Separation, *College of Aeronautics*, Cranfield, Rep. 114.

Migay, V. K., and Golubev, L. K., 1970, Friction and Heat Transfer in Turbulent Swirl Flow with a Variable Swirl Generator in a Pipe, *Heat Transfer – Soviet Research*, vol. 2 pp. 68-73.

Mukhopadhyay, A., Sundararajan, T., and Biswas, G., 1993, An Explicit Transient Algorithm for Predicting Incompressible Viscous Flows in Arbitrary Geometry, *Int. J. Numer Methods Fluids,* vol.17, pp. 975-993.

Nichols, B. D., and Hirt, C. W., 1971, Improved Free Surface Boundary Conditions for Numerical Incompressible-Flow Calculations, *J. Comp. Phys.*, vol. 8, pp. 434-448.

Orlanski, I., 1976, A simple boundary condition for unbounded flows, *J. of Comput. Phys.*, vol. 21, pp 251-269.

Patankar, S.V., Ramadhyani, S., and Sparrow, E. M., 1978, Efeect of Circumferentially Nonuniform Heating on Laminar Combined Convection in a Horizontal Tube, *Journal of Heat Transfer*, vol. 100,pp. 63-70.

Patankar, S.V., and Spalding, D.B., 1972, A Calculation Procedure for Heat Mass and Momentum Transfer in Three-Dimensional Parabolic Flows, *Int. J. Heat Mass Transfer*, vol.15, pp 1787-1806.

Patankar, S.V., 1981, A Calculation Procedure for Two-Dimensional Elliptic Situations, *Numerical Heat Transfer,* vol.4, pp. 409-425.

Pearcy, H.H., 1961, Stock-Induced Separation in Boundary Layers and Flow Control, Vol. 2, Pergamon Press, New York.

Peric, M., 1985, A Finite Volume Method for the Prediction of Three-Dimensional Fluid Flow in Complex Ducts, Ph.D. Thesis, University of London.

Peric, M., Kessler, R., and Scheuerer, 1988, Comparision of Finite-Volume Numerical Methods with Staggered and Collocated Grids, *Computers and Fluids,* vol. 16, pp. 389-403.

Pauley, W. R., and Eaton, J. K., 1988, Experimental Study of the Development of Longitudinal Vortex Pairs Embedded in a Turbulent Boundary Layer, AIAA Journal, vol. 26, pp 816-823.

Rhie, C. M., and Chow, W. L., 1983, Numerical Study of the Turbulent Flow Past an Airfoil with Trailing Edge Seperation, *AIAA J.,* vol. 21, pp. 1525-1532.

Robichaux, J., Tafti, D.K., and Vanka, S.P., 1992, Large-Eddy Simulations of Turbulence on the CM-2, *Numerical Heat Transfer,* Part-B, vol.21, pp.367-388.

Russels, C. M. B., Jones, T.V., and Lee, G. H., 1982, Heat Transfer Enhancement Using Vortex Generators, *Proc. of the Seventh Int. Heat Transfer Conference,* Munich ,vol.3, pp 283-288.

Sanchez, M., Mitra, N. K., Fiebig, M., 1989, Numerical Investigation of Three-Dimensional Laminar Flows in a Channel with Built-in Circular Cylinder Wing-Type Vortex Generators, *Proc. Eighth GAMM Conference on Numerical methods in Fluid Mechanics (Vieweg),* pp-484-492.

Smithberg, E., and Landis, F., 1964, Friction and Forced Convection Heat Transfer Characteristics in Tube with Twisted Tape Swirl Generator, *Journal of Heat Transfer,* vol. 86, pp. 39-49.

Sparrow, E. M., and Chaboki A., 1984, Swirl Affected Turbulent Fluid Flow and Heat Transfer in a Circular Tube, *Journal of Heat Transfer,* vol. 106, pp. 766-773.

Tiggelbeck, S., Mitra, N. K. and Fiebig, M., 1992, Flow Structure and Heat Transfer in a Channel with Multiple Longitudinal Vortex-Generators, *Experimental Thermal and Fluid Science,* vol. 5, pp 425-436.

Torii, K., Nishino, K. and Nakayama, K., 1994, Heat Transfer Augmentation by Longitudinal Vortices in a Flat Plate Boundary Layer, *Proc. of the Tenth International Heat Transfer Conference,* Brighton,vol. 6, pp 123-128.

Turk, A.J., and Junklan, G.H., 1986, Heat Transfer Enhancement Downstream of Vortex generators on a Flat Plate. *Proc. 8th IHTC,* Vol. 6, pp. 2903-2908, San Francisco.

Valencia, A., 1992, Warmeubergang und Druckverlust in Lamellen-Rohr-Warmeubertragernmit Langswirbelerzugern, Doctoral Thesis, Ruhr-Universitat Boschum, Germany.

Valencia, A., Fiebig, M. and Mitra, N. K., 1996, Heat Transfer Enhancement by Longitudinal Vortices in Fin-tube Heat Exchanger Element with Flat tubes, *Journal of Heat Transfer (ASME)}*, vol. 118, pp 209-211.

Van Doormaal, J.P., and Raithby,.G.D., 1984, Enhancements of the SIMPLE method for Predicting Incompressible Fluid Flows, *Numerical Heat Transfer,* vol.7, pp.147-163.

Velusamy, K., and Garg, V. K., 1993, Entrance Flow in Elliptical Ducts, *Int. J. Numer. Methods Fluids*, vol. 17, pp. 1079-1096.

Verma, A.K., and Eswaran, V., 1996 Overlapping Control Volume Approach for Convection-Diffusion Equation, *Int. J. Numerical Methods Fluids*, vol. 23,pp. 865-882.

Verma, A.K., and Eswaran, V.,1997 A Bounded Convection Scheme for the Overlapping Control Volume Approach, *Int. J. Numerical Methods Fluids*

Viecelli, A. J., 1971, A Computing Method for Incompressible Flows Bounded by Moving Walls, *J. Comp. Phys.*, vol. 8 pp. 119-143.

Webb, B. W., and Ramadhyani, S., 1985, Conjugate Heat Transfer in a Channel with Staggered ribs, *Int. J. Heat Mass Transfer*, vol. 28, pp. 1679-1687.

Webb, R. L., 1987, Enhancement of Single-Phase Convective Heat Transfer, *Hand Book of Single-Phase Convective Heat Transfer*, (Ed Kakac, S., Shah,R. K. and Aung, W.) John Wiley & Sons, New York.

Westphal, R. V., and Mehta, R. D., 1987, Interaction of Oscillating Vortex with a Turbulent Boundary Layer, *AIAA 19th Fluid Dynamics and Laser Conference, Hawaii*, AIAA paper no. 87-1246.

Winter, H., 1956, Stromungsvorgange on Plattern and Profilerten Korpern bei Kleinen Spannweiten, *Forschg. Ing. Wes..*, vol. 6, pp. 247-249.

Yanagihara, J. L. and Torii, K., 1990, Heat Transfer characteristics of Laminar Boundary Layer in the Presence of Vortex Generators, *Proceedings of the Ninth International Heat Transfer Conference* ,vol. 6, pp 323-328.

Zhang., Fiebig, M., and Mitra, N. K., 1989, Vortex Breakdown on Heat Transfer Enhancement in Flows Between Parallel Plates, Eurotherm Seminar No.91, Heat Transfer in Single Phase Flows, Bochum, pp 97-104.

Appendix A

The Program Substructure

In order to solve the full Navier-Stokes and energy equations a computer code has been developed based on the numerical scheme described in Chapter-3. The code has been written in FORTRAN-77 language. The code consists of several subroutines each of which has a set of specific tasks to carry out. The main program (DELTAM) and the subroutines are written in the form of modules. The flow chart provided in Figure A-1 shows the operational sequence of the various subroutines with their major communication links with the main program. A brief description of the different indices and the functions of the various subroutines are given below.

INIT	This subroutine initialises the entire calculations for a set of input variables such as Reynolds number, Prandtl number, grid sizes etc.
IREST	This is an index which denotes whether a restart from a set of existing field variables is desired (=1) or the computation should start from the beginning.
START	This subroutine specifies the starting values (guessed field) of the dependent variables and initiates computation.
RESTAR	This is a subroutine where the field variables are equated to a data field which was existing beforehand.
CONTI	This subroutine controls the pressure-velocity iteration loop for compliance with the continuity equation.

BCC	This subroutine deals with the boundary conditions for continuity equation.
BCO	The velocity boundary conditions for the obstacle which are required for the CONTI module are specified in this subroutine.
CEQCP	In this subroutine divergence of velocity vector (D) is evaluated and the pressure correction is done.
EPSI	A small value prescribed as the upper-bound for the velocity divergence in each cell.
BCNS	This subroutine specifies the velocity boundary conditions for Navier-Stokes equation.
VELALT	This subroutine stores the current velocity field for time level (n) in order to start a new time cycle of (n+1) level.
TICORR	In this subroutine the value of the time increment (Δt) and the donor cell coefficient (α_p) are calculated.
DIVMAX	This stands for the maximum value of divergence in the entire flow field.
DTMAX	This is the value of the maximum time increment of the field variables.
STAT	A small value which determines the conditions for steady solution.
ITI	Iteration counter for the CONTI module.
ITA	Number of time steps.
ITAMAX	Maximum allowable number of time steps.
NSEQCP	This is a subroutine where the velocities for the next timestep are explicitly evaluated from the discretised Navier-Stokes equations.
BCOV	This subroutine specifies the velocity boundary conditions for the obstacle which are required in the *predictor* step. (The subroutines BCO and BCOV together define the vortex

	generator).
TIGRAD	In this subroutine the time-gradients of the velocity components are calculated.
ENERGY	This subroutine controls the solution of the energy equation.
BCT	This subroutine deals with the temperature boundary conditions for the computational domain.
BCOT	This subroutine specifies the temperature boundary conditions for the vortex generator.
TEQCP	This subroutine calculates the temperature field.
DT	This denotes the value of the maximum change in temperature between two iterative steps.
TSTAT	A small value that determines the convergence for steady solution of the energy equation.
OUTPUT	This subroutine prints the output in the assigned output files.

A. The Program

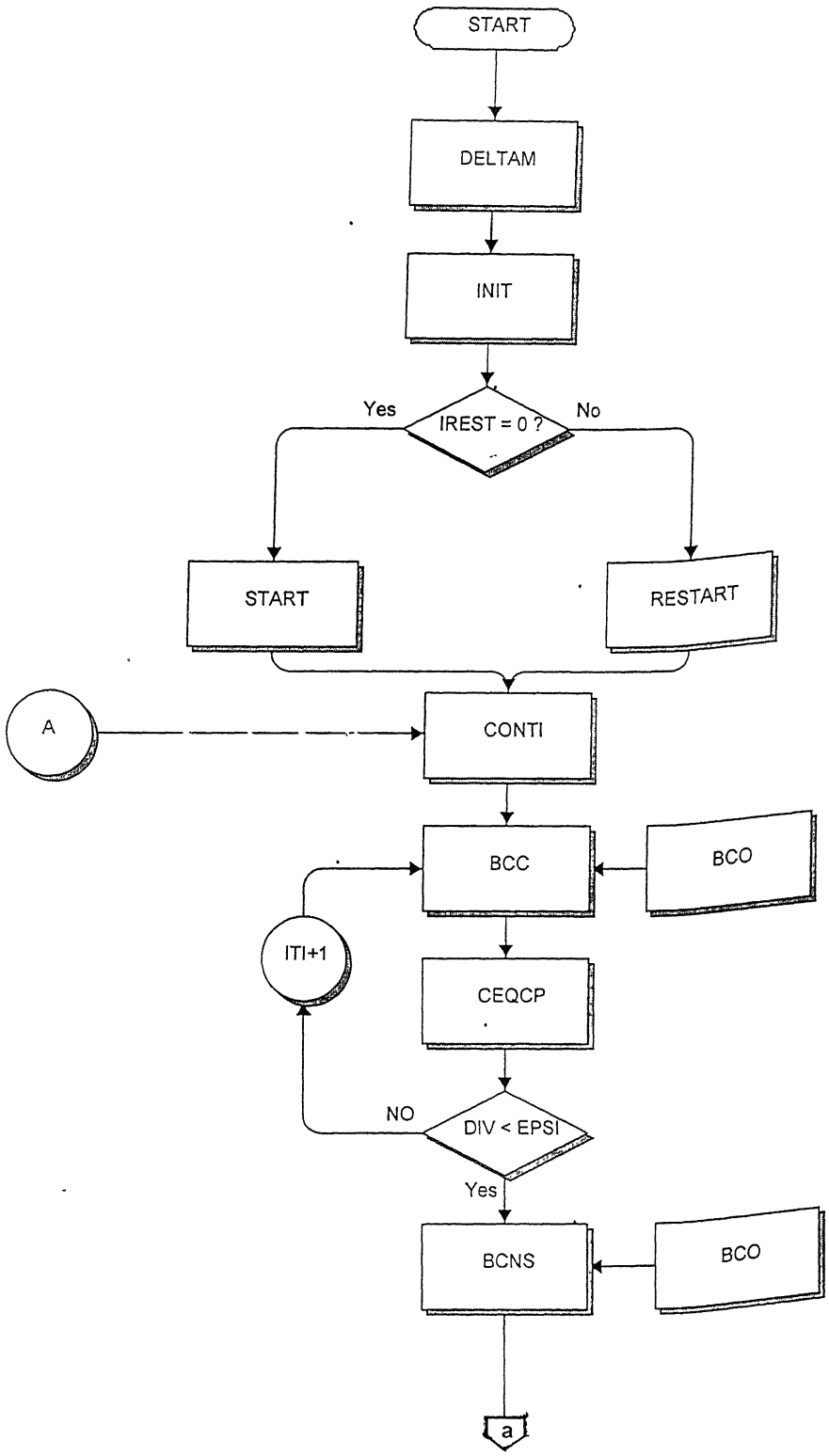

Fig. A-1

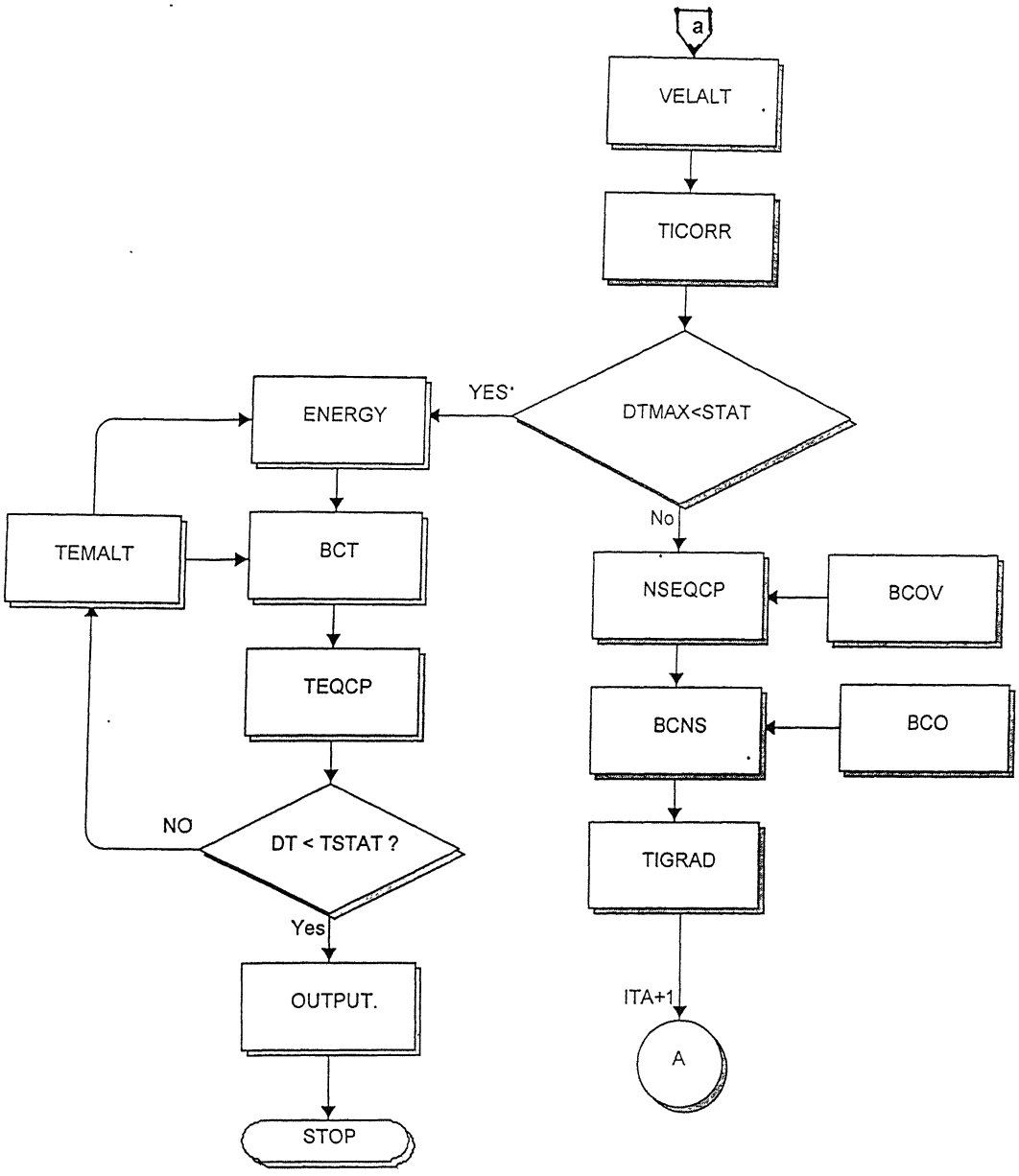
a
VELALT
TICORR
DTMAX<STAT
YES
ENERGY
No
TEMALT
BCT
NSEQCP
BCOV
TEQCP
BCNS
BCO
NO
DT < TSTAT ?
TIGRAD
Yes
OUTPUT.
ITA+1
A
STOP

Fig. A-1

A 131095

Date Slip

This book is to be returned on the date last stamped.